LONG-TERM DEMONSTRATION OF HYDROGEN PRODUCTION FROM COAL AT ELEVATED TEMPERATURES

Year 6 – Activity 1.12 – Development of a National Center for Hydrogen Technology

Topical Report

Prepared for:

AAD Document Control

National Energy Technology Laboratory
U.S. Department of Energy
626 Cochrans Mill Road
PO Box 10940, MS 921-107
Pittsburgh, PA 15236-0940

DOE NETL Cooperative Agreement No. DE-FE0003466
Performance Monitor: Steve Markovich

Prepared by:

Joshua J. Stanislowski
Scott G. Tolbert
Tyler J. Curran
Michael Swanson

Energy & Environmental Research Center
University of North Dakota
15 North 23rd Street, Stop 9018
Grand Forks, ND 58202-9018

March 2012

EERC DISCLAIMER

LEGAL NOTICE This research report was prepared by the Energy & Environmental Research Center (EERC), an agency of the University of North Dakota, as an account of work sponsored by the U.S. Department of Energy (DOE) National Energy Technology Laboratory (NETL), the North Dakota Industrial Commission, and a consortium of industrial sponsors. Because of the research nature of the work performed, neither the EERC nor any of its employees makes any warranty, express or implied, or assumes any legal liability or responsibility for the accuracy, completeness, or usefulness of any information, apparatus, product, or process disclosed or represents that its use would not infringe upon privately owned rights. Reference herein to any specific commercial product, process, or service by trade name, trademark, manufacturer, or otherwise does not necessarily constitute or imply its endorsement or recommendation by the EERC.

DOE ACKNOWLEDGMENT

This report was prepared with the support of DOE NETL Cooperative Agreement No. DE-FE0003466. However, any opinions, findings, conclusions, or recommendations expressed herein are those of the author(s) and do not necessarily reflect the views of DOE.

DOE DISCLAIMER

This report was prepared as an account of work sponsored by an agency of the United States Government. Neither the United States Government, nor any agency thereof, nor any of their employees makes any warranty, express or implied, or assumes any legal liability or responsibility for the accuracy, completeness, or usefulness of any information, apparatus, product, or process disclosed, or represents that its use would not infringe upon privately owned rights. Reference herein to any specific commercial product, process, or service by trade name, trademark, manufacturer, or otherwise does not necessarily constitute or imply its endorsement, recommendation, or favoring by the United States Government or any agency thereof. The views and opinions of authors expressed herein do not necessarily state or reflect those of the United States Government or any agency thereof.

LONG-TERM DEMONSTRATION OF HYDROGEN PRODUCTION FROM COAL AT ELEVATED TEMPERATURES

Year 6 – Activity 1.12 – Development of a National Center for Hydrogen Technology

ABSTRACT

The Energy & Environmental Research Center (EERC) has continued the work of the National Center for Hydrogen Technology® (NCHT®) Program Year 6 Task 1.12 project to expose hydrogen separation membranes to coal-derived syngas. In this follow-on project, the EERC has exposed two membranes to coal-derived syngas produced in the pilot-scale transport reactor development unit (TRDU). Western Research Institute (WRI), with funding from the State of Wyoming Clean Coal Technology Program and the North Dakota Industrial Commission, contracted with the EERC to conduct testing of WRI's coal-upgrading/gasification technology for subbituminous and lignite coals in the EERC's TRDU. This gasifier fires nominally 200–500 lb/hour of fuel and is the pilot-scale version of the full-scale gasifier currently being constructed in Kemper County, Mississippi. A slipstream of the syngas was used to demonstrate warm-gas cleanup and hydrogen separation using membrane technology. Two membranes were exposed to coal-derived syngas, and the impact of coal-derived impurities was evaluated. This report summarizes the performance of WRI's patent-pending coal-upgrading/gasification technology in the EERC's TRDU and presents the results of the warm-gas cleanup and hydrogen separation tests.

Overall, the WRI coal-upgrading/gasification technology was shown to produce a syngas significantly lower in CO_2 content and significantly higher in CO content than syngas produced from the raw fuels. Warm-gas cleanup technologies were shown to be capable of reducing sulfur in the syngas to 1 ppm. Each of the membranes tested was able to produce at least 2 lb/day of hydrogen from coal-derived syngas.

TABLE OF CONTENTS

Continued . . .

TABLE OF CONTENTS (continued)

LIST OF FIGURES

Continued . . .

LIST OF FIGURES (continued)

LIST OF TABLES

Continued . . .

LIST OF TABLES (continued)

LONG-TERM DEMONSTRATION OF HYDROGEN PRODUCTION FROM COAL AT ELEVATED TEMPERATURES

Year 6 – Activity 1.12 – Development of a National Center for Hydrogen Technology

EXECUTIVE SUMMARY

The Energy & Environmental Research Center (EERC) has continued the work of the National Center for Hydrogen Technology® (NCHT®) Program Year 6 Task 1.12 project to expose hydrogen separation membranes to coal-derived syngas. In this follow-on project, the EERC has exposed two membranes to coal-derived syngas produced in the pilot-scale transport reactor development unit (TRDU). Western Research Institute (WRI), with funding from the State of Wyoming Clean Coal Technology Program and the North Dakota Industrial Commission, contracted with the EERC to conduct testing of WRI's coal-upgrading/gasification technology for subbituminous and lignite coals in the EERC's TRDU. This gasifier fires nominally 200–500 lb/hour of fuel and is the pilot-scale version of the full-scale gasifier currently being constructed in Kemper County, Mississippi. A slipstream of the syngas was used to demonstrate warm-gas cleanup and hydrogen separation using membrane technology. Two membranes were exposed to coal-derived syngas, and the impact of coal-derived impurities was evaluated. This report summarizes the performance of WRI's patent-pending coal-upgrading/gasification technology in the EERC's TRDU and includes the results of the warm-gas cleanup and hydrogen separation tests.

Overall, the WRI coal-upgrading/gasification technology was shown to produce a syngas significantly lower in CO_2 content and significantly higher in CO content than syngas produced from the raw fuels. Warm-gas cleanup technologies were shown to be capable of reducing sulfur in the syngas to 1 ppm. Each of the membranes tested was able to produce at least 2 lb/day of hydrogen from coal-derived syngas.

Cost-effective CO_2 separation is a significant technical hurdle, with a potential increase of up to 84% in the cost of electricity produced for existing pulverized coal-fired power plants with retrofit carbon capture. Therefore, novel approaches to the problem are required, including fuel upgrading and hydrogen separation membranes. Fuel-upgrading technologies improve the efficiency of the plant and reduce the overall CO_2 footprint. Efficient and cost-effective membranes for the separation of hydrogen and CO_2 represent a potential cost-effective method for the coproduction of power, hydrogen, and/or fuels and chemicals while leaving CO_2 available for enhanced oil recovery. Significant progress has been made over the past decade in producing membranes that can effectively separate hydrogen from the syngas stream, leaving a relatively pure stream of CO_2 available at high pressure for sequestration.

WRI's proprietary patent-pending coal-upgrading/gasification process is a promising technology for conversion of upgraded low-rank, high-moisture fuels to syngas via various proprietary operational modifications to gasification technologies. Warm-gas cleanup techniques have been shown to improve the economics of coal gasification plants, and since certain volatile

metals are challenging to remove from syngas at elevated temperatures, any technology that can remove even a fraction before gasification is beneficial.

Hydrogen separation membrane development to date has occurred mainly on simulated mixtures of syngas. Impurities from coal-derived syngas that could poison a hydrogen separation membrane include H_2S, COS, NH_3, CO, and HCl. Long-term success of hydrogen separation membranes will require long-term exposure to coal-derived syngas to understand the impact of the impurities. While the majority of the impurities will be removed in a gas cleanup process, concentrations to less than 1 ppmv may be required for long-term viability.

The raw and upgraded fuels were prepared by WRI using WRI's proprietary patent-pending process at WRI and shipped to the EERC and tested in the EERC's TRDU as part of WRI's project, funded by the State of Wyoming Clean Coal Technology Program and the North Dakota Industrial Commission. Each fuel was demonstrated to gasify well with minimal operational issues. The biggest system upset for the week was the loss of the main air compressor for a couple of hours that was caused by cold ambient air temperatures. Fuel feeding for the test run progressed with minimal issues, and no differences were noted in the feedability of the three fuels. The treated fuels were shown to have a significant reduction in moisture and certain volatile metals, and lower levels of silica were also observed in the treated coals.

The most dramatic transition observed throughout the testing was the change in CO and CO_2 concentrations as the gasifier was switched from raw to upgraded fuels. For both the Powder River Basin (PRB) and lignite fuels, CO levels significantly increased, and CO_2 levels significantly decreased when the dried fuel was brought online. This change resulted in a syngas with increased heating value. This transition was also observed when switching from the upgraded PRB to the raw lignite, between Tests 4a-4 and 5a-1.

Particle-size distributions were determined for all of the ash samples collected during the test run and the raw fuels. No major differences were observed in the particle-size distributions for the test runs. The elemental composition of the ash was also analyzed, and the most significant finding was the high level of sulfur capture occurring in the filter ash under the air-blown test conditions. Otherwise, no significant difference was observed in the ash chemistry between the raw and treated fuel. No ash agglomeration issues were observed for any of the tests.

Water samples produced from the gasifier were analyzed for organic content. Lower levels of organics were observed on the dried and treated fuels as compared to the raw fuel runs. Significantly higher concentration organic material was produced during the steam–oxygen gasification tests.

The warm-gas cleanup equipment, sorbents, and catalysts used were shown to be capable of removing sulfur down to less than 2 ppm and the shift catalyst was able to reduce CO levels to below 1%. Water and tars were condensed out of the syngas prior to compression for the membrane exposure.

Both of the hydrogen separation membranes were shown to be able to produce greater than 2 lb/day of hydrogen. Membrane 1 appeared to experience some performance degradation which

may have been caused by coking. The coking could be attributed to a system upset and lack of steam available for the water–gas shift reaction. The membrane was exposed to oxygen at high temperature at the supplier's laboratory to burn out the contaminant, and the membrane performance returned to expected levels. Membrane 2 developed a significant leak during the testing. Both membranes were shown to be capable of producing hydrogen from coal-derived syngas during the entire test period.

LONG-TERM DEMONSTRATION OF HYDROGEN PRODUCTION FROM COAL AT ELEVATED TEMPERATURES

Year 6 – Activity 1.12 – Development of a National Center for Hydrogen Technology

APPROACH

Cost-effective CO_2 separation is a significant technical hurdle, with a potential increase of up to 84% in the cost of electricity produced for existing pulverized coal-fired power plants with retrofit carbon capture. Therefore, novel approaches to the problem are required, including fuel upgrading and hydrogen separation membranes. Fuel-upgrading technologies improve the efficiency of the plant and reduce the overall CO_2 footprint. Efficient and cost-effective membranes for the separation of hydrogen and CO_2 represent a potential cost-effective method for the coproduction of power, hydrogen, and/or fuels and chemicals while leaving CO_2 available for enhanced oil recovery. Significant progress has been made over the past decade in producing membranes that can effectively separate hydrogen from the syngas stream, leaving a relatively pure stream of CO_2 available at high pressure for sequestration.

Hydrogen separation membrane development to date has occurred mainly on simulated mixtures of syngas. Impurities from coal-derived syngas that could poison a hydrogen separation membrane include H_2S, COS, NH_3, CO, and HCl. Long-term success of hydrogen separation membranes will require long-term exposure to coal-derived syngas to understand the impact of the impurities. While the majority of the impurities will be removed in a gas cleanup process, concentrations to less than 1 ppmv may be required for long-term viability.

The Energy & Environmental Research Center (EERC) is continuing the work performed in Years 3–5 of Activity 1.12 to demonstrate the performance of hydrogen separation membranes on coal-derived syngas. This follow-on project will gasify upgraded coal from Western Research Institute (WRI) patent-pending coal-upgrading/gasification process in the EERC's transport reactor development unit (TRDU) and then test the performance of a selected hydrogen separation membrane on a slipstream of the syngas. WRI is providing funding for the test run through the State of Wyoming's Clean Coal Technologies Research Program and the North Dakota Industrial Commission. WRI's coal-upgrading/gasification process is proprietary and has been shown to significantly reduce moisture and certain volatile metals in the fuel and enhance gasification performance with a fluidized-bed gasifier. WRI is interested in evaluating the gasification performance of the upgraded fuel as well as evaluating the syngas impact on potential end products. The EERC will conduct gasification tests with the WRI raw, dried, and treated fuels according to WRI's proprietary gasifier conditions, and a slipstream of the syngas will be sent through a gas-cleaning, WGS, and hydrogen separation train. Hydrogen and CO_2 will be separated using a hydrogen separation membrane to yield relatively pure streams of hydrogen and CO_2. The membrane selected will be one currently part of the U.S. Department of Energy (DOE) membrane development program, and DOE will be consulted on membrane selection. This approach has merit because the drying process has the potential to reduce the

amount of CO_2 emitted from the gasifier and, therefore, will also reduce the overall cost of processes utilizing hydrogen separation membranes with CO_2 capture and storage.

The goal of this activity is to evaluate the gasification performance of WRI's thermally treated coal on the TRDU and to produce a pure stream of hydrogen from a slipstream of the TRDU syngas. Specific objectives are as follows:

- Perform a 7-day gasification test campaign on the EERC's TRDU to evaluate various operating conditions with raw, dried, and treated coals employing WRI proprietary gas injection and other gasifier operational modifications.

- Perform slipstream syngas cleaning and hydrogen separation testing during the gasification test runs.

BACKGROUND

Principles of Coal Gasification

Coal gasification processes employ fixed-bed, fluidized-bed, or entrained-flow reactor systems to react coal with air or oxygen and steam over a range of temperatures from 650°C (1202°F) for catalytic gasification to about 1500°C (2732°F) for entrained-flow gasifiers (EFGs), variously resulting in dry, agglomerated, or slagging ash discharge. Process pressures range from near atmospheric to 1200 psig (82 atm). The principal groups of reactions are pyrolysis, combustion, steam gasification, and secondary reactions among gaseous products and with carbon.

Pyrolysis and Tar Cracking

Coal $\rightarrow$ Char + Tar, Light Oil, H_2O, H_2, CO, CO_2, and HC Gases

Tar, Light Oil $\rightarrow$ CH_4 and Other HC Gases + CO + H_2 + CO_2

Combustion	ΔH, Btu/lb mole
$C + O_2 \rightarrow CO_2$	−169,300
$C + ½O_2 \rightarrow CO$	−47,600
$CO + ½O_2 \rightarrow CO_2$	−121,700
Steam Gasification	
$C + H_2O \rightarrow CO + H_2$	+56,490
Secondary Reactions	
$H_2 + ½O_2 \rightarrow H_2O_{(g)}$	−104,000
$C + 2H_2O_{(g)} \rightarrow CO_2 + 2H_2$	+ 38,780

Water–Gas Shift (WGS) Reaction

$CO + H_2O_{(g)} \rightarrow CO_2 + H_2$	−17,700

Methanation Reactions

$C + 2H_2 \rightarrow CH_4$	−32,200
$CO + 3H_2 \rightarrow CH_4 + H_2O$	−88,700
$CO + H_2 \rightarrow ½CH_4 + ½CO_2$	−53,200

Note: (−) Exothermic
(+) Endothermic

The primary products of gasification are CO, H_2, and CH_4, along with some carbon dioxide and nitrogen when air is used as the oxidant. Coproducts may include tar, oil, phenol, char, hydrogen sulfide, carbonyl sulfide, ammonia, and hydrogen cyanide. The primary reactions involving pyrolysis and steam gasification are endothermic; thus heat must be provided either externally or by the combustion of carbon. Heat from combustion can also be supplied indirectly by recycling bed material to provide either sensible heat or chemical energy (e.g., the CO_2 acceptor process). The WGS and methanation reactions are exothermic and contribute to the energy balance at lower temperatures and at low temperature and high pressure where CH_4 is a principal product. The particular gas composition obtained from various types of gasifiers depends on the effects of temperature, pressure, flow patterns (e.g., cocurrent versus countercurrent), fluid dynamic intensity, solid and gas residence times, and catalysis on chemical kinetics and equilibrium.

Coal Drying and Friability

The friability and volume of coal particles change with drying or heating. The thermal and mechanical friabilities and volumetric shrinkage influence the size distribution of coal or char particles in fixed-bed gasification systems. Shrinkage during drying and devolatilization will have an effect on the size distribution in addition to that caused by the fracturing of particles. Drying and pyrolysis can cause bulk shrinkage of 35% in lignite (1). In fixed-bed applications, particle shrinkage can be an important factor in the settling behavior of low-rank coals in the process vessels. Typically, the properties of fixed beds such as shear strength and permeability are defined by the size distribution of the particles regardless of how that size distribution was produced. The mechanical friability of low-rank coals increases sharply with the amount of drying. For example, removing approximately half the original moisture content of Indian Head lignite increased the mechanical friability from 20% to 70% (1). In addition to mechanical friability, thermal friability also plays a role in the particle-size evolution of coal particles. Thermal friability is a measure of the thermal fracturing resulting from differential expansion of different portions or components of coal particles because of expanding water vapor and volatile organic materials. For some coals, such as lignites, the thermal friability is significantly greater than the mechanical friability. The EERC has conducted work in the area of thermal and mechanical friabilities in support of gasification projects.

Coal mechanical friability and thermal friability depend strongly on the lithotype composition of coal (1). Each lithotype has significantly different physical properties. Fusain is commonly the origin of fine particles. During handling and transportation, fusain is easily removed from larger particles as fines. Fusain is generally rich in inertinite macerals. The huminite and liptinite maceral groups are less friable relative to inertinite. Petrographic analyses of coal combined with knowledge of their moisture contents can be used to empirically predict the mechanical and thermal friabilities of various coals (1, 2).

Coal Pyrolysis, Tar Formation, and Tar Cracking

Pyrolysis is a thermal decomposition process that produces gases, liquids (tar), and char (solid residue). In general, the thermal decomposition occurs in an oxygen-free atmosphere, but oxidative pyrolysis is an inherent component of combustion processes. Gaseous, liquid, and solid pyrolysis products can all be used as fuels, with or without prior upgrading, or they can be utilized as feedstocks for chemical or material industries.

During heating, all coals follow the same transformation pathway, which includes the loss of moisture and loss of weight because of thermal decomposition or pyrolysis. The materials driven off during thermal decomposition are referred to as volatile matter, which consists of decomposition products, gases, and vapors. The gases and vapors produce tars when cooled. The residual material consists of char or fixed carbon. The abundance and characteristics of tars and char are highly coal-dependent. Some bituminous coals when heated exhibit plastic properties over a specific range of temperatures, while lower-ranked subbituminous and lignite coals do not exhibit plastic properties and produce a ridged, friable char.

Coal rank and type also influence the abundance and characteristics of the volatile or tar components. Low-rank coals have generally higher yields of volatiles. Oxygen functional groups abundant in low-rank coals, especially in lignites, are evolved during pyrolysis mainly as water and carbon oxides. High-volatile bituminous coals produce large amounts of tars, 50%–80% of total weight loss, in contrast to <25% for lignites.

The maceral (organic) components of coals also influence the products of pyrolysis. The three principal maceral groups are exinite, vitrinite, and inertinite. Exinite possesses the highest hydrogen and volatile matter contents and heating value, whereas inertinite has the lowest. Vitrinite is the most abundant maceral, generally comprising 60%–95% of coal's organic matter. The total yield of pyrolysis gases increases in the order exinite > vitrinite > inertinite. Tar composition is also maceral-dependent; for example, liquids from exinite contain primarily neutral oils, whereas those from vitrinite are generally lighter and more phenolic.

Coal pyrolysis generally proceeds in two stages: primary release of volatile matter (gas and tar), followed by secondary reactions involving mainly tar cracking and carbon deposition. A similar sequence of reactions occurs during the pyrolysis of biomass. The final products are characterized by different hydrogen-to-carbon ratios, with gas and char having the highest and lowest hydrogen contents, respectively. Variations in pyrolysis conditions, such as temperature and pressure, result in different product yields and compositions. This feature renders pyrolysis an attractive coal conversion technique.

Mass Transfer, Chemical Kinetics, and Thermodynamics

Equilibrium of the Carbon–Steam–Oxygen System

The effects of temperature on gas composition at equilibrium are presented in Figure 1 for a pressure of 20 atm (294 psia) and in Figure 2 comparing 1 versus 70 atm (14.7 versus 1029 psia). At 1 atm pressure, the equilibrium concentration of hydrogen in dry nitrogen-free syngas approaches 50% at 650°C (1202°F) and then drops with increasing temperature (Figure 2). At elevated pressures, the hydrogen concentration increases with increasing temperature. Above 1000°C (1832°F), hydrogen levels off at between 35% and 40% regardless of pressure. The concentration of CO increases along with temperature to exceed the concentration of H_2 above a temperature level between 700° to 900°C (1292° to 1652°F) depending on pressure. At high temperatures above 1100°C (2012°F), representative of an EFG, CO and H_2 comprise 90% to 99% of the syngas at equilibrium (Figure 1), with the ratio of CO/H_2 increasing along with temperature from about 1.5 at 1100°C (2012°F) to 1.8 at 1500°C (2732°F). The equilibrium concentrations of CO_2 and H_2O decrease with increasing temperature to reach negligible levels above 1100°C (2012°F) (Figure 1), indicating that the steam gasification and reverse WGS reactions tend to approach completion at higher temperatures. The equilibrium curves presented here were calculated for the minimum amounts of steam and oxygen required to satisfy the energy balance and achieve 95% carbon conversion. In practice, excess steam and oxygen will always be needed to drive the reaction kinetics and compensate for heat losses. Equilibrium calculations do not precisely predict gas compositions for different types of gasifiers, but they do reflect trends relating to differences in temperature and pressure.

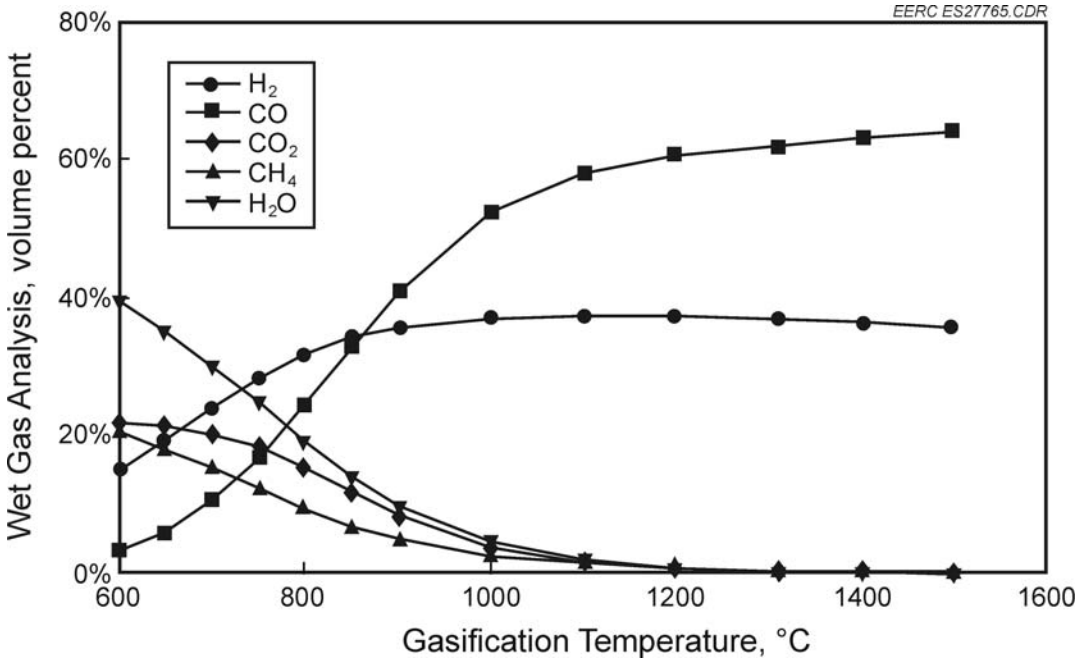

Figure 1. Effect of temperature on gas composition.

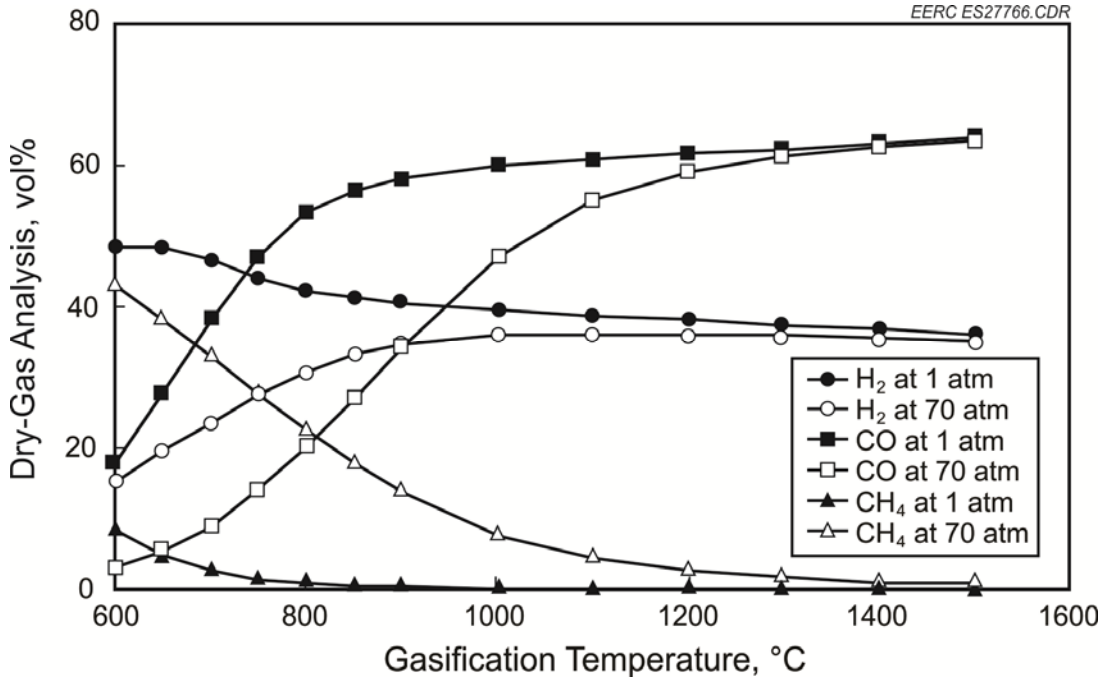

Figure 2. Effect of temperature and pressure on gas composition.

For example, low-temperature catalytic gasification processes operating in the range of 650° to 750°C (1202° to 1382°F) produce hydrogen at low pressure and methane at high pressure. High-temperature EFGs with exit gas temperatures in the range of 1040° to 1430°C (1904° to 2606°F) produce mainly CO and H_2 at ratios generally between 1:1 and 2:1, along with CO_2 in proportion to the amount of oxygen used to supply heat—which is greater for a slurry feed gasifier compared to a dry feed gasifier. Fixed-bed gasifiers with exit gas temperatures between 260° and 540°C (500° and 1004°F) and fluidized-bed gasifiers (FBGs) between 820° and 1000°C (1508° and 1832°F) produce syngas typically containing 3% to 5% CH_4 and ratios of CO to H_2 governed by the effect of excess steam on the WGS reaction.

Gasification Reaction Kinetics

Mass transfer and chemical reaction kinetics are the controlling factors determining the overall rate of gasification (3). Mass transfer is probably the dominant mechanism at temperatures above 2100°F (1149°C) where rates can be significantly improved by increasing the relative velocities of reactants and thus mixing. Below 2100°F (1149°C), the mass action effect of reactants on chemical kinetics is more pronounced, although the mixing effect remains significant. An analysis of the controlling mechanisms must consider that different reactions predominate in different zones of a gasifier. For example, combustion, steam gasification, and pyrolysis/drying occur from the bottom to the top of a fixed-bed gasifier, wherein coal is fed at the top and steam and oxygen are introduced at the bottom and pass counter currently upward through the descending bed of char.

The contributions of different chemical reactions occurring in a gasifier were recently evaluated by EERC researchers Sondreal et al. (4), using the characteristic reaction rates for lignite compiled in Table 1 from University of North Dakota (UND) researchers (5–7). For the three heterogeneous gasification reactions between gas and carbon (Reactions 1–3 in Table 1), combustion is nearly seven orders of magnitude faster than steam gasification, and steam gasification, in turn, is about two orders faster than hydrogasification. The Boudouard reaction is even slower. During partial combustion (Reaction 1 in Table 1), the relative yield of CO versus CO_2 increases along with temperature and the ratio of carbon to oxygen in the combustion zone of a gasifier (8). In a fixed-bed gasifier or FBG, where the residence time of solids is far greater than that of gas, combustion is confined to the region where oxygen is introduced, and oxygen is essentially absent outside this region. In a high-temperature EFG, where the rate of reaction for carbon particles is controlled by heat and mass transfer and the residence times of both gas and carbon particles are on the order of seconds, some oxygen will be found throughout a substantial part of the reactor volume.

The rate of steam gasification for North Dakota lignite has been estimated to be proportional to the partial pressure of steam raised to the 0.63 power, total pressure to the −0.70 power, and $(CO/CO+CO_2)^{-1.91}$, reflecting a relatively greater effect for an incremental increase in steam where steam is a small fraction of the total gas and an inhibiting effect due to the buildup of CO as a reaction product (7).

The homogeneous gas-phase Reactions 5 and 6 in Table 1 are performed industrially using mixed metal oxide/sulfide catalysts to promote the WGS conversion of CO to H_2 at temperatures below 500°C (932°F) and nickel-based catalysts to accomplish methanation at temperatures below 300°C (572°F). Even without an added catalyst, the rate of the WGS reaction is relatively rapid (Table 1), causing the gas composition exiting an FBG at between 820° and 1000°C (1508° and 1832°F) to approach the equilibrium concentration of hydrogen, which is higher when more steam is present and when the operating temperature is lower. For slurry-fed EFGs operating at higher temperatures, the hydrogen content of the product gas will increase as the gas cools through a temperature range favorable for the forward reaction of CO and steam to produce H_2. Table 1 does not include a reaction rate for methanation, but the rate can be inferred to be slower than that of the WGS reaction from the fact that the concentration of CH_4 exiting a gasifier at a moderately low temperature of 800°C (1472°F) does not begin to approach the relatively high equilibrium concentration (4).

Examples of Predicting Fuel Gas Composition for Various Gasifier Types

Predictions of fuel gas or syngas composition were made for selected gasification system types utilizing the tools developed by Sondreal et al. (4). The characteristics of the major gasifier types are summarized in Table 2, and temperature profiles are shown in Figure 3. Gasifiers are first categorized as entrained-flow, fixed-bed, or fluidized-bed systems and then further classified by their use of either dry or slurry coal feed and either dry ash or slag discharge. The selection of an optimum design depends on the effect of coal properties on the operation of the gasifier and the desired gas exit conditions in relation to downstream process conditions. The temperature, pressure, and composition of the gas leaving the gasifier should match the

Table 1. Lignite Reaction Rate Parameters[a]

		Lignite Reaction Rate Parameters[a]		Reaction Rate Constant, k[b]	
Model Reactions	Process	A	E (cal/mol)	815°C	955°C
1. $xC + yO_2 \rightarrow zCO_2 + dCO$[c]	Combustion	3.51 (10^6)	2.18 (10^4)	1.5 (10^2)	4.6 (10^2)
2. $H_2O + C \leftrightarrow CO + H_2$	Steam gasification	8.10 (10^2)	3.51 (10^4)	7.2 (10^{-5})	4.6 (10^{-4})
3. $2H_2 + C \leftrightarrow CH_4$	Hydro gasification	6.11 (10^{-3})	1.92 (10^4)	8.5 (10^{-7})	2.3 (10^{-6})
4. $H_2O + CO \leftrightarrow CO_2 + H_2$	WGS	3.23 (10^7)	1.18 (10^4)	1.4 (10^5)	2.6 (10^5)
5. $CO + 3H_2 \leftrightarrow CH_4 + H_2O$	Methanation	Observed to be slower than WGS			

[a] Table adapted from Mann et al. (7). The reaction rate parameters are from Carpenter (5) and Hossain (6).
[b] $k = A \exp(-E/RT)$.
[c] $x = z + d$, $y = z + d/2$.

requirements of the gas-cleaning and separation processes and end-use application to minimize cost and efficiency penalties associated with gas cooling, compression, and downstream processing. The properties of coals that are most important in determining the choice of a gasifier are their moisture, calcium, and sodium contents. High moisture contents limit the use of slurry feed, and high levels of sodium and calcium affect slag viscosity and the corrosion, clinkering, and deposition properties of the ash and slag as well as enhance reactivity.

Gasification Process Testing Experience at the EERC

The early efforts in the area of gasification at the EERC date back to when the laboratory began in the late 1940s on low-rank and other coals. Testing was conducted initially on the very reactive high-sodium lignitic coals. One of the first programs was on the annular externally heated retort (AEHR) conducted from 1945 to 1951. The AEHR efforts were focused on the production of fuel gas and char. The char was used for steelmaking.

The EERC conducted extensive work on slagging fixed-bed gasification of North Dakota lignite (9). Numerous tests were performed to determine the gasification potential of North Dakota lignites in slagging FBGs. The EERC operated the first slagging FBG in the United States. The pilot plant gasifier was initially operated under the Bureau of Mines during the period 1958–1965 to demonstrate the feasibility of slagging operations and assess operational parameters. Operations were resumed in 1976 to investigate the environmental concerns associated with commercial-scale, fixed-bed coal gasification facilities. In September 1978, gasifier operation was suspended for modifications and updating of the existing equipment and to expand the operational capabilities. The facilities as originally constructed were designed for gasification of noncaking coals. Experiments were generally of 8 to 12 hours in duration because of equipment and personnel limitations. Operation of the pilot plant resumed during 1980–1985.

Research on catalytic gasification was initiated at the EERC in the early 1980s and continued into the early 1990s in cooperation with a number of contract organizations to determine the feasibility of producing low-cost hydrogen from low-rank coals for various commercial applications.

Table 2. Characteristics of Major Gasifier Types

	Fixed-Bed Dry Ash	Fixed-Bed Slagging	Fluidized Bed	Transport Reactor	Entrained Slurry-Fed	Entrained Dry Feed
Commercial Units	Lurgi	BGL[1]	U-Gas KRW[2] HTW[3]	KBR[4]	GE E-Gas	Shell Prenflow Future Energy
Coal Feed System	Lock hopper	Lock hopper, stirrer for caking coal	Lock hopper	Dry rotary pressure seal and surge bin	Coal–water slurry	Lock hopper with pneumatic conveying
Ash Discharge	Dry ash	Slag	Dry ash or agglomerated	Dry ash	Slag	Slag
Coal Feed Size	2 × ¼ in.	2 × ¼ in. with some fines	−¼ in.	−1/16 in.	−100 mesh	−100 mesh
Coal Moisture Tolerance, %	35	28	10–25	25 or higher		Dried to 5–10
Gasifier Pressure, psig[5]	450	450	450	450	500–1000	450
Exit Gas Temperature, °F	500–1200	300–1200	1500–1900	1500–1900	1900–2500	2500–3000
Issues	Tars and oils in raw gas		Carbon conversion		Gas cooling load	
	Typical Conditions for Oxygen-Blown Gasifiers Operating on Low-Rank Coals					
Source	DGC[6]	EERC	Nexant (10)/ U-Gas	Southern Co./KBR	EPRI[7]/E-Gas	EPRI/Shell
Feed Coal	ND lignite	ND lignite	ND lignite	PRB subbit.	PRB subbit.	TX lignite
O/C, mol	0.35	0.72	0.65	0.4–0.6	0.88	0.93
Steam/C, mol	1.50	0.40	0.30	0–0.7	0.00	0.00
Syngas Composition, dry vol%						
H_2	39.4	29.0	29.6	36.2	39.4	28.5
CO	15.7	58.7	39.8	41.3	38.9	62.6
CH_4	10.9	5.2	8.4	3.1	0.1	0.0
CO_2	32.8	5.9	20.2	17.7	19.5	2.9

[1] British Gas-Lurgi.
[2] Kellogg Rust Westinghouse.
[3] High-temperature Winkler.
[4] Kellogg, Brown and Root.
[5] Dry feed systems can meet the pressure requirements of current-generation gas turbines of nominally 450 psi. Slurry feed systems are better suited for higher pressures that may be required for some chemical processes.
[6] Dakota Gasification Company.
[7] Electric Power Research Institute.

A research program on mild gasification was conducted from 1987 to 1995. The focus of the program was on the production of solids, liquids, and gases from coal. This research was conducted using lower-severity conditions, with a focus on producing valuable solids or char.

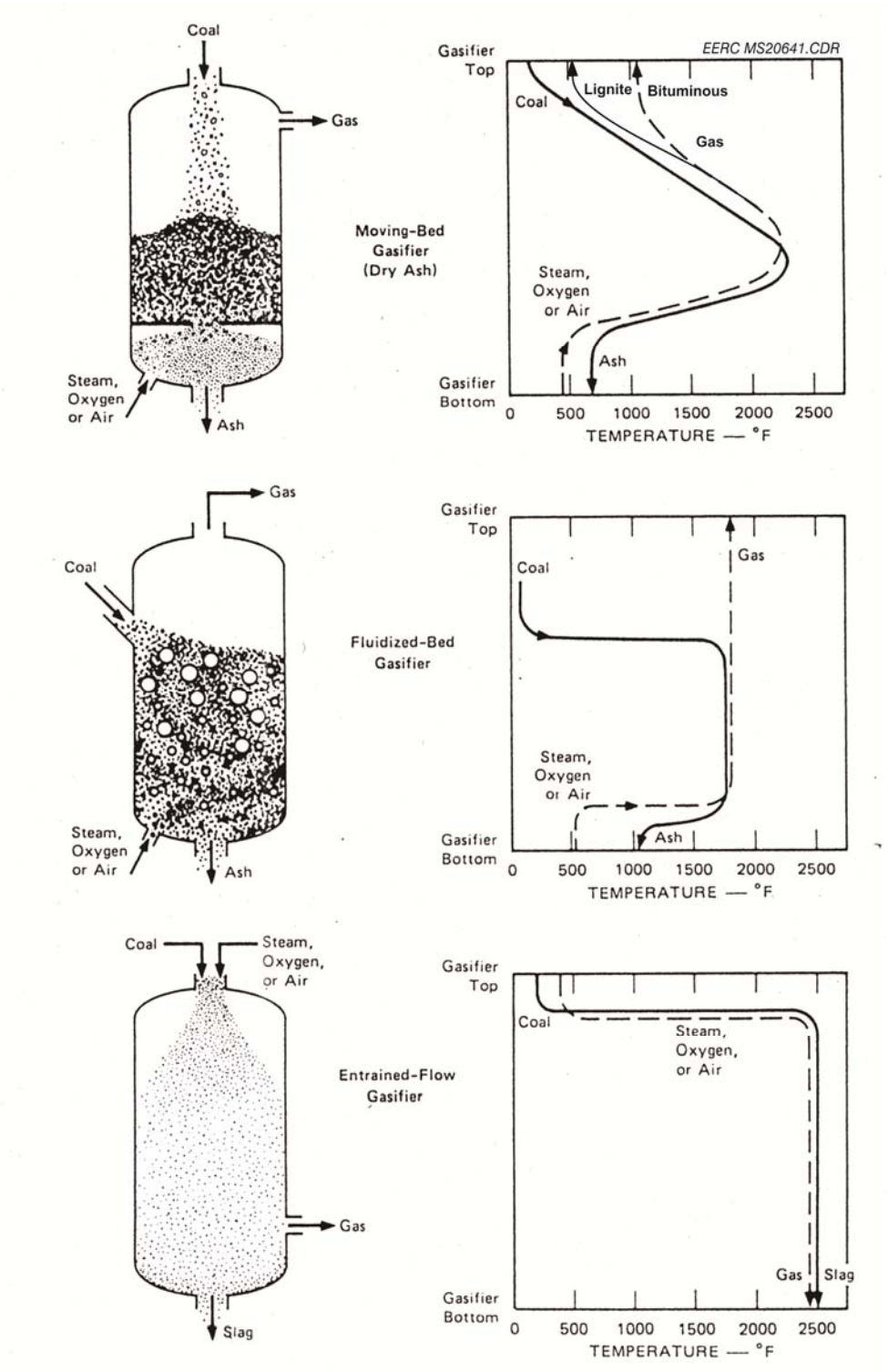

Figure 3. Three major types of gasifiers.

A TRDU, also referred to as a transport reactor integrated gasification (TRIG) system, has been under development for the past 10 years through programs conducted at the EERC and Southern Company. The EERC installed a pilot-scale KBR transport reactor, or TRIG, gasification system to conduct testing of the gasification process, gas-cleaning, and gas separation technologies. This project was supported by DOE's National Energy Technology Laboratory (NETL), Southern Company, and KBR. Since the original installation, the EERC has conducted several projects on bituminous, subbituminous, and lignite coals for industry and has continued development of the technology through funding from DOE NETL. Data from the EERC TRIG system were used to scale up the technology at the Power Systems Development Facility (PSDF) near Wilsonville, Alabama.

Hot- and warm-gas cleanup for the control of particulate and mercury has been the focus of ongoing programs at the EERC. The removal of particulate and unburned carbon has been demonstrated for several coals using the TRIG system and at the proof-of-concept-scale PSDF system. In addition, the EERC tested the use of highly reactive mercury sorbents for use at temperatures over 500°F (260°C) in gasification systems. The results of this work showed a greater than 95% removal of mercury from the warm fuel gas (11), a significant finding since the existing technology (12) required cooling the gases to less than 100°F (38°C) prior to removing mercury with presulfided activated carbon.

Overview of Gasification Impurities and Purification Technologies

Gas Cleanup for Particulate and Trace Elements Including Mercury

Hot- and warm-gas cleanup for the control of particulate and mercury has been the focus of ongoing programs at the EERC. The removal of particulate and unburned carbon has been demonstrated for several coals using the TRIG system and at the proof-of-concept-scale PSDF system. In addition, the EERC tested the use of highly reactive mercury sorbents for use at temperatures over 260°C (500°F) in gasification systems. The results of this work showed a greater than 95% removal of mercury from the warm fuel gas (11), a significant finding since the existing technology (12) requires cooling the gases to less than 38°C (100°F) prior to removing mercury with presulfided activated carbon. Cooling the gases results in a decrease in the overall efficiency of the system.

Highly Efficient Sulfur and Halogen Removal to below 1 ppm

Removal of sulfur as well as halogens is best conducted in stages to ultimately get to a near-zero level. The first step would be removal of some of the sulfur, with limestone or dolomite added to the TRIG system for bulk removal. This will remove the sulfur components down to equilibrium levels for the $CaCO_3 + H_2S = CaS + CO_2 + H_2O$ reaction, with about 20% to 30% removal occurring under the oxygen-blown conditions that would be utilized for hydrogen production. This lower sulfur removal as compared to air-blown operation is a result of the high CO_2 and H_2O partial pressures that result under oxygen-blown operation. This removal will take place with the particulate and mercury step in the gas cleanup phase. A conceptual diagram of the process is illustrated in Figure 4. The process consists of two primary steps. The

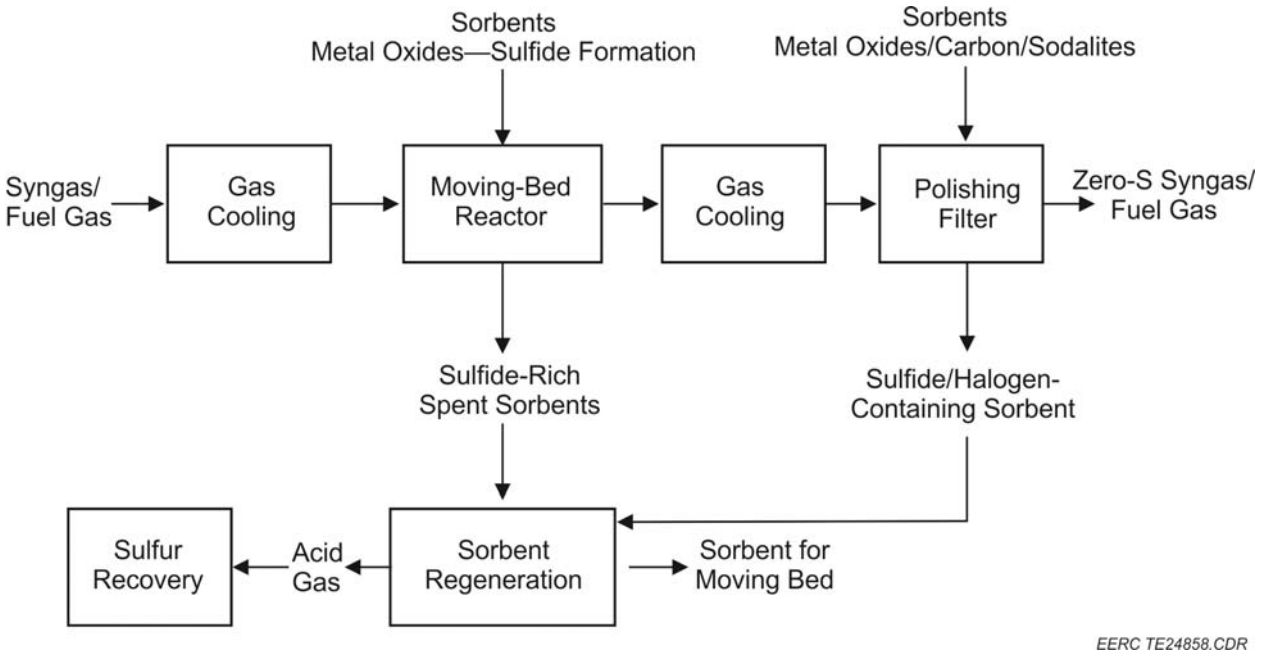

Figure 4. Sulfur removal concept for near-zero sulfur levels.

first step is to capture the sulfur in the form of sulfides through the use of selected metal oxides. Metal oxides have been used to remove sulfur species from coal-derived synthesis gas (13). These metal oxides include transition metals such as iron oxide, zinc oxide, copper oxide, and others. The components have the potential to be regenerated, and the sulfur can be recovered. The reactions of the synthesis gas or fuel gas would be conducted in either a moving-bed or fluid-bed reactor, which would reduce the level of sulfur to the 10–20-ppm range. A second step would involve using a fixed bed to reduce sulfur and other species such as halogens and, possibly, any mercury that remained. The sorbents to be injected would include metal oxides, carbons, and sodalites. Sodalites are aluminosilicate phases that have a cubo-octahedral structure that can react with sulfur and halogen species (14). These phases have been identified in various ash residual materials and offer the opportunity for use as polishing sorbents. The exiting gases would be ultrapure relative to the levels of sulfur, with concentrations of less than 1 ppm.

Carbon Dioxide Separation and Removal

The first choice for the separation of carbon dioxide would involve a higher-temperature CO_2 separation membrane. The performance of this membrane on an actual coal-derived syngas would be investigated as a part of this program. As a fallback position, the use of recently developed cold-gas CO_2 separation membranes could be tested. Data on fuel gas constituents also will be provided to suppliers of conventional cold-gas removal processes such as Rectisol® or an amine scrubber for their evaluation as a possible process. The cold CO_2 removal step would probably then be conducted after the hydrogen separation step, shown above, in order to obtain higher efficiencies from the TRIG process's thermal energy.

Hydrogen Recovery

Once the sulfur has been removed from the gases, the technologies of the production of ultrapure hydrogen streams can be tested. These include higher-temperature palladium-based membranes that are capable of providing 99.9+% hydrogen purity. Some palladium-based membranes such as Pd–Cu are also capable of tolerating some sulfur, potentially reducing the amount of sulfur removal necessary and possibly even eliminating the polishing filter.

Hydrogen Separation Membranes and Integration with Warm-Gas Cleanup

Why Hydrogen

DOE views hydrogen as an energy carrier of the future because it can be derived from domestic resources that are clean and abundant and because hydrogen is an inherently clean fuel. According to DOE, the deployment of hydrogen technologies could lead to the creation of 675,000 green jobs in the United States (15). Coal gasification plants can separate hydrogen from the synthesis gas, purify the carbon for storage, and burn the hydrogen to produce power in an integrated gasification combined cycle (IGCC) configuration. In this type of configuration, the only major emission from the plant is water. Hydrogen can also play a key role as a transportation fuel. If all vehicles in Los Angeles were converted to hydrogen, the urban smog problems would be virtually eliminated. Hydrogen fuel cell technologies have undergone rapid development over the past decade, and the technology exists today to produce commercial hydrogen fuel cell vehicles that have a transportation range of up to 280 miles (16). The main challenges that remain today are the economical production of hydrogen; economical production of fuel cell vehicles; and development of hydrogen transportation, storage, and dispensing infrastructure.

The National Hydrogen Association views hydrogen as the best pathway to both reduce the oil consumption in the United States and reduce transportation-based CO_2 emissions. Figure 5 compares three different vehicle market penetration scenarios for light-duty vehicles (17). The bar on the left represents 100% gasoline internal combustion engine vehicles (ICEVs), the middle bar represents market penetration for plug-in hybrid electric vehicles (PHEVs), and the bar on the right represents hydrogen fuel cell vehicles. Each scenario is compared to the annual oil consumption for that time period. It can be seen that if nothing changes and the United States continues to rely solely on gasoline-powered vehicles, the annual oil consumption is predicted to increase from 4 billion barrels a year (bby) to over 7 bby by the year 2100. With a significant market penetration of PHEV, oil consumption can be reduced to about 2.5 bby by 2100. However, with 98% market penetration of fuel cell vehicles, dependence on oil is virtually eliminated. While the future of transportation will certainly be a mix of several technologies, this graph illustrates that hydrogen is one of the only pathways toward eliminating the use of oil.

Figure 6 shows a similar set of scenarios, but compares the market penetration with annual CO_2 emissions from vehicles (17). It should be noted that the study assumes hydrogen production is occurring with carbon capture and storage or hydrogen supplied from a renewable source. The graph shows that carbon dioxide emissions from vehicles will almost double by the

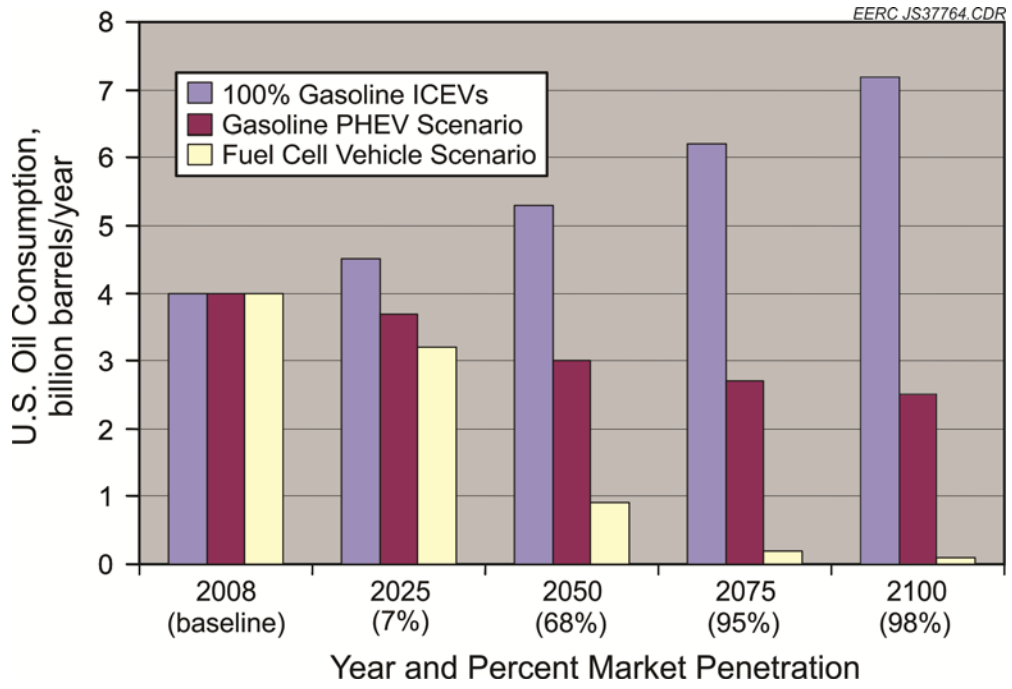

Figure 5. U.S. oil consumption for various vehicle scenarios (17).

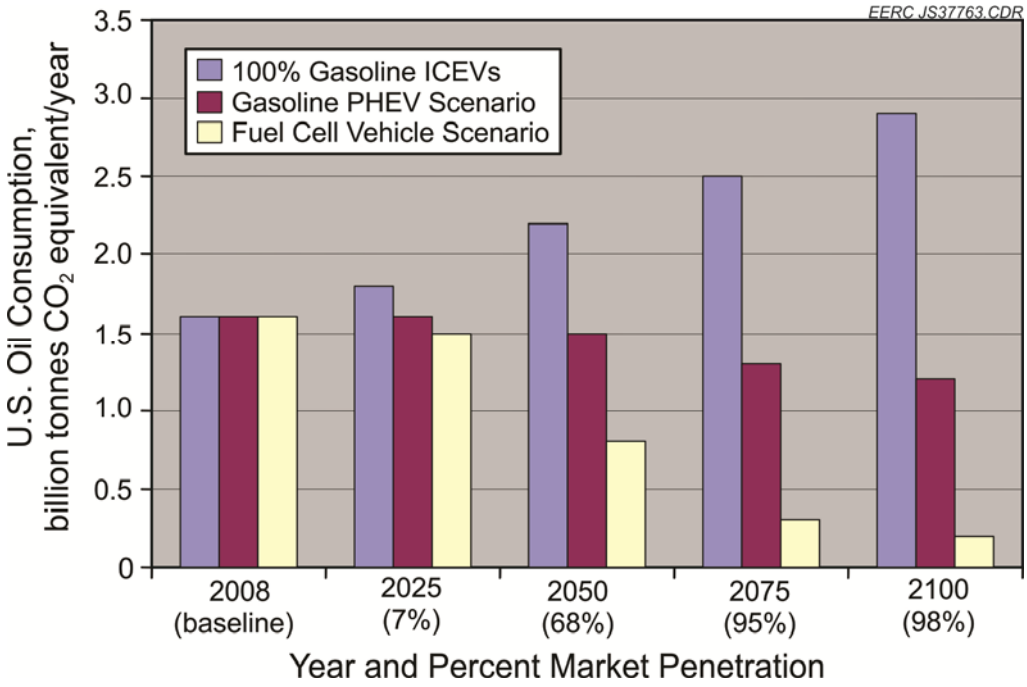

Figure 6. Carbon dioxide emissions for various vehicle scenarios (17).

year 2100 if gasoline vehicles continue to be used exclusively. A reduction in CO_2 emissions is achieved if the course of the PHEV is followed. However, with the fuel cell vehicle scenario, CO_2 emissions are reduced by over 80% in the year 2100. This illustrates that hydrogen is a potential fuel pathway in a carbon-constrained world.

Coal Gasification Fundamentals

Coal gasification is a process in which coal is reacted at temperature and pressure with steam and oxygen to form H_2 and CO. Pressures can range from atmospheric to 1200 psi, and temperatures can range from about 649°C to over 1480°C (1200° to over 2700°F). Besides the typically desired products, H_2 and CO, many other by-products are formed during gasification, such as CO_2, N_2, CH_4, H_2S, COS, HCl, NH_3, higher hydrocarbons, tars and oils, and particulate matter. The biggest challenge with any gasification system is dealing with the inorganic components in the coal and matching gasifier design to fuel-specific properties and desired end products. Gasifiers are typically configured as fixed beds, fluidized beds, moving beds, or entrained flow. Each gasifier type has strengths and weaknesses depending on the fuel used and the desired end products.

Coal gasification has taken on a renewed interest in the last 5 years because of the rising price of oil and pending carbon legislation. Historically, studies have shown that if carbon capture and storage are required, IGCC plants will have a significant cost advantage over conventional pulverized coal boilers with retrofit carbon capture (4, 18). However, the most recent studies to come out have stated that the costs may be similar between the two technologies, especially when considering ultrasupercritical boilers (18–20). At this point, it is difficult to accurately estimate the cost of carbon capture from a pulverized coal power plant because no commercially available technology exists. Therefore, these studies must be reevaluated once technologies are commercially available.

Gas Cleanup Fundamentals

Conventionally, cold-gas cleanup methods have been employed to remove contaminants from coal gasification syngas streams. Methods such as Rectisol or Selexol® are commercially available and do a very good job removing contaminants but are also very costly from capital and operational perspectives. Significant economic benefits can be realized by utilizing warm- or hot-gas-cleaning techniques. DOE has stated thermal efficiency increases of 8% over conventional techniques can be realized by integrating warm-gas cleanup technologies (21) into IGCC plants. Hydrogen separation membranes typically operate at warm-gas cleanup temperatures, so they are a good match for IGCC projects looking to employ warm-gas cleanup and carbon capture.

Conventional Hydrogen Separation Processes

The most commonly employed method used today for hydrogen separation is a pressure swing adsorption (PSA). PSA technology is based on an adsorbent bed that captures the impurities in the syngas stream at higher pressure and then releases the impurities at low pressure. Multiple beds are utilized simultaneously so that a continuous stream of hydrogen may be produced. This technology can produce hydrogen with a purity greater than 99.9% (22).

Temperature swing adsorption is a variation on PSA, but it is not widely used because of the relatively long time it takes to heat and cool sorbents. Electrical swing adsorption has been proposed as well but is currently in the development stage. Cryogenic processes also exist to purify hydrogen but require extremely low temperatures and are, therefore, very expensive (23).

Principles of Hydrogen Separation Membranes

Most hydrogen separation membranes operate on the principle that only hydrogen can penetrate through the membrane because of the inherent properties of the material. The mechanism for hydrogen penetration through the membrane depends on the type of membrane in question. Most membranes rely on the partial pressure of hydrogen in the feed stream as the driving force for permeation, which is balanced with the partial pressure of hydrogen in the permeate stream. Kluiters has categorized membranes into five main types that are commercial or appear to have commercial promise: dense polymer, microporous ceramic, porous carbon, dense metallic, and dense ceramic (24). Each membrane type has advantages and disadvantages, and research organizations and companies continue to work to develop better versions of each. Figure 7 illustrates the basic operating principles of hydrogen separation membranes for use in coal-derived syngas. Figure 7 shows a tubular membrane, but plate and frame-style membranes have also been developed. The "syngas in" stream refers to the feed gas into the membrane module. The permeate stream has permeated through the membrane wall and, in this case, is made up of mostly hydrogen. The raffinate stream is what is left of the feed stream once the permeate is separated. A sweep gas such as nitrogen may be used on the permeate side to lower the partial pressure and enable more hydrogen to permeate the membrane.

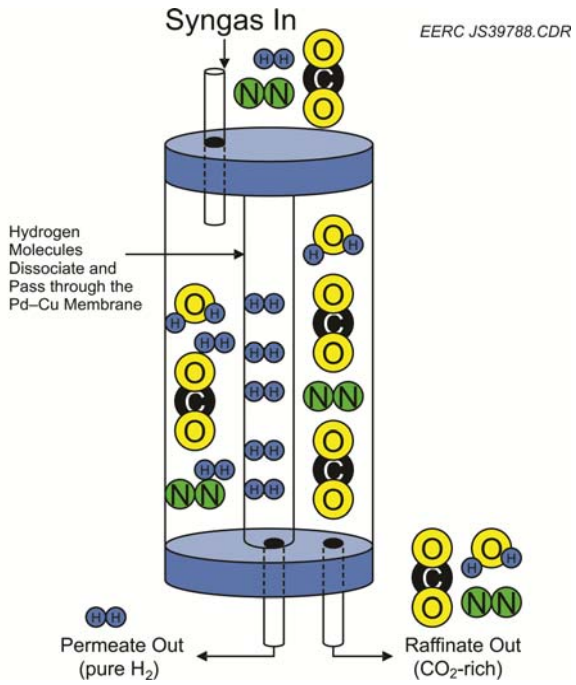

Figure 7. Illustration of the operating principle of hydrogen separation membranes (25).

The mechanisms for hydrogen transport through each membrane type are different. However, the performance of each membrane is gauged by two main principles: hydrogen selectivity and hydrogen flux. Hydrogen selectivity is defined by Equation 1 (24):

$$\alpha_{A/B} = \frac{y_A / y_B}{x_A / x_B} \quad \text{[Eq. 1]}$$

Where α is the selectivity factor of Component A over Component B in the mixture, y_A and y_B are the fractions of those components in the permeate, and x_A and x_B are the fractions of those components in the feed. Components A and B are usually defined so that a higher selectivity factor refers to better membrane performance. A selectivity factor of 1 means there is no component separation.

Hydrogen flux is a measure of the rate of permeation of hydrogen through a membrane wall. The general equation for flux is shown by Equation 2 (23, 24):

$$J_x = \frac{P(p^n_{x,\,feed} - p^n_{x,\,permeate})}{t} \quad \text{[Eq. 2]}$$

Where J_x represents the flux of species x, P_x represents the permeability of species x, $p_{x,feed}$ and $p_{x,permeate}$ are the partial pressures of species x in the feed and permeate streams, t is the membrane thickness, and n is the partial pressure exponent. The value of n is usually between 0.5 and 2 and, like the value of P, depends on the transport mechanism assumed. When n = 1, the equation is called Fick's law. For hydrogen transport through a metal membrane, the value of n is usually 0.5, and the equation reduces to what is referred to as Sievert's law. Sievert's law is a useful way of measuring membrane performance because it takes into account the membrane thickness and the partial pressure of hydrogen on each side of the membrane.

Since most membranes operate on a partial pressure differential, there will always be some hydrogen left behind in the raffinate stream. Therefore, an additional measurement of performance is the recovery or yield as shown by Equation 3:

$$S = \frac{q_p}{q_f} \quad \text{[Eq. 3]}$$

Where S is the yield, q_p is the permeate flow, and q_f is the feed flow. There are numerous other ways to quantify the yield, including calculating the volume reduction in the raffinate or the percentage hydrogen recovery from the feed.

The five basic types of membranes mentioned earlier each have inherent advantages and disadvantages, depending on the desired operating conditions and necessary product specifications. With data presented by Kluiters (24) and modified with Adhikari and Fernando

(23) and Ockwig and Nenoff (26), Table 3 compares, in general, the relative operational performance of these five membrane types. Typical operational temperature will vary by specific membrane type, but it can be seen that the dense polymer membranes are only applicable at low temperature. Dense ceramic and dense metallic membranes have the highest hydrogen selectivity, and hydrogen flux is highest for dense metallic or microporous ceramic membranes. While dense metallic membranes seem to have the best performance relative to hydrogen, they are also very susceptible to poisoning from many compounds found in syngas, and palladium alloys are very expensive. Dense ceramic membranes also have high potential for commercial applications. They are less susceptible to poisoning than metallic membranes and, depending on the material, can be much more inexpensive. Development work is under way with each of these membrane types to increase the resistance to poisoning and reduce cost.

For porous membranes, four types of diffusion mechanisms can affect hydrogen separation: Knudsen diffusion, surface diffusion, capillary condensation, and molecular sieving. Knudsen diffusion occurs when the Knudsen number, Kn, defined by Equation 4, is high.

$$Kn = \frac{\lambda}{L} \qquad \text{[Eq. 4]}$$

The variable λ in Equation 4 represents the mean free path of the gas molecules, and L is the pore radius. At Knudsen numbers greater than 10, Knudsen diffusion becomes significant. Surface diffusion refers to gas molecules that are absorbed on the pore wall and migrate along the surface to the other side. Surface and Knudsen diffusion can occur simultaneously. Capillary condensation occurs if a partially condensed phase fills the pores and does not let other molecules penetrate. Molecular sieving occurs when the pores are so small that only the smaller molecules can fit through. Selectivity toward hydrogen is greatest with molecular sieving and is least with the Knudsen diffusion mechanism.

Table 3. Properties of Five Hydrogen Selective Membranes (23, 24, 26)

	Dense Polymer	Microporous Ceramic	Dense Ceramic	Porous Carbon	Dense Metallic
Temperature Range	<100°C	200°–600°C	600°–900°C	500°–900°C	300°–600°C
H_2 Selectivity	Low	Moderate	Very high	Low	Very high
H_2 Flux	Low	High	Moderate	Moderate	High
Known Poisoning Issues	HCl, SO_x, CO_2		H_2S	Strong vapors, organics	H_2S, HCl, CO
Example Materials	Polymers	Silica, alumina, zirconia, titania, zeolites	$SrCeO_{3-\delta}$, $BaCeO_{3-\delta}$	Carbon	Palladium alloys, Pd–Cu, Pd–Au
Transport Mechanism	Solution/diffusion	Molecular sieving	Solution/diffusion	Surface diffusion, molecular sieving	Solution/diffusion

The solution–diffusion mechanism is somewhat more complex than the diffusion mechanisms, although relatively straightforward in nature. Ockwig and Nenoff (26) presented a seven-step mechanism in which 1) the hydrogen mixture moves to the surface of the membrane; 2) the H_2 molecules dissociate into H^+ ions and electrons; 3) the ions adsorb into the membrane bulk; 4) the H^+ ions diffuse through the membrane; 5) the H^+ ions desorb from the membrane; 6) the H^+ ions and electrons recombine back to H_2 molecules; and 7) the H_2 diffuses from the surface of the membrane. In the case of metal membranes, only hydrogen undergoes the solution–diffusion mechanism; therefore, the membranes are considered 100% selective to hydrogen.

Current Development Activities

DOE has developed a set of performance goals based on some of the measurement equations listed in this report. These goals are listed in Table 4 (27). In order to meet these goals, membranes will have to be developed that have high hydrogen flux and selectivity and are durable to the contaminants found in coal-derived syngas.

Many companies and organizations are actively researching new hydrogen separation materials that have the potential to meet the performance goals as laid out by DOE. This section describes several membranes currently under development and discusses the pros and cons of each. Comparisons are also made to the current DOE targets.

DOE, through NETL, has developed a comprehensive program on hydrogen membrane research. NETL is performing in-house laboratory-scale research on hydrogen separation materials and is mainly focused on metallic membranes. NETL is also cofunding basic membrane research activities with numerous other companies and organizations, including (but not limited to) Argonne National Laboratory; REB Research and Consulting; Eltron Research; Southwest Research Institute; the EERC; Ohio State University; Media and Process Technology, Inc; Praxair, Inc.; United Technologies Research Center; WRI; Worcester Polytechnic Institute; Lehigh University; and Carnegie Mellon University. Most of the companies listed are performing basic research on material types and testing these materials in the laboratory under

Table 4. DOE Technical Targets for Hydrogen Separation Membranes (27)

Performance Criteria	Units	2010 Target	2015 Target
Flux, 100 psi dP basis	$ft^3/hour/ft^2$	200	300
Temperature	°C	300–600	250–500
Sulfur Tolerance	ppmv	20	>100
Cost	$\$/ft^2$	100	<100
WGS Activity	–	Yes	Yes
ΔP Operating Capability	psi	Up to 400	Up to 800 to 1000
CO Tolerance	–	Yes	Yes
Hydrogen Purity	%	99.5%	99.99%
Stability/Durability	years	3	5

simulated syngas conditions. Of the membrane developers listed, the membranes with the most potential were provided by Eltron Research, Praxair, and United Technologies Research Center (28).

In-house research at NETL is focused on membrane-screening test units that can quickly establish capacity for hydrogen separation and hydrogen membrane test units that expose the material to simulated syngas. One of the reactor systems is focused on sulfur-laden gas streams and can evaluate the membrane's performance with exposure to sulfur-laden gases. Testing at NETL has shown that a Pd foil can withstand some exposure to H_2S, but flux is reduced quickly, and a slow deactivation is noted during the test period. By contrast, exposure of a Pd–Cu alloy to the same syngas shows almost immediate, irreversible deactivation (29). A wide variety of additional alloys continues to be evaluated at NETL to determine which perform the best in the presence of sulfur. Some alloys have been identified through these studies that show almost no performance loss in the presence of sulfur (30).

Summary of Results of Year 5 Activity 1.12 – Hydrogen Separation Tests

The EERC acquired three hydrogen separation membranes as part of Year 5 Activity 1.12 test activities and ran them using syngas from small pilot-scale EERC gasifiers. A total of six separate test weeks was completed on two gasifiers. The performance of the membranes was evaluated as a function of time over the course of the testing.

Test Run Summary

Overall, approximately 331 hours of run time was accomplished on the gasifiers during the test campaign. With the simultaneous membrane skid capable of testing up to three membranes at once, an estimated 836 membrane-hours was accomplished during the program. On the fluid bed, 665 membrane-hours was accomplished, and 171 membrane-hours was completed on the EFG. Full stream (FS) membrane was exposed to syngas for 331 hours. SS1 membrane was exposed for 328 hours, and SS2 membrane was exposed for approximately 177 hours. Table 5 summarizes each of the test runs.

Table 5. Hydrogen Separation Membrane Run Summary

Run	Start Date	End Date	Membrane Run, hr	Membrane Run	Notes
FBG012	12/13/2010	12/17/2010	46	3	First shakedown run
EFG031	1/3/2011	1/4/2011	3	1	Gasifier plugged
EFG032	1/10/2011	1/13/2011	56	3	Shutdown after 3 days because of plugging
FBG013	1/24/2011	1/28/2011	75	3	Intermittent shutdowns
FBG014	1/31/2011	2/4/2011	67	2	Intermittent shutdowns
FBG015	2/14/2011	2/18/2011	84	2	Ran well

Hydrogen Purity

Figure 8 shows hydrogen purity from the permeate side of each membrane throughout the test campaign. FS membrane had very high hydrogen purity during the initial weeks of the test period, with purities over 99.99%. The purity dropped off in Week 5 because of a leak in the membrane. The leak rate increased substantially in Week 6 and led to lower-purity hydrogen in the permeate. SS1 membrane also showed high purity, achieving 99.2% purity. Purity dropped off slightly during the week, with a potential leak noticed in Week 5 and a substantial leak found in Week 6. SS2 membrane did not achieve high hydrogen purity during the test run, but the hydrogen purity did improve through the course of the testing. The highest purity achieved was 60%.

Flux and Partial Pressure Differential

Figure 9 shows the performance of the FS membrane throughout the course of the run and compares it to the partial pressure differential of hydrogen for each point on the graph. The highest flux was achieved during the January EFG runs, despite the fact that partial pressure differential was higher for some of the membrane test runs later in the campaign. Also, a leak developed later in the test campaign that should have worked to increase flux for two reasons: 1) hydrogen is bypassing the membrane and penetrating to the permeate side through the leak and 2) the other syngas components leaking through the membrane act as a sweep gas to increase partial pressure differential across the membrane. Even with the leak and the increased partial pressure, flux was decreased from where it was earlier in the test campaign. This indicates that

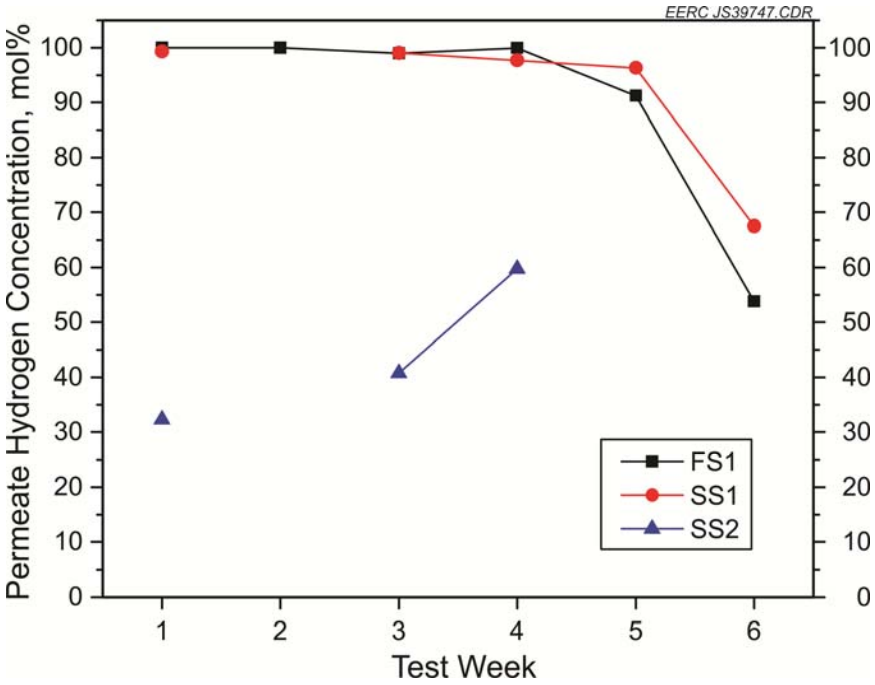

Figure 8. Membrane hydrogen permeate concentrations for each test week.

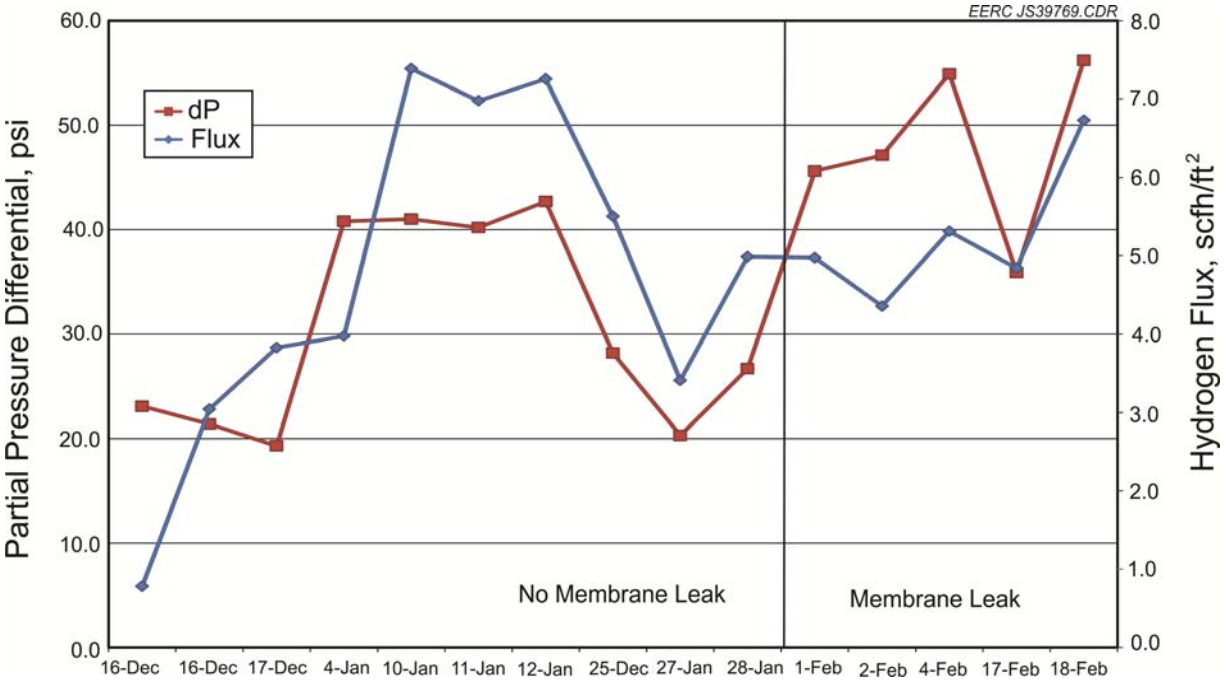

Figure 9. Hydrogen flux across the FS membrane during the test campaign.

there may have been some performance degradation because of syngas contaminants, but more investigation would be necessary to verify.

Figure 10 shows the hydrogen flux across SS1 membrane during the test campaign and compares to partial pressure differential. The one problem with this graph is that measurements earlier in the test campaign were performed with the gas meter, and later measurements were made with the Gilibrator. The gas meter measurements do show a correlation with partial pressure differential, even if the absolute value is not correct. With the Gilibrator measurements, the run during the first week of February actually showed decreasing flux with increasing partial pressure differential. The run the next week indicated increasing flux with increasing partial pressure differential. Unfortunately, the membrane also had a significant leak during this run, and the flux increase with increasing pressure could be attributed to the leak. These data might suggest some degradation because of contamination, but more investigation is required. It should be noted that the absolute value of the flux measurements was significantly higher on this membrane than on FS membrane or SS2 membrane.

Figure 11 shows the hydrogen flux across SS2 membrane during the test runs when it was online. The gas meter was not capable of accurately measuring permeate flow for this membrane, but there does seem to be a flux increase with increasing partial pressure early in the week. Measurements made during the week of January 24 with the Gilibrator seem to indicate increasing flux with increasing partial pressure differential. There is no indication that contamination is having an impact on flux rates, but more data points would be needed to verify

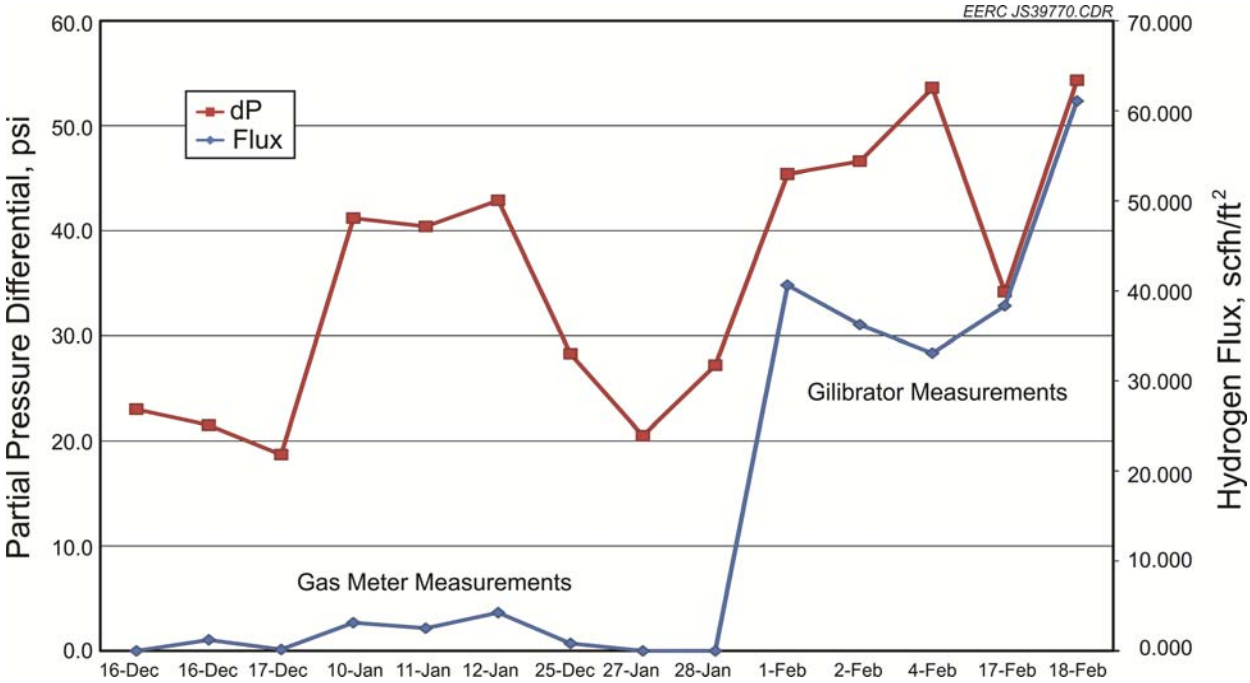

Figure 10. Hydrogen flux across SS1 membrane during the test campaign.

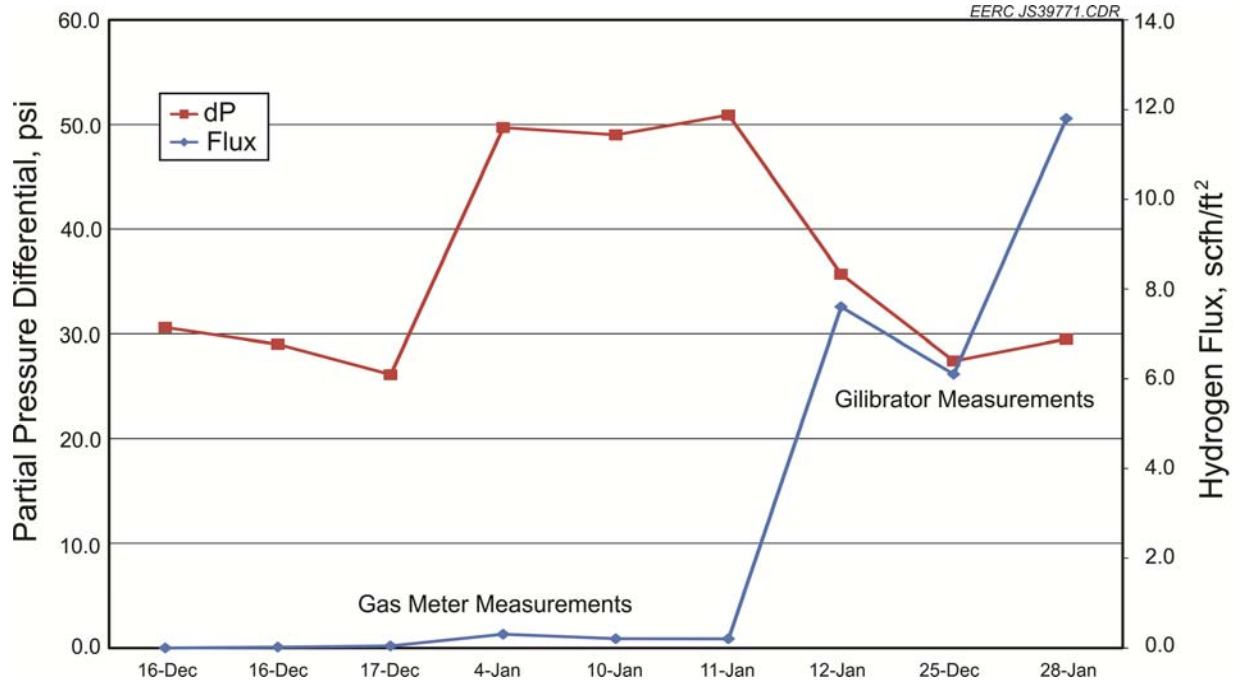

Figure 11. Hydrogen flux across SS2 membrane during the test campaign.

this. The best performance for this membrane was observed at the end of the test campaign, but a significant leak was still observed.

Sievert's Law and Performance vs. DOE Targets

The highest partial pressure differential achieved during the test program was 56 psi. This is well short of the DOE evaluation criteria of 100 psi. Therefore, Sievert's law was used to calculate the theoretical flux rate for the membranes at a partial pressure differential of 100 psi. Permeability for each membrane was calculated using the available data, and then that value was used in Sievert's law at 100 psi differential pressure. Table 6 shows the calculated values for each membrane. Only data derived from the Gilibrator measurements are presented for the slipstream membranes. The maximum flux achieved by the FS membrane was 21.4 scfh/ft^2, and this was during the time period that the membrane did not have a leak. Much lower hydrogen flux was observed when the membrane had a leak, indicating that the membrane material may have been poisoned to some degree during the test campaign.

SS1 membrane achieved much higher flux rates at 131 scfh/ft^2, but this was also when the membrane was thought to have a leak. A flux rate of 117 scfh was achieved when the membrane had no leak. SS2 membrane achieved 29.4 scfh/ft^2, but hydrogen purity was only about 60%.

Table 7 shows the DOE goals for membrane development in 2010 and 2015 and then evaluates the performance of the membranes in this test program versus those targets. It should be noted that this comparison represents the results found in this program only and does not represent other tests that have occurred on these membranes. All three membranes were below

Table 6. Calculated Expected Membrane Flux at 100 psid Using Sievert's Law

	Expected Flux @ 100 psid, scfh/ft^2		
Date	FS Membrane	SS1 Membrane	SS2 Membrane
16-Dec	3.5		
16-Dec	14.8		
17-Dec	20.1		
3-Jan	11.5		
10-Jan	21.3		
11-Jan	20.7		
12-Jan	20.3		
25-Jan	21.4		20.6
27-Jan	17.3	117.5	20.5
28-Jan	18.5	112.8	29.4
1-Feb	12.9	105.9	
2-Feb	11.1	93.6	
4-Feb	12.1	78.1	
17-Feb	13.4	115.0	
18-Feb	13.6	131.3	

Table 7. Membrane Performance in This Test Campaign vs. DOE Targets

Performance Criteria	Units	2010 Target	2015 Target	FS Membrane	SS1 Membrane	SS2 Membrane
Flux (100 psi dP basis)	$ft^3/(hour*ft^2)$	200	300	21.3	117	29.4
Temperature	°F	572–1112	482–932	650	750	900
S Tolerance	ppmv	20	>100	ND	ND	ND
Cost	$/ft^2$	100	<100	ND	ND	ND
WGS Activity	–	Yes	Yes	ND	ND	ND
ΔP Operating Capability	psi	Up to 400	Up to 800 to 1000	600	300	200
Carbon Monoxide Tolerance	–	Yes	Yes	Yes	Yes	Yes
Hydrogen Purity	%	99.5%	99.99%	99.99	99.2	59.7
Stability/Durability	Years	3	5	ND	ND	ND

Meets DOE 2015 goal.
Meets DOE 2010 goal.
Under DOE 2010 goal.

the 2010 target for flux rates, although SS1 membrane came the closest to hitting 200 $scfh/ft^2$. All three membranes were operated below the 2015 target temperature. Sulfur tolerance was not able to be specifically determined as part of this test campaign, because sulfur was kept well below 1 ppm for the duration of the testing. Undoubtedly, small levels of sulfur reached the membranes, and they will be evaluated for sulfur poisoning in the postmortem analysis that is being conducted by the providers. Cost of the small separators is also not relevant to commercial-scale operations, and cost numbers were not provided by the membrane producers. The membranes did not appear to provide significant WGS activity, but this was difficult to determine in this test program because in order to achieve the highest possible partial pressure differential, the syngas was shifted as far as possible before hydrogen separation.

FS membrane met the 2010 goal for differential pressure operation capability according to the specifications, even though it was not tested that high in this program. The others were rated far below the specification. The membranes all appeared to have CO tolerance, since none of them completely deactivated, with approximately 2% CO in the syngas during the test program. FS membrane met the purity goal of 99.99% for the DOE 2015 target. SS1 membrane came close to the DOE 2010 goal with 99.2% purity. SS2 membrane probably had a significant leak and did not meet the purity goals.

The stability and durability of the membranes are difficult to determine because of the relatively short test periods that were run. FS membrane seemed to experience a reduction in flux toward the end of the program. Both FS and SS1 membrane appeared to develop a significant leak during the course of the testing. All three membranes will have to be evaluated postmortem to understand if the leaks were developed in the membrane material, membrane joints, or fittings.

It is possible that the leaks developed in the fittings from the heat-up and cooldown experience through the test program and not in the membrane material.

Future Research Needs

Many good membrane candidates have been found through the DOE program. Additional laboratory-scale testing needs to occur to establish baseline durability and improvements in hydrogen flux. If operation with a coal gasification system is desired, long-term testing on coal-derived syngas must occur to understand the impacts of trace impurities over the life of the membranes. Additional materials development will also occur to find even better candidates for hydrogen separation, but some of today's materials are promising enough to move to commercial scale-up.

The next step for several of these membranes is testing on a bench- or pilot-scale coal gasification unit, where the syngas is cleaned to levels that would mimic a typical commercial-scale gasification operation. Successful demonstration at the pilot scale would include demonstrating that high hydrogen flux can be maintained over long durations, little or no performance degradation due to impurities, high hydrogen recovery rates, and low operating cost. Membranes that successfully meet these criteria and the 2015 criteria listed by DOE may be candidates for scale-up to a demonstration-scale facility, followed by potential inclusion in an advanced gasification or IGCC-style facility.

RESULTS AND DISCUSSION

The results section is divided into four main sections. The first section describes the test plan and equipment that was required and constructed for the project. The TRDU test results are presented next, followed by membrane test results. First, the coal properties are detailed, followed by the test plan and gasifier operating conditions. Then the gas analysis, carbon conversion, and other relevant operational parameters are provided, followed by an evaluation of the membrane performance. Additional detailed analyses are presented where further discussion is warranted.

Fuel Acquisition and Test Plan Development

WRI's proprietary patent-pending coal-upgrading/gasification process is a promising technology for conversion of upgraded low-rank, high-moisture fuels to syngas via various proprietary operational modifications to gasification technologies. WRI is providing funding for the test runs through the State of Wyoming's Clean Coal Technologies Research Program and the North Dakota Industrial Commission. This proprietary coal-upgrading/gasification process has been shown to significantly reduce moisture and certain volatile metals in the fuel and enhance gasification performance with a fluidized-bed gasifier. Warm-gas cleanup techniques have been shown to improve the economics of coal gasification plants, and since mercury is challenging to remove from syngas at elevated temperatures, any technology that can remove it before gasification is beneficial.

Two coal types were used in this testing—a PRB coal from Wyoming and a lignite from North Dakota. Each of the fuels was acquired from WRI's coal-drying and upgrading process. Three fuel conditions were then sent to the EERC for each coal type: raw (or run of mine), dried, and upgraded. This resulted in six total fuel types to be tested at the EERC. Each fuel was shipped in Super sacks and then put in nitrogen-purged bunkers just prior to fuel preparation. The fuels were sized to approximately 10 mesh and placed in nurse hoppers in preparation for feed into the TRDU.

The test plan for evaluating each fuel was developed jointly between WRI and the EERC. WRI provided the primary input for the types of tests to be run on the system following the nature of the upgraded coals and the proprietary gasifier operational modifications, and the EERC developed the operational plan and gasifier set points. An overview of the test plan is shown in Table 8. The basic plan for the test run was to first evaluate the performance of each of the fuels on the TRDU and then to conclude the run with test conditions that maximize the hydrogen content, thereby optimizing the hydrogen separation membrane performance. The testing started with TRDU heat-up which is denoted as Test 1. Then the PRB fuel was run next, starting with the raw, then moving to the dried and treated. Two temperatures were tested for each fuel type run, 1650° and 1850°F. The lignite coal was tested after the PRB, with the raw, dried, and treated tested sequentially. In Test 8, steam and oxygen inputs were optimized to produce a high-hydrogen syngas for testing on the separation membranes. However, the membranes were online for all of the test conditions.

TRDU Description

The EERC TRDU has an operating gas temperature of up to 1040°C, a nominal gas flow rate of 400 scfm, and an operating pressure of approximately 120 psig.

The coal/biomass is first crushed to less than 2 inches and then ground to a 400-µm mass mean diameter in a coal pulverizer. The coal is then loaded into "nurse hoppers" where they are placed over a bin for feeding into the drag chain conveyer. The drag chain conveyor then conveys the coal to the fuel feed lock hopper system.

The TRDU, as shown in Figure 12, consists of a riser reactor with an expanded mixing zone at the bottom, a disengager, a primary cyclone, a standpipe (SP), and a dipleg. The loop seal is not shown on the figure and is located where the dipleg makes a bend toward the SP. The SP collects solids from the disengager and is connected to the mixing section of the riser by an L-valve transfer line that utilizes steam to move the solids back to the mixing zone. Additional solids are collected by the primary cyclone into the dipleg that returns these solids into the SP through a seal leg. All of the components in the system are refractory-lined and designed mechanically for a maximum pressure of 150 psig and a maximum internal temperature of 1040°C.

The coal feed can be admitted to the transport reactor through a nozzle located near the top of the mixing zone. Coal is fed through a pressurized lock hopper feeder. A commercial system would use a different feed system but the same lock hopper concept. The feeder has two parallel

Table 8. Planned Test Matrix for the TRDU

	Time Duration, hr	Total Time, hr	Fuel	Mix Zone Temp., °F	Coal Feed, lb/hr	Comment
Test 1	6	6	PRB –as received	1550	140	TRDU start-up
Test 2a	12	18	PRB – as received	1850	360	Parametric fuel evaluation
Test 2b	12	30	PRB – as received	1650	360	Parametric fuel evaluation
Test 3a	12	42	PRB – dried	1650	290	Parametric fuel evaluation
Test 3b	11	53	PRB – dried	1850	290	Parametric fuel evaluation
Test 4a	9	62	PRB – treated	1850	270	Parametric fuel evaluation
Test 4b	9	71	PRB – treated	1650	270	Parametric fuel evaluation
Test 5a	12	83	Lignite – as received	1650	445	Parametric fuel evaluation
Test 5b	12	95	Lignite – as received	1850	445	Parametric fuel evaluation
Test 6a	11	106	Lignite – dried	1850	320	Parametric fuel evaluation
Test 6b	10	116	Lignite – dried	1650	320	Parametric fuel evaluation
Test 7a	9	125	Lignite – treated	1650	300	Parametric fuel evaluation
Test 7b	8	133	Lignite – treated	1850	300	Parametric fuel evaluation
Test 8	28	161	PRB – as received	1700	360	Optimization for membranes
Test 9	4	165	PRB	1550	100	TRDU shutdown

lock hoppers, with one feeding and the other depressurizing, filling, being pressurized, and in standby mode. During operation of the TRIG, the coal feed is measured by an rpm-controlled metering auger and microwave-based solids flow indicator.

Oxygen is fed through three nozzles into the mixing zone. Hot solids from the SP are circulated into the mixing zone where they contact the nitrogen and the steam being injected into the L-valve. This feature enables spent char to contact steam prior to the fresh coal feed. This staged gasification process enhances the process efficiency. Gasification or combustion reactions are carried out in the riser as coal and oxygen (with steam for gasification) flow up the reactor. The solids circulation into the mixing zone is controlled by the solids level in the SP. The riser,

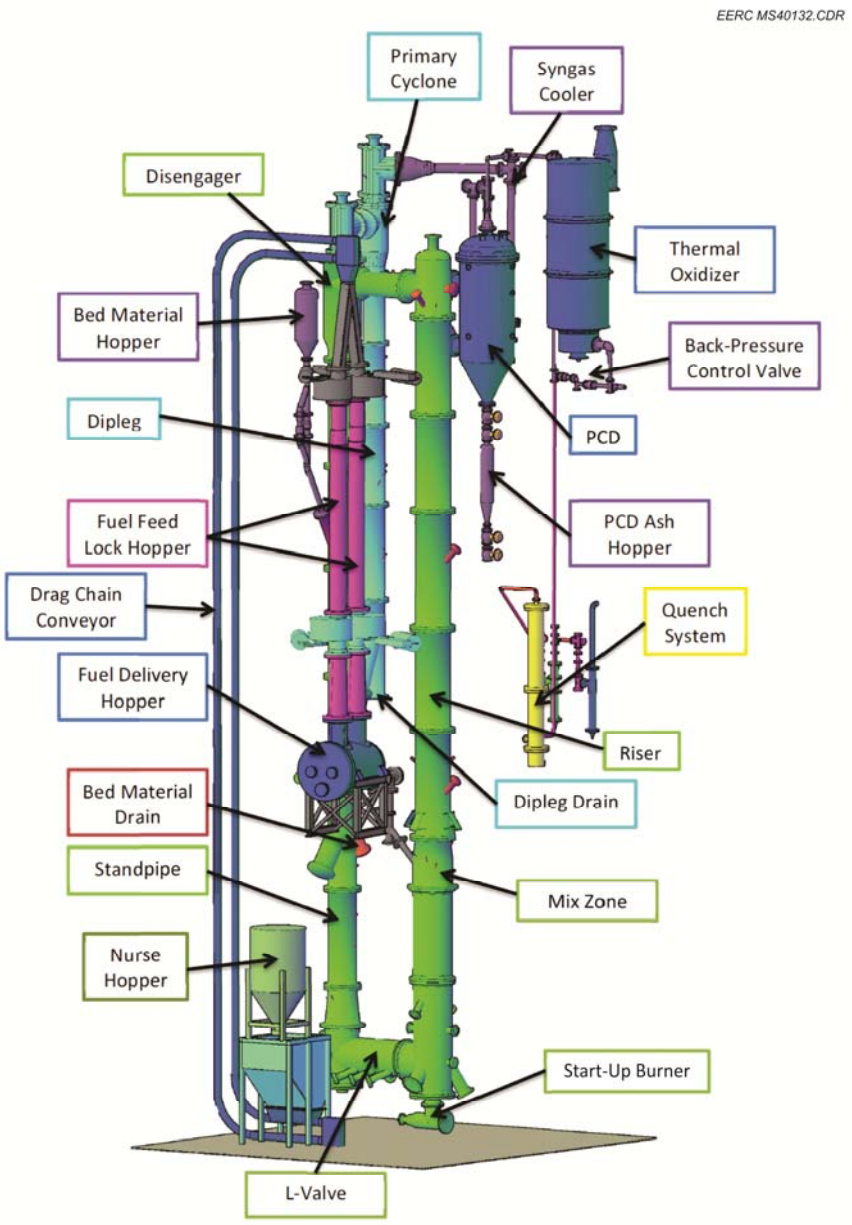

Figure 12. TRDU.

disengager, SP, and cyclones are equipped with several internal and skin thermocouples. Nitrogen-purged pressure taps are also provided to record differential pressure across the riser, disengager, dipleg, and cyclones. The bulk of entrained solids leaving the riser is separated from the gas stream in the disengager and circulated back to the riser via the SP. A solids stream is withdrawn from the SP via an auger to maintain the system's solids inventory. Gas exiting the disengager enters a primary cyclone. Gas exiting this cyclone enters a jacketed-pipe heat exchanger before entering the particulate control device. Table 9 summarizes the design and operating conditions of the system.

Table 9. Summary of TRDU Design and Operation on the Design Coal

Parameter	Design	Actual
Coal	Illinois No. 6	Illinois No. 6
Moisture Content, %	5	8.5
Pressure, psig	120 (9.3 bar)	120 (9.3 bar)
Steam/Coal Ratio, mol	0.34	0.34
Air/Coal Ratio, mol	4.0	2.3
Ca/S Ratio, mol	1.5	2.0
Air Inlet Temperature, °C	427	180
Steam Preheat, °C	537	350
Coal Feed Rate, lb/hr	198 (89.9 kg/hr)	220 (99.9 kg/hr)
Gasifier Temperature, maximum °C	1010	950
ΔT, maximum °C	17	60 to 100
Carbon Conversion,[1] %	>80	76.5
HHV[2] of Fuel Gas, Btu/scf	100	110
Heat Loss as Coal Feed, %	19.5	13
Riser Velocity, ft/sec	31.3	25
Heat Loss, Btu/hr	252,000	320,000
SP Superficial Velocity, ft/sec	0.1	0.38

[1] Carbon conversion = (wt carbon feed − wt carbon removed)/wt carbon feed * 100.
[2] Higher heating value.

Hot-Gas Filter Vessel

The hot-gas filter vessel (HGFV) is designed to handle all of the gas flow from the TRDU at its expected operating conditions. The vessel is approximately 48-in. i.d. (121.9 cm) and 185 in. (470 cm) long and is designed to handle gas flows of approximately 325 scfm at temperatures up to 815°C (1500°F) and pressure of 120 psig (8.3 bar). The refractory has a 28-in. (71.1-cm) i.d. with a shroud diameter of approximately 22 in. (55.9 cm). The vessel is sized such that it could handle candle filters up to 1.5 m long; however, 1-m candles have been utilized in the 540°C (1000°F) gasification tests to date. Candle filters are 2.375-in. (6-cm) o.d. with 4-in. (10.2-cm) center line-to-center line spacing. The filter design criteria are summarized in Table 10.

The total number of candles that can be mounted in the current geometry of the HGFV tube sheet is 19. This enables filter face velocities as low as 2.0 ft/min to be tested using 1.5-m candles. Higher face velocities are achieved by using fewer candles. The majority of testing has been performed at a face velocity of approximately 4.0 to 4.5 ft/min. This program has tested an Industrial Filter & Pump (IF&P) ceramic tube sheet and Fibrosic and REECER SiC candles, silicon carbon-coated and SiO_2 ceramic fiber candles from the 3M company, along with sintered

Table 10. Design Criteria and Actual Operating Conditions for the Pilot-Scale HGFV

Operating Conditions	Design	Actual
Inlet Gas Temperature	540°C	450°–580°C
Operating Pressure	150 psig (10.3 bar)	120 psig (8.3 bar)
Volumetric Gas Flow	325 scfm (0.153 m^3/s)	350 scfm (0.165 m^3/s)
Number of Candles	19 (1 or 1.5 meter)	13 (1 meter)
Candle Spacing	4 in. 6 to 6 (10.2 cm)	4 in. 6 to 6 (10.2 cm)
Filter Face Velocity	2.5–10 ft/min (1.3 to 2.3 cm/s)	4.5 ft/min (2.3 cm/s)
Particulate Loading	<10,000 ppmw	<38,000 ppmw
Temperature Drop Across HGFV	<30°C	25°C
Nitrogen Backpulse System Pressure	Up to 600 psig (42 bar)	250 to 350 psig (17 to 24 bar)
Backpulse Valve Open Duration	Up to 1-s duration	¼-s duration

metal (iron aluminide) and Vitropore silicon carbon ceramic candles from Pall Advanced Separation Systems Corporation. In addition, granular SiC candles from U.S. Filter/Schumacher and composite candle filters from McDermott Technologies and Honeywell were tested. Current testing has focused on Pall's iron aluminide metal filters. Also, candle filter fail-safes from Siemens-Westinghouse Science and Technology Center have been tested.

The ash letdown system consists of two sets of alternating high-temperature valves with a conical pressure vessel to act as a lock hopper. Additionally, a preheat natural gas burner attached to a lower inlet nozzle on the filter vessel can be used to preheat the filter vessel separately from the TRDU. The hot gas from the burner enters the vessel via a nozzle inlet separate from the dirty gas.

The high-pressure nitrogen backpulse system is capable of backpulsing up to four sets of four or five candle filters with ambient-temperature nitrogen in a time-controlled sequence. The pulse length and volume of nitrogen displaced into the filter vessel are controlled by regulating the pressure (up to 600 psig [42 bar]) of the nitrogen reservoir and controlling the solenoid valve pulse duration. Figure 12 also shows the filter vessel location and process piping in the EERC gasifier tower. A recently installed heat exchange surface now allows the hot-gas filter to operate in the 500° to 1200°F range instead of the higher temperature range of 800° to 1000°F utilized in previous testing. This additional heat exchange surface was added to allow gas cooling to the temperature where Hg removal is likely to occur. Ports for obtaining hot high-pressure particulate and trace metal samples both upstream and downstream of the filter vessel were added to the filter system piping.

Membrane Test System Setup Activities

In order to simultaneously test two hydrogen separation membranes on a slipstream of syngas from the TRDU, the EERC's membrane test system that normally resides in the National Center for Hydrogen Technology® (NCHT®) facility was moved to the TRDU gasification

tower. Four fixed-bed reactors and associated heaters, controllers, and piping were moved to the tower. Additional components were purchased as necessary to accommodate different electrical connections and changes to the gas flow path. The hydrogen separation membrane skid contains all of the controllers and instrumentation necessary to control and monitor hydrogen separation membrane tests. Again, slight modifications were made to accommodate electrical connections and gas flow piping.

The overall test flow setup for the gas cleanup equipment, hydrogen separation membranes, and integration with the TRDU is shown in Figure 13. A slipstream of syngas was pulled from the TRDU after the HGFV on the seventh floor of the gasification tower. The syngas ran through a heat-traced tubing bundle maintained at approximately 550°F. Two fixed beds for WGS were used to shift the CO in the syngas to hydrogen. KATALCOJM™ K8-11 produced by Johnson Matthey was used as the sour-shift catalyst for this test. Steam was injected just prior to the beds to ensure there was enough water available to perform a complete shift. A smaller gasifier with steam injection capability was used as the steam generator for this test. A variable-frequency pump with a loss-on-weight calculation was used to control the steam rate into the shift catalyst. After shift, two sorbent beds loaded with regenerable RVS-1 sulfur sorbent were available for sulfur control. One bed was used at a time, with the one always being regenerated, which allows for continuous operation between the two beds.

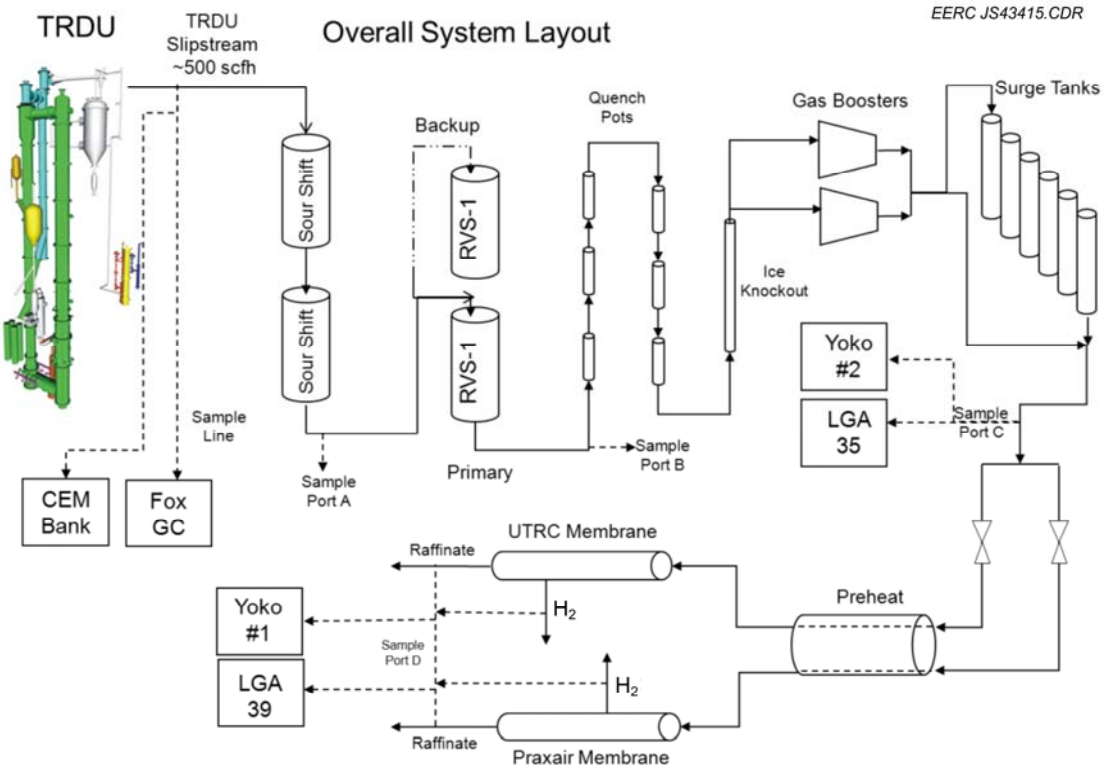

Figure 13. Process flow diagram.

After desulfurization, the syngas traveled through a series of quench pots and a final ice bath knockout pot to remove as much moisture and tars from the syngas as is possible. All of the quench pots were indirectly cooled. Two compressed-air-driven gas boosters were then used to boost the pressure of the cleaned and cooled syngas above the operating pressure of the hydrogen separation membranes. A series of 12 connected gas cylinders was used as a surge tank for the syngas. This also provided for a small reservoir of syngas available if the gasifier were to go offline. The syngas was then divided and sent through separate regulators for each membrane so that each could be operated at independent pressure settings. Each of the syngas streams passed through a large preheater to reheat the gas to near membrane operating conditions.

Specifications for each membrane are shown in Table 11. Membrane 1 operates at higher pressure and temperature. Both were sized to be able to receive 250 scfh of syngas, and both can handle sulfur concentrations in the 1–10-ppm range, with exact tolerance dependent on operating conditions. A picture of the membrane test setup is shown in Figure 14.

Table 11. Membrane Specifications

Membrane	Feed Flow, scfh	Temperature, °F	Pressure, psi
Membrane 1	250	932	500
Membrane 2	250	750	250

Figure 14. EERC membrane test skid.

Both membranes were fully equipped with monitoring and control instrumentation. A detailed piping and instrumentation diagram (P&ID) was developed. Details of the P&ID can be seen in Figure 15. Each of the membranes' parallel pathways was designed to be double-valved to facilitate safe isolation, if needed, while the other membrane was operating under pressure. Low-cracking-pressure check valves were used to prevent backflow of process gases and cross-contamination of samples. Mechanical design of the system proceeded under the precept that the entire unit must be transportable and subsystems must be modular. Redundancy of components was also promoted. Gases discharged from the membrane test system, identified as "To Vent" in Figure 15, are recombined prior to going to the thermal oxidizer. The thermal oxidizer is a down-fired natural gas-fired combustor specifically designed to run with a high level of excess oxygen to promote complete syngas oxidation. Process control and monitoring of the membrane test system was of critical importance to meet the objectives of the project and to operate the system safely, since the system would process flammable, pressurized syngas for the production of pure hydrogen. The EERC uses a hazardous operations review process for risk assessment.

Membrane Test System Description

The membrane test skid is designed to test up to three membranes in parallel using syngas generated by the EFG, the high-pressure FBG (HPFBG), or the TRDU at the EERC. A photo of

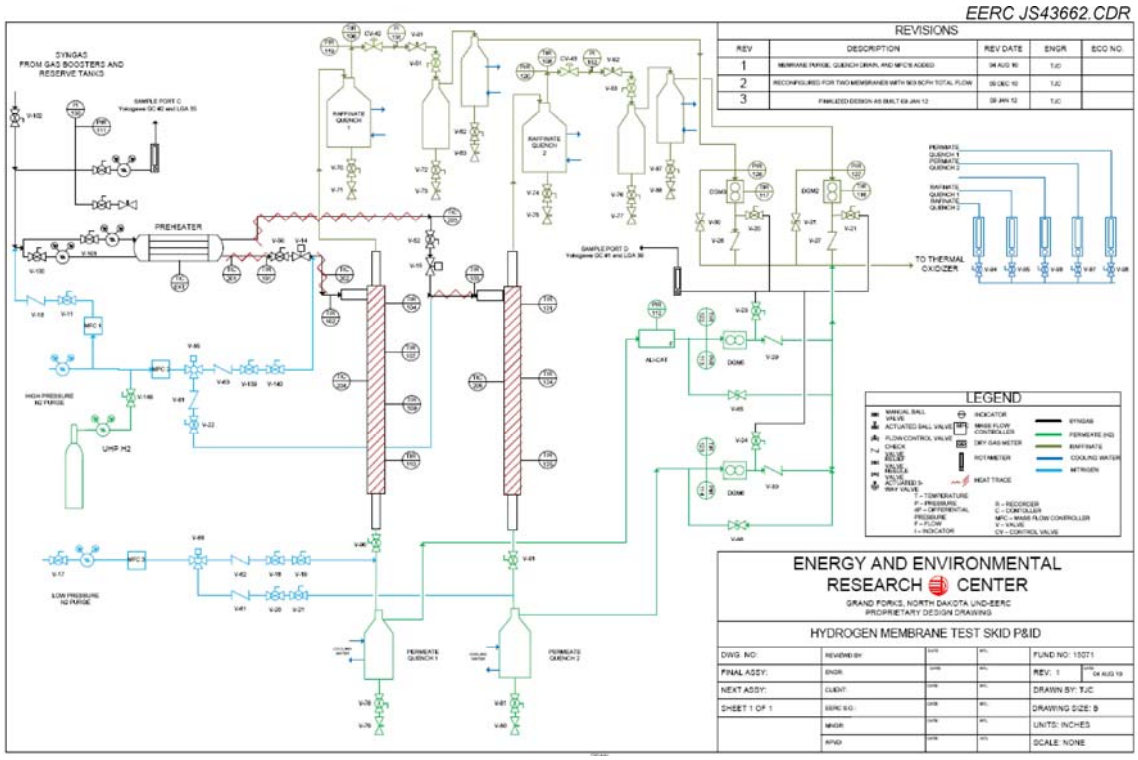

Figure 15. Membrane test skid P&ID diagram.

the test skid is shown in Figure 14. Referring to the P&ID shown in Figure 15, each membrane subsystem has the following individual components:

- Syngas preheat temperature control
- Membrane temperature control
- Raffinate cooling
- Permeate cooling
- Raffinate flow control
- Raffinate flow measurement
- Permeate flow measurement
- Sweep and purge gas flow control
- Permeate and raffinate gas sample ports downstream of dry gas meters
- Data logging of flows, temperatures, pressures, and gas composition

The membrane test skid was fabricated and constructed entirely within the EERC, including welded pressurized quench vessels and the electrical and control systems. All fittings, valves, and quench pots that are in contact with process gases are stainless steel. Swagelok tube fittings, instrumentation valves, and stainless steel tubing were used throughout. Tubing is of moderately heavy wall designation for the sizes used, for example, 0.500-in.-diameter tubing has a wall thickness of 0.065 and 0.250-in.-diameter tubing has a wall thickness of 0.049 in. All tubing is of fully annealed, drawn, 316/316L grade with a hardness of 80 HRB or less. All connections were inspected for scratches and other imperfections prior to final assembly. Assembly of the tubing and fittings followed procedures outlined in Swagelok's Tube Fitter's Manual. All fittings were leak-checked under pressure with a soap-and-water solution.

Each membrane has purge gas capability for flushing either side of the membrane during heat-up and cooldown. Purging residual hydrogen during the cooldown period is critically important since hydrogen in contact with membrane media degrades membrane performance. Purge flow rates are controlled by mass flow controllers (MFCs). Pressure is controlled by a pressure regulator upstream of the MFC. The purge system may also be used for permeate-side sweep gas control. Although various purge gases may be used, this testing was limited to nitrogen.

Quench pots (Figure 16) were of sufficient size to cool permeates and raffinates to approximately 12°C (54°F). Municipal water is used to externally cool quench pots that the gases pass through. The temperature of the cooling water was approximately 3°C (38°F) during the testing period. Cooling water flow is controlled by needle valve and monitored by a rotameter. Since water may be present in the raffinate streams, double-valved drains are used on the bottom of each quench pot to facilitate removal of condensates. Although water should not be present in the permeate, permeate quench pots may be periodically checked for condensate, which would be an indicator that syngas is flowing through the membrane into the permeate stream. Because of tubing runs being sufficiently long and of large enough diameter, from the quench pots to the dry gas meters, the gases were rewarmed to room temperature prior to flow measurement at the dry gas meters.

Figure 16. Quench pots.

Flow control valves (Figure 17) are used on the raffinate streams to regulate the syngas flow rate past the membrane. In this way, the percent capture of hydrogen may be measured as a function of the flow across the membrane. The flow control valves are of a pneumatic fail-open design. The supply valves at the syngas inlet to the system are a pneumatic fail-closed type. If the operator initiates an emergency stop, power is lost, or compressed air pressure is lost, the pneumatically actuated supply valves close and the back-end flow control valves open, allowing the system to depressurize. The valve flow coefficient of the flow control valves is sufficient to provide a gradual depressurization, thereby eliminating the possibility of flooding the thermal oxidizer with raffinate gas. The valves employ a position encoder giving resulting closed-loop operation and accurate position data being fed back to the control computer.

Instrumentation consists of Type K thermocouples, pressure transmitters, dry gas meters, gas chromatographs, and laser gas analyzers. Yokogawa EJA series pressure transmitters use a silicon resonant sensor formed from monocrystal silicon, which has no hysteresis in pressure or temperature changes. The sensor minimizes overpressure, temperature change, and static pressure effects, thus offering long-term stability. Output signals are of the 4–20-mA analog

Figure 17. Raffinate flow control.

type. A 24-bit analog-to-digital converter is employed in the data acquisition and control system, thereby yielding high resolution to the measurements.

Control is done with National Instruments LabVIEW software, National Instruments Compact RIO hardware, and a personal computer. All control components, with the exception of the personal computer, are located in a purged cabinet that is mounted on the skid. The computer is located in the control room. Communication between the computer and the skid uses a conventional Ethernet protocol. The physical network communications media is dedicated to the systems used for testing. Thermocouple and analog input modules have 24-bit resolution. The time span between saved data is a user-selectable parameter. For these tests, 30 seconds was used. Many of the saved data values were a time-weighted average to reduce the effects of spurious signals or nonuniform pulse train signals. Watlow temperature controllers are panel-mounted to the front of the control cabinet. The temperature controllers are networked with the main control system to provide integrated temperature control and temperature-ramping features. Gradual temperature ramping of the membrane assemblies is required to maintain uniform linear thermal expansion between the internal and external components of the membrane.

The membrane test system uses a control system that was developed in-house using National Instruments LabVIEW software. The main control page can be seen in Figure 18. The layout is similar to the P&ID. All control and sensor data are accessible on the main page. The flow rate of purge gases is controlled by mass flow controllers. Three-way valves are used to direct the flow across the outface membrane face media or through the inner permeate portion of the membrane. The latter also enables a membrane to be tested using a sweep gas. Gas meter values shown on the main page are based on a time-weighted average.

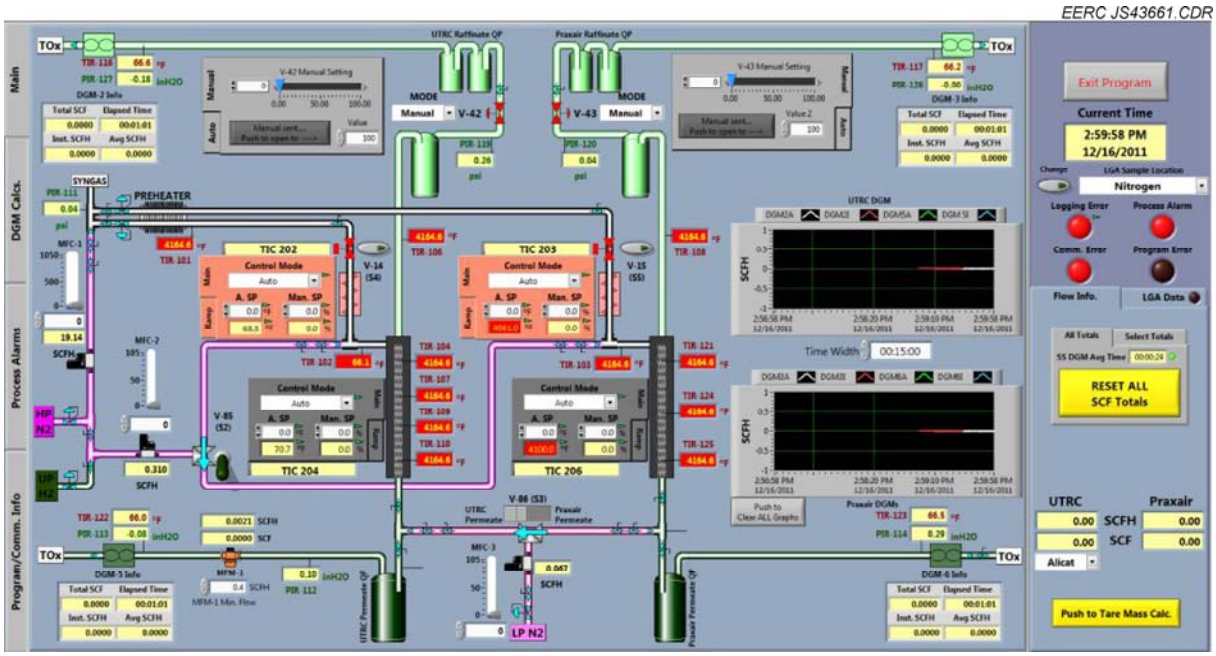

Figure 18. Control program – main page.

Numerous variables are set up with alarm conditions if their value lies outside a set range. The alarm condition is signaled by a flashing red background color for the displayed value. The low (LO) and high (HI) alarm limits are operator-defined values in the left columns. The current status is also displayed in the right columns. The LO or HI red light indicator will enunciate an alarm condition, thereby giving the operator a quick indication why an alarm condition may exist.

Power to the heaters is controlled by Watlow EZ-Zone PM temperature controllers. The heater controllers use low-voltage signals to control solid-state power relays. Generally, the operator inputs temperature set points in a heater controller's block on the main page. Those values flow through to the HTR Controls page. The Watlow temperature controllers have built-in ramp functions. The control program utilizes the ramp function to allow the operator to specify the ramp rate, seen in the bottom of each temperature controller's block. The operator may specify ramp up, ramp down, or both. By specifying a gas preheat temperature set point to be the same as the membrane temperature set point and using the same ramp rate, thermal stress in the membrane can be minimized. During heat-up, the low flow rate of heated purge gas helps to heat up the internal portion of the membrane at the same rate as the external portion.

Dry gas meters do not produce a uniform output signal. This is because of the diaphragm type: dry gas meter translates reciprocating linear motion into rotary motion, which results in dial speeds that appear to stop and start. Pulse counting by the control system results in the time-weighted averages displayed on the main page.

Gas Analysis

Syngas, permeates, and raffinate gas compositions are monitored with two gas analyzers. Sample ports are located downstream of gas meters. Sample gas streams are manually switched via valves at the sample ports. Sample gas tubing from sample ports to the analyzers is polyethylene, with no line longer than 50 feet. Sample gas transit times to the analyzers are estimated to be less than 1 minute, depending on the individual sample gas flow rate. The first analyzer is a laser gas analyzer (LGA) that is capable of detecting and measuring the concentration of eight gases at once: H_2, CO, CO_2, N_2, O_2, H_2S, CH_4, and total hydrocarbons. The LGA provides real-time feedback of the gas composition and is typically used to aid in the control of the system. The second analyzer used is a gas chromatograph (GC) equipped with two thermal conductivity (TC) detectors and a pulsed-flame photometric detector for ultralow sulfur detection. The first TC detector is dedicated solely to analyzing hydrogen and provides three hydrogen measurements for each 15-minute analysis cycle. The second detector analyzes the gas stream for CO, CO_2, N_2, O_2, H_2S, COS, CH_4, ethane, ethene, propane, and propene. One measurement is provided every 15 minutes for each of those gases. The third detector is capable of ultralow sulfur detection, down to 50 ppb. It provides three H_2S and COS measurements per 15-minute cycle. In a similar but continuous and dedicated manner, the FS raffinate is analyzed by a separate set of paired analyzers, LGA and GC. Dräger tube and gas bag samples may be drawn from each of the sample ports on the membrane skid as well as from several other ports on the gasifier system. Gas bag samples were analyzed by a GC in one of the EERC's chemistry labs as an additional check of gas compositions. A sampling plan for the testing is shown in Table 12.

Sorbent traps were used to quantify levels of mercury and other trace metals in the syngas. Mercury sampling was performed at the Port C sampling location, which is after the mercury control column and before the hydrogen separation membranes. Additional sampling was performed just after the TRDU HGFV. Sampling at this location measures the mercury concentrations to which the hydrogen separation membranes are exposed. Mercury concentrations were determined by syngas sampling using sorbent traps (U.S. Environmental

Table 12. Gas Sampling Plan

	Analyzers	Dräger Tubes					
Sample Port/ Location	Bulk Gas Comp.	H_2S	NH_3	HCN	HCl	Hg	Gas Bag
Sample Port A	None	None	None	None	None	None	None
Sample Port B	None	None	1x/shift	1x/shift	1x/shift	None	None
Sample Port C	Yoko2/LGA35	Hourly	None	None	None	TBD	None
Sample Port D: (Yoko1, LGA39)							
Mem. 1 Raffinate	3.5 hr/shift	None	None	None	None	None	None
Mem. 1 Permeate	0.5 hr/shift	None	None	None	None	None	None
Mem. 2 Raffinate	3.5 hr/shift	None	None	None	None	None	None
Mem. 2 Permeate	0.5 hr/shift	None	None	None	None	None	None

[1] To be determined.

Protection Agency Method 30B). Previous research at the EERC indicated that sorbent traps were able to provide reliable and accurate syngas mercury concentrations. The samples were collected using OhioLumex sorbent traps and analyzed using an OhioLumex RA915+ mercury analyzer. This instrument utilizes a pyrolysis technique followed by Zeeman atomic absorption detection. The multielement sorbent trap, or ME-ST, method is an experimental method used to quantify the levels of trace elements in gas streams. Trace elements were measured at Port C and on the TRDU gas stream using the ME-ST method.

Proprietary Gas Injection

WRI had an interest in determining the impact of its patent-pending proprietary gas injection into certain areas of the gasifier. To facilitate the injection, WRI provided additional funding to purchase and install a gas injection system for the TRDU. The system uses a proprietary gas that was plumbed directly into the TRDU. The system was of sufficient size to provide 1000 scfh of the proprietary gas. The gas injection system was utilized during the test runs with the treated fuel.

Fuel Preparation and Coal Properties

Each of the six fuel types was received by the EERC in Super sacks. The raw fuels were shipped from WRI to the EERC in early October 2011 and stored indoors in the same Super sacks in which they were delivered. The fuels were moved to EERC bunkers in late December, and the coal preparation process began in early January. The dried and treated fuels arrived from WRI at the EERC in early January and were moved to bunkers and prepared the week prior to and the week of testing.

The fuel preparation process for the TRDU consists of conveying the selected fuel from the bunker to a bucket elevator which will convey the coal to the Williams patent crusher. The crushed coal drops into a second bucket elevator which then drops the crushed coal into a 48-in. Kason classifier. This classifier is utilized to separate the +10-mesh coal for recycle back to the bucket elevator feeding the Williams crusher. The –10-mesh coal is collected as feedstock to the TRDU without any fines removal. All fuels were processed in the same manner for testing so particle-size differences between any samples would be a function of the fuel type and any upfront drying or thermal treatment processes.

During the test run, fuel samples were collected from each fuel hopper and compiled into a composite sample for each fuel type. The composite samples were then analyzed in the EERC coal lab. The results of the proximate, ultimate, and heating value analyses are shown in Table 13. The results of both analysis sets are on an as-received basis with hydrogen and oxygen, not including hydrogen and oxygen from moisture. There is some question of the moisture level of the PRB dried coal as submitted by WRI. It may also be possible that the treated fuel picked up moisture through the EERC fuel preparation and storage processes. The raw lignite appears to have lost some moisture which is typically observed for lignites fired in the TRDU. The dried and treated lignites (and treated PRB) have picked up some moisture through the coal

Table 13. Proximate, Ultimate, and Heating Value Analysis as Analyzed from As-Fed Composites at the EERC

Coal Analysis/Parameter		Raw PRB Coal	Dried PRB Coal	Treated PRB Coal	Raw ND Lignite	Dried Lignite	Treated Lignite
Proximate Analysis, wt%	Moisture	26.19	4.58	2.44	27.32	5.28	6.18
	Ash	4.96	6.57	6.17	9.22	11.07	9.11
	Volatile Matter	32.46	43.23	42.07	29.38	40.79	38.26
	Fixed Carbon	36.39	45.62	49.33	34.08	42.86	46.45
Ultimate Analysis, wt%*	Carbon	50.86	65.06	68.33	45.01	58.62	60.76
	Hydrogen	3.67	4.68	4.31	3.16	4.12	3.87
	Nitrogen	0.61	0.78	0.86	0.48	0.63	0.68
	Sulfur	0.44	0.59	0.59	1.09	1.31	1.2
	Oxygen	13.28	17.74	17.3	13.72	18.97	18.21
HHV	Btu/lb	8622	11,150	11,606	7323	9852	9962

* As-received basis, hydrogen and oxygen not including hydrogen and oxygen from moisture.

preparation facilities. It should be noted that the coal preparation process occurs off-line, and the prepared fuel has time to lose or gain moisture. If the drying, treating, and preparation process occurred in a continuous fashion, which is how it would be completed commercially, the gain in moisture would not be expected.

Ash content was relatively low in the PRB, and sulfur was very low, around 0.4%. The HHV of the treated fuel was near 12,000 Btu/lb as compared to near 8700 Btu/lb for the raw fuel. The lignite coal had around 8% ash on an as-received basis and was close to 1% sulfur. The heating value of the treated lignite was near 10,000 Btu/lb as compared to about 7300 Btu/lb for the raw fuel.

The fuels were ashed in the EERC coal laboratory, and the elemental composition of the ash was analyzed using x-ray fluorescence (XRF). The pressed pellet method was used for preparing the samples, and a Rigaku ZSX PRIMUS II wavelength-dispersive x-ray system was used for analysis of the samples. The results of the analysis for the six fuels are shown in Table 14. The inorganic chemistry is similar for the two fuels. Sodium and potassium contents in the fuels are relatively low, enabling the use of silica sand as a start-up bed material in the gasifier.

The data indicate that the silica, alumina, and potassium content of each of the fuels was reduced through the treatment process. This reduction was accompanied by an apparent increase in the other components, but it is more likely that the reduction was real and the increase was due to the renormalization of the data. The reduction in potassium and, possibly, sodium was anticipated as these elements are semivolatile and could be removed in the upgrading process.

Table 14. Elemental Analysis of Coal Ash Produced from Each Fuel

% Elements	PRB Raw	PRB Dried	PRB Treated	Lignite Raw	Lignite Dried	Lignite Treated
Si	23.0	23.0	18.9	24.3	20.0	15.0
Al	17.1	16.8	15.1	12.3	12.2	11.8
Fe	8.1	7.7	8.5	11.3	10.1	9.6
Ti	1.6	1.6	1.7	0.7	0.6	0.5
P	0.7	0.8	0.8	0.2	0.2	0.3
Ca	30.5	31.4	35.1	24.8	27.5	31.1
Mg	6.5	6.4	7.0	10.7	12.3	14.7
Na	1.3	1.3	1.2	2.2	2.7	2.4
K	0.6	0.5	0.2	1.3	0.9	0.7
S	10.6	10.5	11.4	12.2	13.6	14.0

The reduction in silica and aluminum was likely due to the presence of these materials in the fine size fraction and the separation of fine material is also possible in the upgrading process.

The fuels were also analyzed for chlorine, fluorine, and trace metal contents. The results of the analyses are shown in Table 15.

As-Run Test Plan

Slight modifications were made to the test plan as the runs progressed based on input from WRI personnel, who were on-site during the runs. The final as-run test matrix is shown in Table 16. Each of the six fuel types were evaluated, but changes were made to temperatures and proprietary gas injection points. Proprietary gas was injected in two places in the gasifier. The PRB treated runs all occurred at an 1850°F target temperature and evaluated proprietary gas injection locations. Additional proprietary gas injection testing was also performed with the raw lignite. Test 8 was intended to optimize the syngas for hydrogen separation in the membranes and was oxygen-fired with steam injection.

Gasifier Operations and Operational Data

Gasifier operation was started on January 15, 2012, with heat-up on natural gas. Silica sand was used as a start-up bed material to help carry heat through the gasifier. Coal combustion was started around late that evening, and the system was transitioned to gasification mode around 05:00 on January 16, 2012. The first parametric fuel evaluation, Test 2a, reached steady state (SS) by 12:00 on January 16. Overall, the system ran well for the entire test period. Very minimal fuel-related issues were noted. The biggest challenge noted with the different fuel types was achieving accurate feed rates because of the changing coal types. A couple of minor upsets occurred during the week with the dipleg solids getting pushed up and through the cyclone, but only resulted in 1- to 2-hour upsets.

Table 15. Concentration of Halides and Trace Metals in the Fuel Samples

Sample ID	PRB Composite, as received	PRB Composite, dry	PRB Composite, treated	Lignite Composite, as received	Lignite Composite, dry	Lignite Composite, treated
Parameter, µg/g dry						
Chlorine	16.7	15.2	14.8	28.9	22.6	17.8
Fluorine	<50	<50	<50	<60	<50	<50
Antimony	0.18	0.18	0.16	0.24	0.29	0.25
Arsenic	2.81	2.24	1.50	4.66	4.74	4.47
Beryllium	0.259	0.255	0.224	0.279	0.207	0.237
Cadmium	0.091	0.079	0.078	0.065	0.061	0.048
Chromium	5.42	5.58	4.58	5.20	5.07	4.22
Cobalt	2.45	2.66	2.51	1.47	0.962	1.08
Lead	2.64	2.38	2.22	1.82	1.81	2.10
Manganese	11.0	11.1	18.9	79.0	90.8	78.0
Mercury	0.108	0.0851	0.0461	0.0736	0.0808	0.0616
Nickel	4.42	4.20	4.06	3.43	3.22	2.27
Selenium	0.814	0.768	0.744	0.41	0.38	0.38

Table 16. As-Run Test Matrix

Test	Fuel	Proprietary Gas Injection	Temp., °F	Comments
1	PRB – as received	None	1550	TRDU start-up
2a	PRB – as received	None	1850	Parametric fuel evaluation
2b	PRB – as received	None	1650	Parametric fuel evaluation
3a	PRB – dried	None	1650	Parametric fuel evaluation
3b	PRB – dried	None	1850	Parametric fuel evaluation
4a-1	PRB – treated	None	1850	Parametric fuel evaluation
4a-2	PRB – treated	Location 1	1850	Parametric fuel evaluation
4a-3	PRB – treated	Location 1 and 2	1850	Parametric fuel evaluation
4a-4	PRB – treated	Location 2	1850	Parametric fuel evaluation
5a-1	Lignite – as received	None	1850	Parametric fuel evaluation
5a-2	Lignite – as received	Location 1	1850	Parametric fuel evaluation
5a-3	Lignite – as received	Location 1 and 2	1850	Parametric fuel evaluation
5a-4	Lignite – as received	Location 2	1850	Parametric fuel evaluation
5b-1	Lignite – as received	Location 2	1650	Parametric fuel evaluation
5b-2	Lignite – as received	None	1650	Parametric fuel evaluation
6a	Lignite – dried	None	1650	Parametric fuel evaluation
6b	Lignite – dried	None	1850	Parametric fuel evaluation
7a-1	Lignite – treated	Location 2	1850	Parametric fuel evaluation
7a-2	Lignite – treated	None	1850	Parametric fuel evaluation
7a-3	Lignite – treated	Location 1 and 2	1850	Parametric fuel evaluation
8	PRB – as received	None	1700	Optimization for membranes
9	PRB	None	1550	TRDU shutdown

The biggest system upset for the week was the loss of the air compressor that occurred during the transition to Test 3b. Cold ambient air temperatures resulted in freezing of the intake lines and compressor shutdown. Changes were made to the intake system, and vents were adjusted in the compressor room to help ensure the compressor was taking in warmer air. The compressor ran without issue for the remainder of the week. The shutdown resulted in about 2 hours of coal feed downtime and about 5 hours of total time needed to bring the system back to SS.

Operational data for each of the test runs are shown in Table 17. SS periods were chosen within each test run, and the average data for those time periods are presented in the table. Operating pressure, flow rates, temperatures, velocities, and circulation rates are all presented in the table. Gasifier pressure held steady for the duration of the test run. The O_2-to-moisture ash-free (MAF) coal ratio also varied based on the temperature targets and changes in coal feed rate. The data indicate that the average mixing zone temperature was typically below the target settings. Carbon content in the SP was below 5% for most of the test periods, but a few anomalous samples occurred throughout the week of testing. These samples were most likely the

Table 17. Average Gasifier Operating Conditions

Test:	2a	2b	3a	3b	4a-1	4a-2	4a-3	4a-4	5a-1	5a-2
Date	1/16/12	1/17/12	1/17/12	1/18/12	1/18/12	1/18/12	1/18/12	1/19/12	1/19/12	1/19/12
SS Start Time	12:00	0:00	13:30	7:00	11:00	16:45	19:00	1:45	6:00	11:15
SS Stop Time	15:30	4:00	16:00	8:30	12:00	18:15	21:10	3:00	11:00	12:40
Oxidant	Air	Air	Air	Air	Air	Air	Air	Air	Air	Air
Pressure, psig	121	121	121	121	121	121	121	121	121	121
O_2:MAF Coal Ratio	0.89	0.75	0.81	0.88	0.82	1.04	1.04	1.00	0.99	0.95
Coal Feed Rate, lb/hr	366	366	253	284	276	192	192	195	385	422
Mixing Zone, °F, avg.	1731	1589	1611	1736	1785	1793	1719	1688	1710	1729
L-Valve Zone, °F, avg.	1397	1261	1252	1434	1452	1415	1366	1315	1352	1363
Riser, °F, avg.	1599	1475	1492	1611	1635	1665	1620	1573	1612	1632
SP, °F, avg.	1656	1527	1551	1681	1719	1734	1656	1627	1661	1679
Dipleg, °F, avg.	944	1093	1136	1156	1161	1094	1089	1110	1174	1229
Carbon in Bed, %, SP	0.3	0.6	4.5	2.8	17.6	0.8	14.2	1.80	0.7	0.7
Riser Velocity, ft/s	42.0	35.1	32.2	46.1	41.3	40.7	40.9	41.4	46.5	44.9
SP Velocity, ft/s	0.19	0.17	0.20	0.21	0.22	0.23	0.13	0.14	0.21	0.21
Circulation Rate, lb/hr	2670	6435	5523	5300	3879	3663	4453	4551	3509	3811

Continued . . .

Table 17. Average Gasifier Operating Conditions (continued)

Test:	5a-3	5a-4	5b-1	5b-2	6a	6b	7a-1	7a-2	7a-3	8
Date	1/19/12	1/19/12	1/19/12	1/20/12	1/20/12	1/20/12	1/21/12	1/21/12	1/21/12	1/22/12
SS Start Time	13:00	14:15	19:00	0:00	14:00	22:00	8:00	10:30	14:00	3:00
SS Stop Time	14:00	17:00	22:00	6:00	16:15	4:00	10:00	11:45	18:30	7:30
Oxidant	Air	Air	Air	Air	Air	Air	Air	Air	Air	Oxygen
Pressure, psig	121	121	121	121	121	121	121	121	121	121
O_2:MAF Coal Ratio	0.95	0.90	0.84	0.83	0.78	0.84	0.61	0.61	0.89	0.83
Coal Feed Rate, lb/hr	422	412	403	401	274	309	389	389	290	394
Mixing Zone, °F, avg.	1706	1701	1591	1589	1630	1693	1701	1718	1714	1564
L-Valve Zone, °F, avg.	1346	1348	1283	1274	1281	1335	1338	1345	1352	1261
Riser, °F, avg.	1621	1616	1505	1490	1511	1575	1595	1602	1611	1460
SP, °F, avg.	1659	1656	1534	1528	1565	1620	1636	1651	1652	1481
Dipleg, °F, avg.	1242	1280	1257	1246	1295	1324	1246	1326	1352	1058
Carbon in Bed, %, SP	0.4	0.2	1.4	1.6	11.7	3.9	1.3	6.40	4	0.4
Riser Velocity, ft/s	44.2	44.4	41.2	40.9	33.5	38.3	37.0	38.0	37.5	35.2
SP Velocity, ft/s	0.14	0.17	0.17	0.18	0.19	0.19	0.16	0.21	0.16	0.20
Circulation Rate, lb/hr	4292	4468	6249	6026	5524	5340	5717	5826	6233	5015

result of gasifier coal feed upsets. Velocity was variable based on the required temperature set point, and as temperature settings increased, so did the requirement for air; therefore, velocity also increased. The solids circulation rate is variable based on solids inventory in the system and changed frequently from the need to drain and add solids throughout the run.

Gasifier Syngas Analysis Results

The concentrations of the major syngas components for each test are shown in Table 18. Three analyzers were monitoring the syngas composition from the TRDU throughout the week. The continuous emission monitor (CEM) bank and the Foxboro GC were dedicated to the gasifier exit syngas stream throughout the test run. The Yokogawa GC periodically sampled the gasifier syngas but also sampled the premembrane location after WGS and desulfurization. The Foxboro GC had some peak-shifting issues that were difficult to resolve; therefore, there is a section of data that is suspect or not included, as indicated by the table. Some differences were observed between the analyzers for the air-blown runs. The oxygen-blown test indicated better agreement between measurement systems, as is indicative of the range of components in the calibration gas.

In general, higher CO yields were noted with the dried and upgraded fuels for both the PRB and lignite coals. As intended by the run conditions, the H_2-to-CO ratio was below 1 for all of the air-blown tests. The most dramatic transition observed throughout the testing was the change in CO and CO_2 concentrations as the gasifier was switched from raw to upgraded fuels. For both the PRB and the lignite, CO levels significantly increased and CO_2 levels significantly decreased when the dried fuel was brought online. This transition was also observed when switching from the upgraded PRB to the raw lignite, between Tests 4a-4 and 5a-1.

Smaller but significant changes in CO_2 concentration were observed when switching gasifier temperatures. As expected, the higher temperatures resulted in higher CO_2 concentration, increased carbon conversion, and reduced syngas heating value.

Operation at lower temperatures resulted in reduced carbon conversion but also increased syngas heating value. Carbon conversion ranged from the low 80% range to the mid-90% range under higher-temperature conditions. The syngas heating value was below 100 Btu/scf for all of the air-blown test conditions and approximately 120–125 scfh for the oxygen-blown condition. The heating value as calculated from the CEM data is most likely higher than actual because of a high total hydrocarbon (HC) reading.

The concentration of the minor syngas components is shown in Table 19. Large discrepancies were observed between the H_2S measurements from each of the analyzers. A basic Aspen modeling calculation was performed for Test Conditions 4a-4 and 5a-1 to provide another estimate of sulfur levels in the system. The model calculations estimated 770 ppm H_2S for Test Condition 4a-4 and 1522 ppm for Test 5a-1. The modeling results suggest that the CEM was reading high for the test and the GCs may have been reading low. Noncondensable higher HCs are also shown in Table 19. The GCs do not agree on the levels of C_3H_8 in the system, but some correlation can be seen with C_2H_6. The concentration of higher noncondensable HCs was not significant in the syngas stream.

Table 18. Concentration of Major Syngas Components, Syngas Heating Value, and Carbon Conversion

	Gas Concentration %																				
	CEM							Foxboro GC[1]							Yokogawa GC							
Test	H_2	CO	CO_2	HC	N_2[2]	H_2/CO	HHV Btu/SCF	H_2	CO	CO_2	CH_4	N_2	H_2/CO	HHV Btu/SCF	H_2	CO	CO_2	CH_4	N_2	H_2/CO	HHV Btu/SCF	Carb. Conv. %
2a	5.0	11.8	13.3	2.8	68.5	0.4	86.3	6.3	8.1	10.7	1.3	72.4	0.8	64.1	5.9	7.8	10.2	1.3	64.2	0.8	67.7	93.3
2b	5.0	12.3	12.7	3.3	68.3	0.4	92.9	5.9	9.5	10.7	1.7	75.0	0.6	68.7	NA[3]	NA	NA	NA	NA	NA	NA	94.2
3a	4.0	15.5	8.5	2.5	70.4	0.3	92.5	3.3	14.0	6.4	1.5	76.1	0.2	74.0	NA	NA	NA	NA	NA	NA	NA	81.8
3b	3.5	16.1	8.9	2.2	71.2	0.2	88.8	**3.1**	**0.1**	**6.3**	**0.2**	**0.3**	NA	NA	NA	NA	NA	NA	NA	NA	NA	89.2
4a-1	3.4	17.3	8.0	2.2	70.4	0.2	92.9	**3.0**	**10.2**	**6.7**	**0.8**	**56.8**	NA	NA	4.3	13.6	5.8	1.0	65.6	0.3	80.0	88.8
4a-2	2.0	14.1	11.6	1.8	71.9	0.1	73.0	**0.8**	**5.2**	**9.9**	**0.4**	**37.5**	NA	NA	3.5	10.9	8.8	0.8	66.6	0.3	63.5	92.8
4a-3	3.0	16.2	12.3	2.8	68.2	0.2	93.2	**1.6**	**5.7**	**10.5**	**0.3**	**31.8**	NA	NA	NA	NA	NA	NA	NA	NA	NA	92.8
4a-4	2.5	15.3	10.4	1.8	71.3	0.2	79.0	**2.6**	**2.4**	**8.5**	**0.4**	**14.3**	NA	NA	3.4	11.6	7.7	0.9	66.3	0.3	67.9	96.1
5a-1	3.7	7.5	13.0	1.8	75.3	0.5	56.9	**3.3**	**1.4**	**11.5**	**0.5**	**18.8**	NA	NA	5.0	6.9	10.4	0.8	68.5	0.7	53.8	95.0
5a-2	3.9	8.9	14.9	1.8	72.1	0.4	62.0	NA	NA	NA	NA	NA	NA	NA	5.2	7.5	12.1	0.8	65.2	0.7	57.3	96.6
5a-3	3.5	9.4	16.0	1.8	70.9	0.4	62.1	NA	NA	NA	NA	NA	NA	NA	5.3	8.1	13.4	0.8	64.0	0.7	60.0	96.6
5a-4	3.7	9.1	15.0	1.8	71.8	0.4	62.0	NA	NA	NA	NA	NA	NA	NA	5.2	7.8	12.5	0.8	64.4	0.7	58.7	96.6
5b-1	3.8	8.8	15.0	2.4	71.4	0.4	67.6	4.3	6.7	14.4	1.0	63.3	0.6	53.8	5.2	7.5	12.3	0.9	64.3	0.7	59.0	94.8
5b-2	4.3	7.6	13.0	2.2	73.9	0.6	63.7	4.3	6.2	11.6	1.3	64.7	0.7	56.5	5.5	6.7	10.2	0.9	65.7	0.8	58.0	91.4
6a	3.7	14.6	9.4	2.1	71.2	0.3	84.2	3.9	10.3	8.1	1.0	65.6	0.4	67.0	NA	NA	NA	NA	NA	NA	NA	83.9
6b	4.8	17.2	9.2	2.4	67.6	0.3	99.5	4.1	12.0	7.5	1.3	62.4	0.3	79.2	NA	NA	NA	NA	NA	NA	NA	87.4
7a-1	3.4	17.8	11.0	2.1	66.9	0.2	93.4	3.6	12.9	9.8	0.9	61.3	0.3	74.1	4.3	13.8	8.5	0.9	61.5	0.3	80.4	91.7
7a-2	3.9	17.3	9.0	2.1	69.0	0.2	93.5	3.1	12.4	7.9	0.8	61.6	0.2	71.2	4.6	13.4	7.0	0.8	62.4	0.3	80.0	91.7
7a-3	3.0	16.9	12.1	2.0	64.9	0.2	90.2	1.2	13.8	15.1	3.1	60.0	0.1	90.4	4.1	12.6	9.4	0.8	63.6	0.3	72.8	92.7
8	16.0	9.4	22.9	8.4	48.2	1.7	169.2	16.4	7.8	26.0	3.6	47.2	2.1	120.9	16.9	7.9	22.1	3.1	45.6	2.1	124.3	95.9

[1] Data in bold are suspect because of analyzer problem.
[2] Balance assumed N_2.
[3] Not available (analyzer off-line or sampling different stream).

Table 19. Concentration of Minor Syngas Components

	Gas Concentration, ppm									
	CEM	Foxboro GC[1]			Yokogawa GC					
Test	H_2S	H_2S	C_2H_6	C_3H_8	H_2S	COS	C_2H_4	C_2H_6	C_3H_6	C_3H_8
2a	791	445	140	915	244	27	977	95	4	6
2b	1383	756	358	2260	NA[2]	NA	NA	NA	NA	NA
3a	1052	1057	181	1317	NA	NA	NA	NA	NA	NA
3b	1257	**488**	**64**	**747**	NA	NA	NA	NA	NA	NA
4a-1	1140	**5**	**233**	**1026**	98	17	803	111	6	8
4a-2	1154	**431**	**23**	**127**	307	49	162	19	1	24
4a-3	1198	**228**	**124**	**736**	NA	NA	NA	NA	NA	NA
4a-4	1268	**257**	**329**	**1111**	206	30	776	49	4	21
5a-1	2358	**826**	**103**	**541**	959	6	475	55	3	21
5a-2	2437	**1504**	**264**	**331**	1170	2	256	35	4	21
5a-3	2394	**1270**	**39**	**682**	1100	0	427	47	0	9
5a-4	2424	**974**	**58**	**529**	1116	0	434	48	2	6
5b-1	2826	904	89	1429	984	0	1294	194	8	5
5b-2	2851	955	262	1453	1111	0	1197	198	7	3
6a	1787	566	113	970	NA	NA	NA	NA	NA	NA
6b	1895	527	104	741	NA	NA	NA	NA	NA	NA
7a-1	1753	1337	11	596	707	25	436	60	3	3
7a-2	1548	1753	103	506	819	0	350	42	4	5
7a-3	1910	241	4012	4360	1073	3	310	50	3	8
8	3175	1207	1744	3914	1995	0	3814	1443	25	5

[1] Data in bold are suspect because of analyzer problem.

[2] Not available (analyzer off-line or sampling different stream).

The daily syngas composition as measured by the CEMs is presented in Figures 19–25. The nitrogen concentration is as measured by the Foxboro GC where available. The SS test periods for which the average data are presented in the tables are indicated on the graphs. The graphs also describe the transient data between the test runs and indicate when the transition started between test periods.

The concentration of trace metals in the syngas was also measured using carbon traps with Method 30B and the ME-ST method. The concentration of Sb, As, Be, Cd, Cr, Co, Pb, Mn, Hg, Ni, and Se in the gasifier was evaluated for selected test conditions on the TRDU. Mercury samples were taken with both Method 30B and with the ME-ST method. The remaining trace metals were sampled only with the ME-ST method. Samples were pulled just after the HGFV. The treated fuels are anticipated to have lower levels of some of the more volatile trace metals, including mercury.

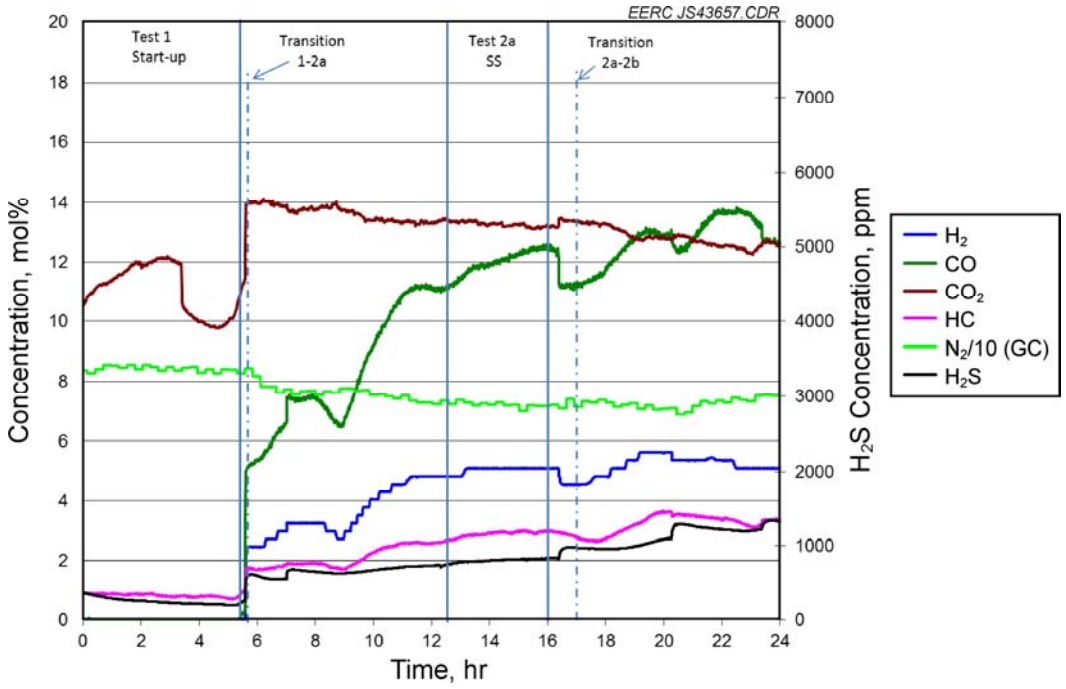

Figure 19. Syngas composition as measured by the CEM on January 16.

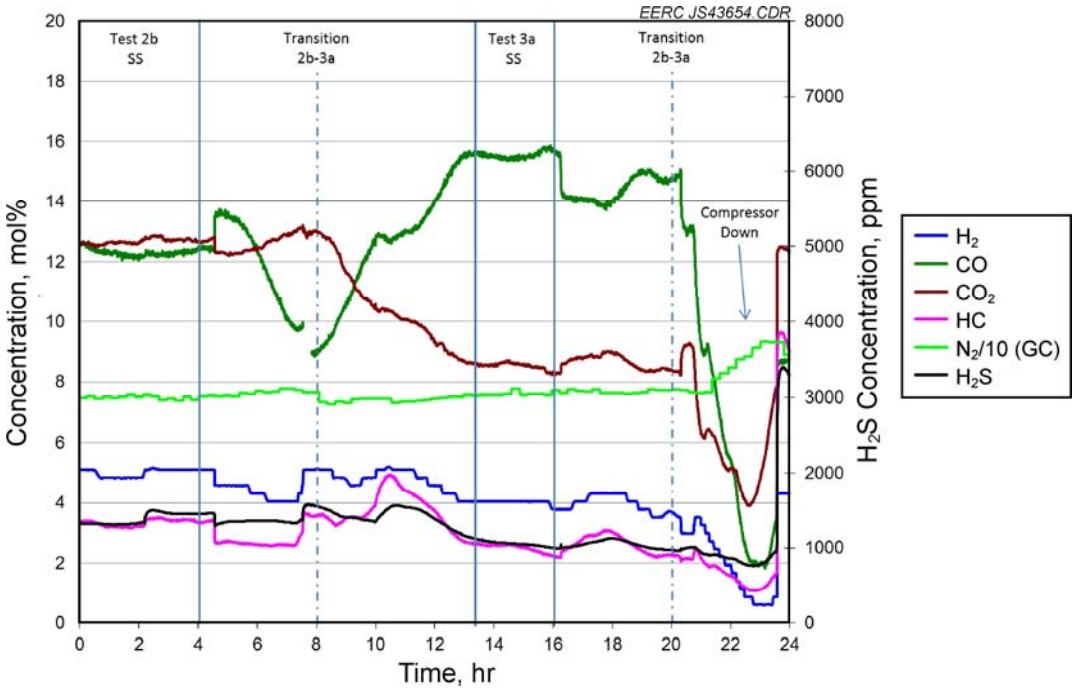

Figure 20. Syngas composition as measured by the CEM on January 17.

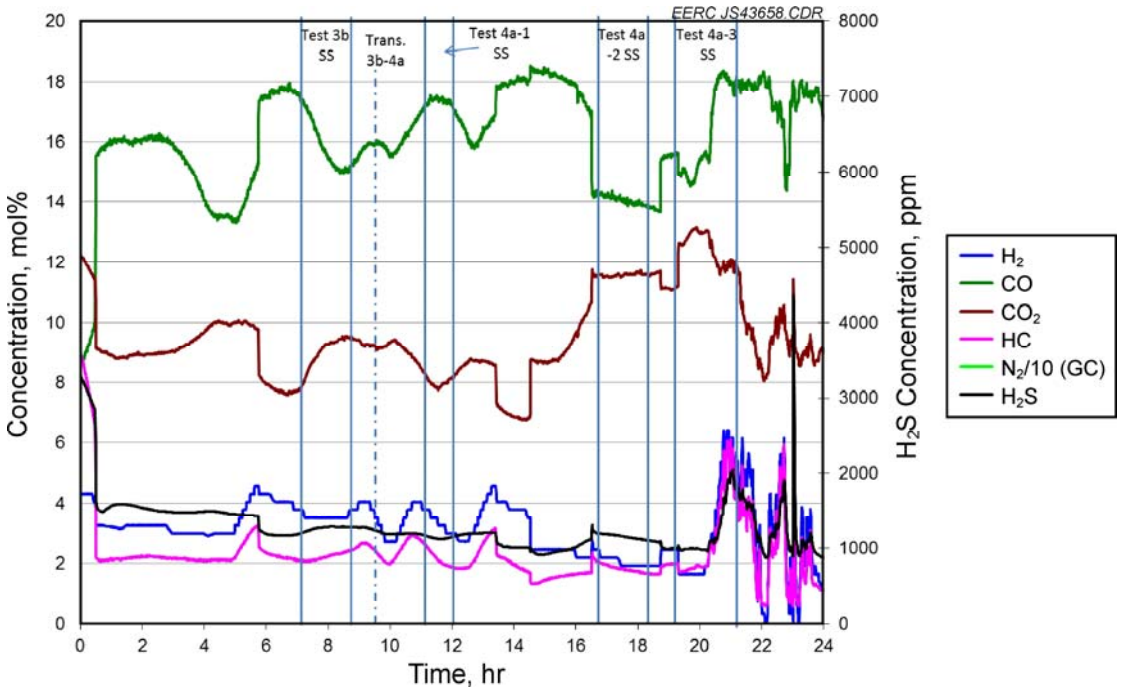

Figure 21. Syngas composition as measured by the CEM on January 18.

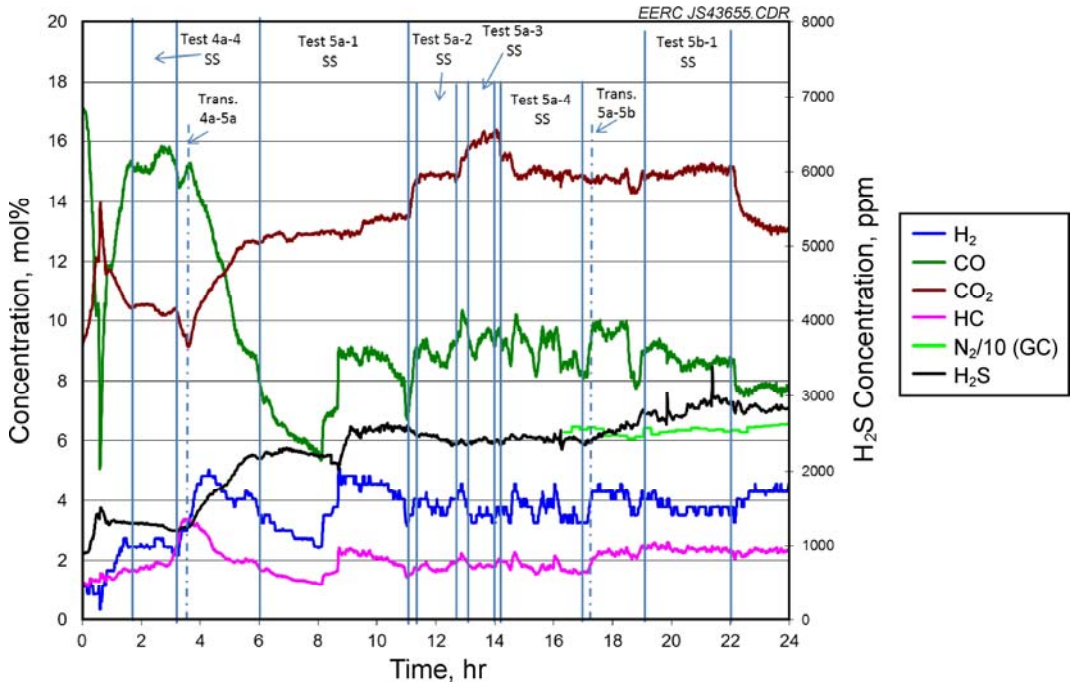

Figure 22. Syngas composition as measured by the CEM on January 19.

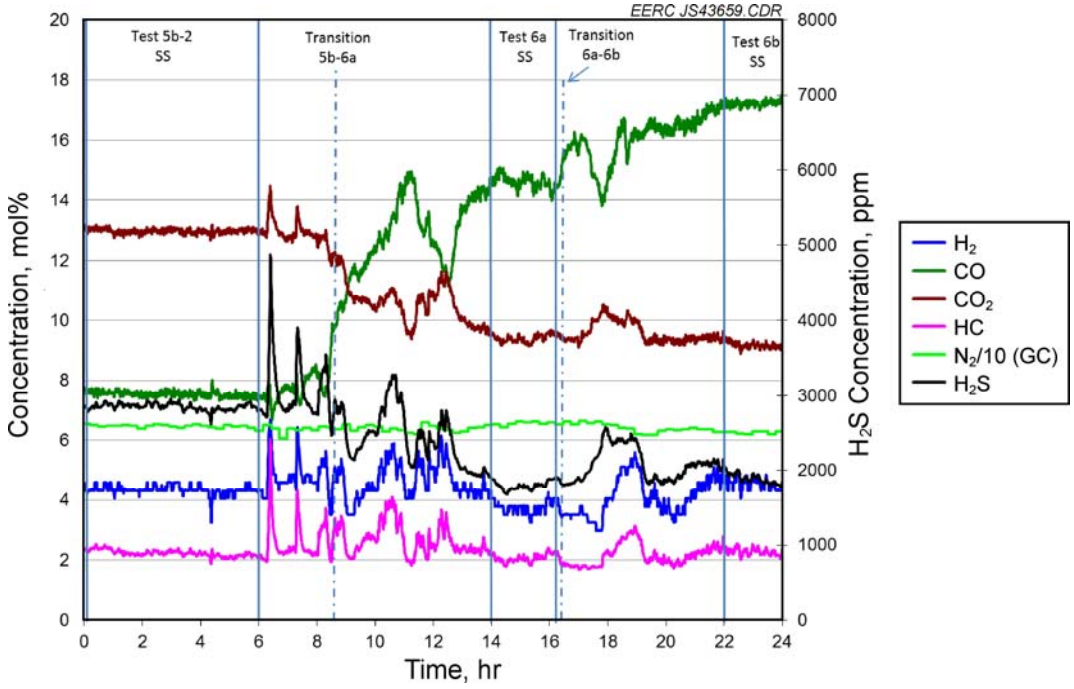

Figure 23. Syngas composition as measured by the CEM on January 20.

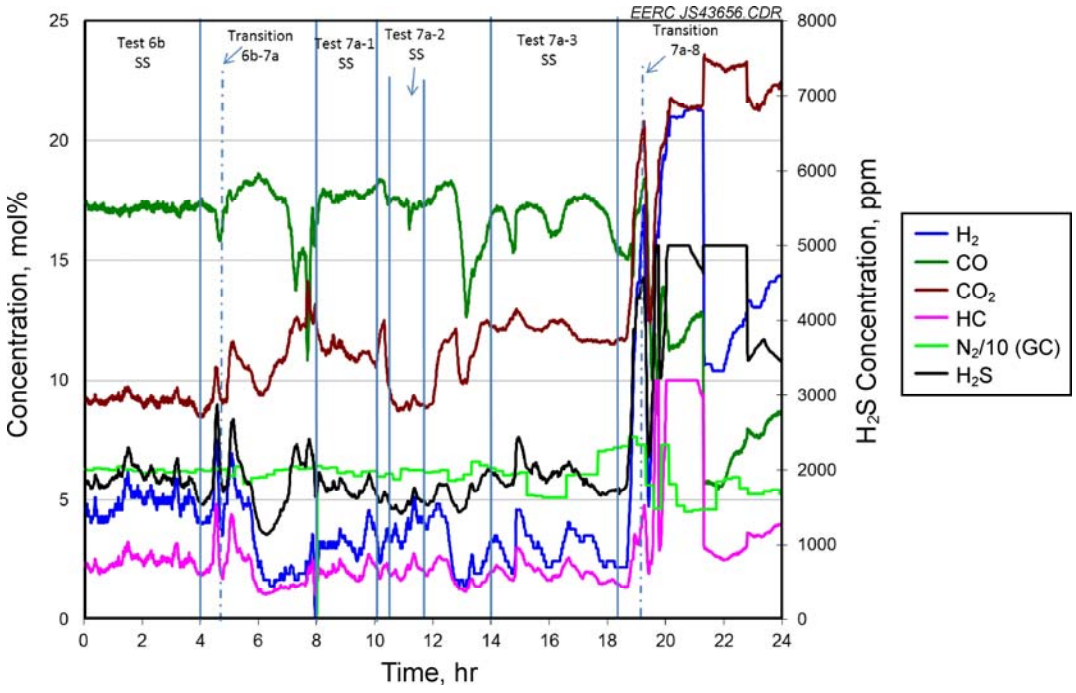

Figure 24. Syngas composition as measured by the CEM on January 21.

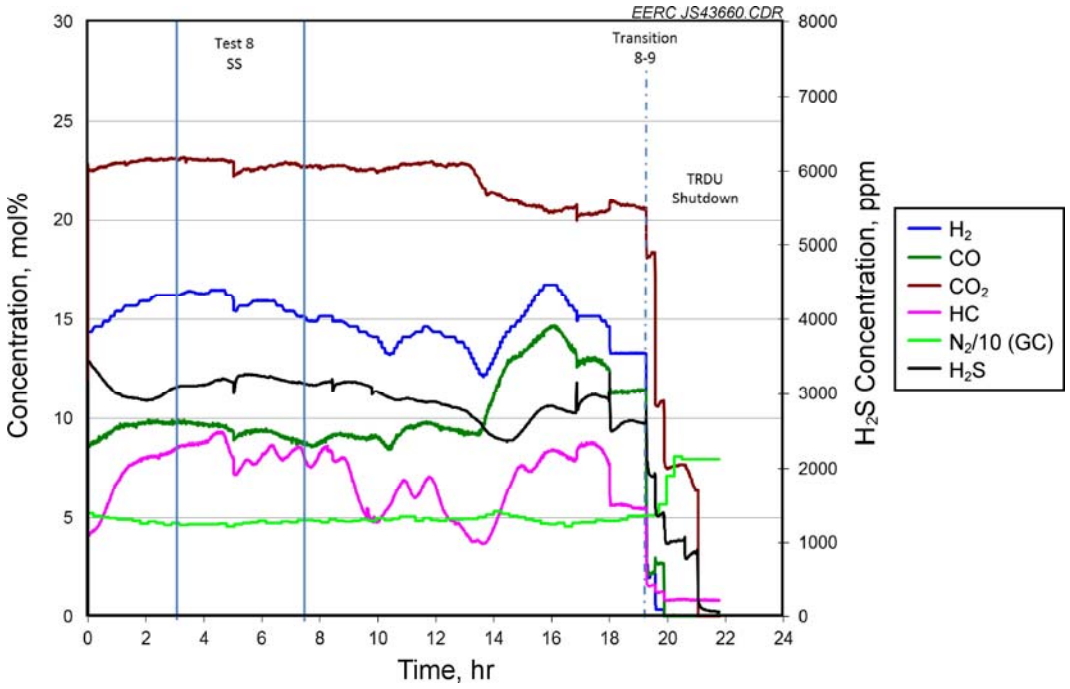

Figure 25. Syngas composition as measured by the CEM on January 22.

Table 20 shows the results of the mercury data by Method 30B and ME-ST samples for the other trace metals. Many nondetects were encountered for the analysis of at least one of the ME-ST trap stages.

Analysis of Solid and Liquid Samples

Throughout the run, solid samples were taken from the coal hopper, SP, and filter vessel. The particle-size distribution was determined for selected runs for each of the solid sample points. Coal and SP samples were analyzed using a dry sieve technique, and filter vessel particle sizes were determined using a Malvern particle-size detector. The largest sieve used was 1680 µm for the coal and 400 µm for the SP samples. Figure 26 shows the particle-size distribution for samples taken during the raw, dried, and treated PRB tests. As expected, the coal particles were the largest with smaller particles extracted from the SP. Particle sizes for the filter vessel samples ranged from 1 to 100 µm. It is difficult to distinguish if there is a significant trend in the filter vessel particle-size distributions based on the test conditions. Temperature and fuel type can have some impact on particle-size, but changing velocity in the reactor also will have a significant impact because it affects the cyclone efficiency. Changes in temperature are also accompanied by changes in the primary airflow rates; therefore, cyclone efficiency is impacted. No clear-cut trend is observed from these data.

Figure 27 shows the particle-size distributions for samples taken during the lignite test runs. For the raw fuel, smaller particles appear to be produced in the filter vessel at lower temperatures. This is counterintuitive based on the kinetics of the carbon–steam reaction; therefore, the cyclone efficiency may be impacted in a negative way at higher airflow rates.

Table 20. Syngas Trace Element Concentration for Selected Tests

	Trace Element Concentration, µg/m^3									
	Raw PRB Test 2a	Dried PRB Test 3a	Dried PRB Test 3b	Treated PRB Test 4a-1	Treated PRB Test 4a-2	Raw Lignite Test 5a-2	Raw Lignite Test 5b-2	Dry Lignite Test 6b	Treated Lignite Test 7a-3	Raw PRB Test 8
Method	30B	ME-ST	M30B	M30B	ME-ST	M30B	ME-ST	M30B	ME-ST	M30B
Sb	NA	<1.1	NA[1]	NA	<1.2	NA	<0.9	NA	<0.8	NA
As	NA	<4.3	NA	NA	<4.3	NA	<3.2	NA	<2.4	NA
Be	NA	<0.2	NA	NA	<0.2	NA	<0.2	NA	<0.1	NA
Cd	NA	<0.3	NA	NA	<0.3	NA	<0.2	NA	<0.1	NA
Cr	NA	38.1	NA	NA	99.6	NA	27.7	NA	28.3	NA
Co	NA	1.6	NA	NA	<8.7	NA	1.0	NA	<0.8	NA
Hg	9.0	<10.9	10.8	7.4	<4.6	6.3	<1.2	8.4	<7.3	10.0
Pb	NA	<1.2	NA	NA	<0.4	NA	1.5	NA	1.1	NA
Mn	NA	41.0	NA	NA	<115.4	NA	36.5	NA	30.3	NA
Ni	NA	29.3	NA	NA	181.3	NA	5.9	NA	5.9	NA
Se	NA	<4.0	NA	NA	<3.6	NA	<0.3	NA	<1.1	NA

[1] Not applicable.

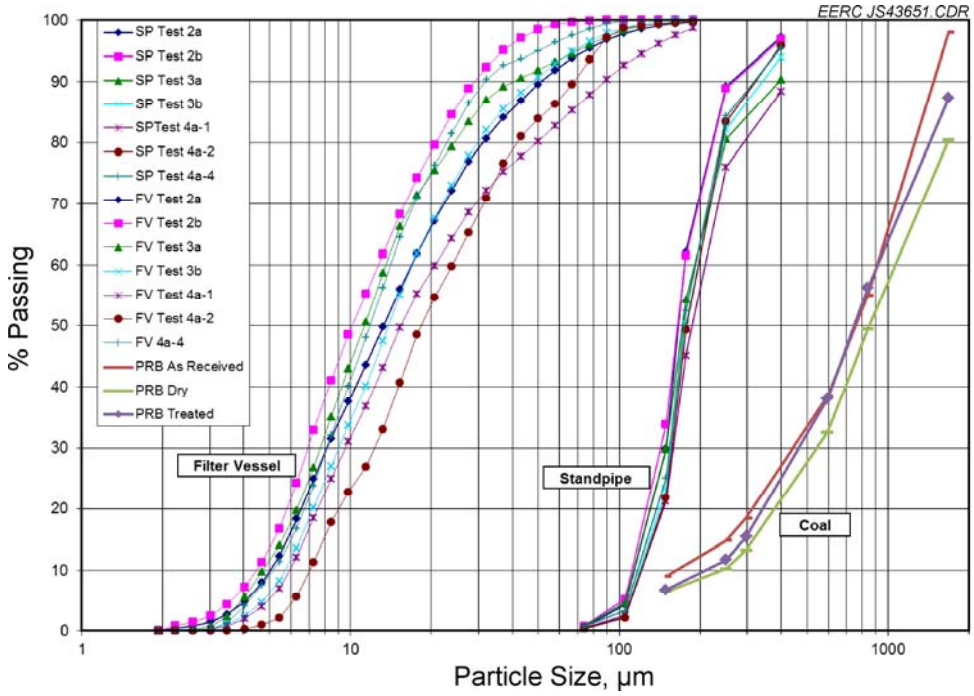

Figure 26. Particle-size distribution for the parametric PRB tests.

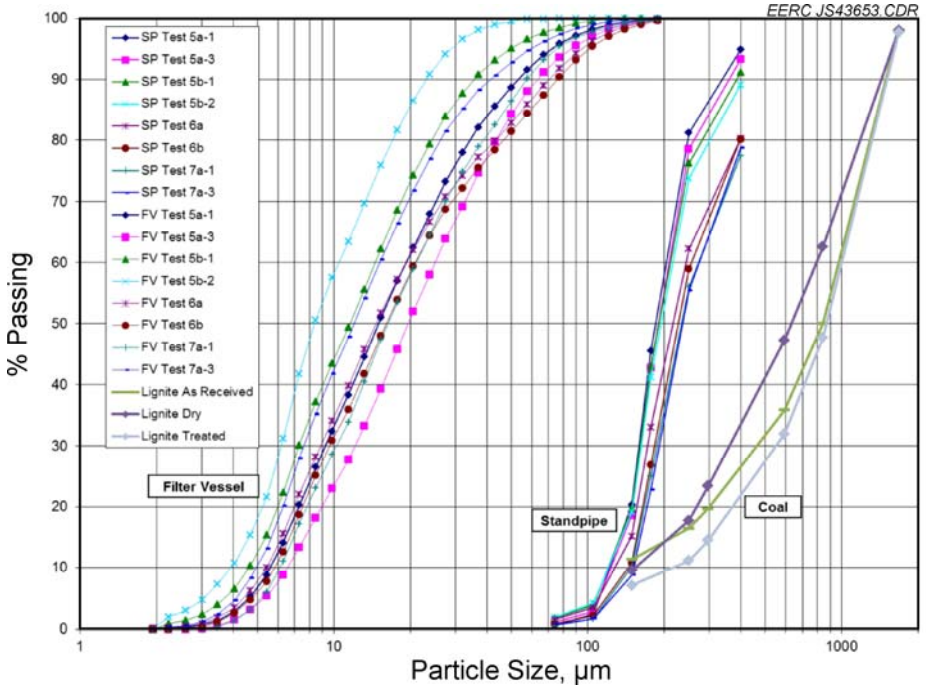

Figure 27. Particle-size distribution for the parametric lignite tests.

Changes in temperature had no impact on the particle-size distribution of the dried fuel. The particle-size distribution of the treated fuels fell within the distributions of the other fuels, indicating the upgrading process has no impact on the filter vessel particle sizes produced from the gasifier. The SP samples did appear to have some top-size differences when evaluating the raw fuel versus the treated and dried. Smaller particles were observed in the SP for the raw fuel as compared to the dried and treated fuels.

Figure 28 shows the particle-size distribution for the oxygen–steam condition, Test 8. The distribution falls in line with the distributions for the other tests, and no significant deviation is observed.

Elemental analysis was also performed on each of the solid samples collected utilizing XRF. Elemental analysis of individual test periods is presented with data from the fuel, SP, and filter vessel in Figures 29–35. Silica in the SP samples was very high because silica sand was used as a start-up bed material for the testing. The silica sand concentration in the SP was reduced over time as it was gradually replaced with coal ash. The filter vessel ash compositions resemble the coal ash composition very closely, indicating that there was no significant ash partitioning occurring between the SP and filter vessel. Higher levels of silica were noted in the filter vessel during Test 3a, which also corresponded to an event where the solids in the gasifier dipleg had blown over to the filter.

Of special interest is the concentration of sulfur in the filter vessel ash. The ash for both fuels was high in calcium, which enables it to capture some sulfur in lower-temperature

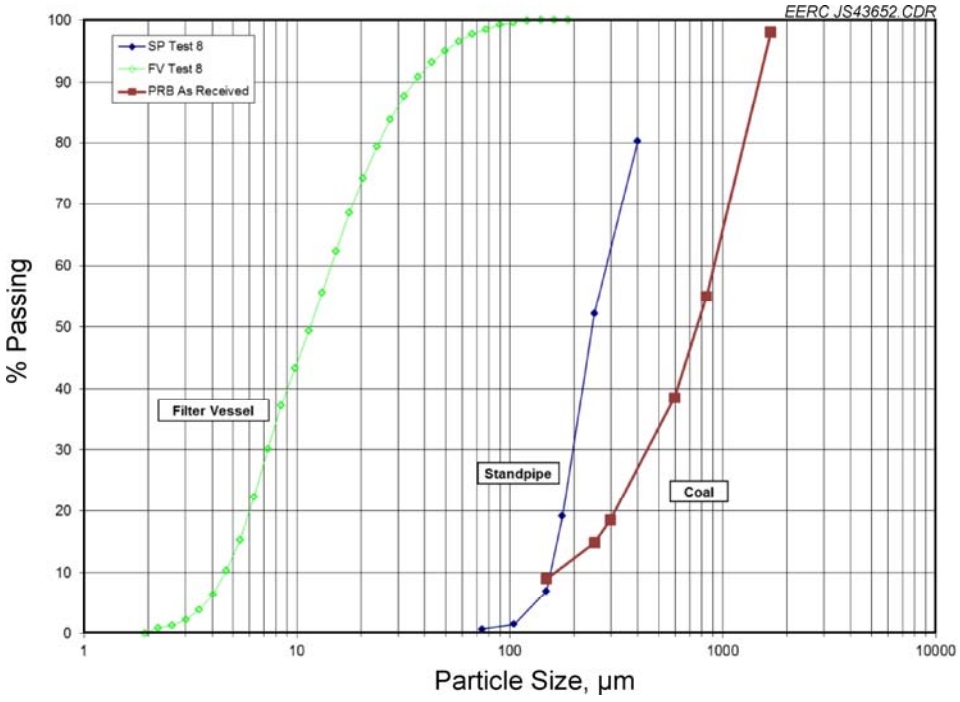

Figure 28. Particle-size distribution for the membrane optimization tests.

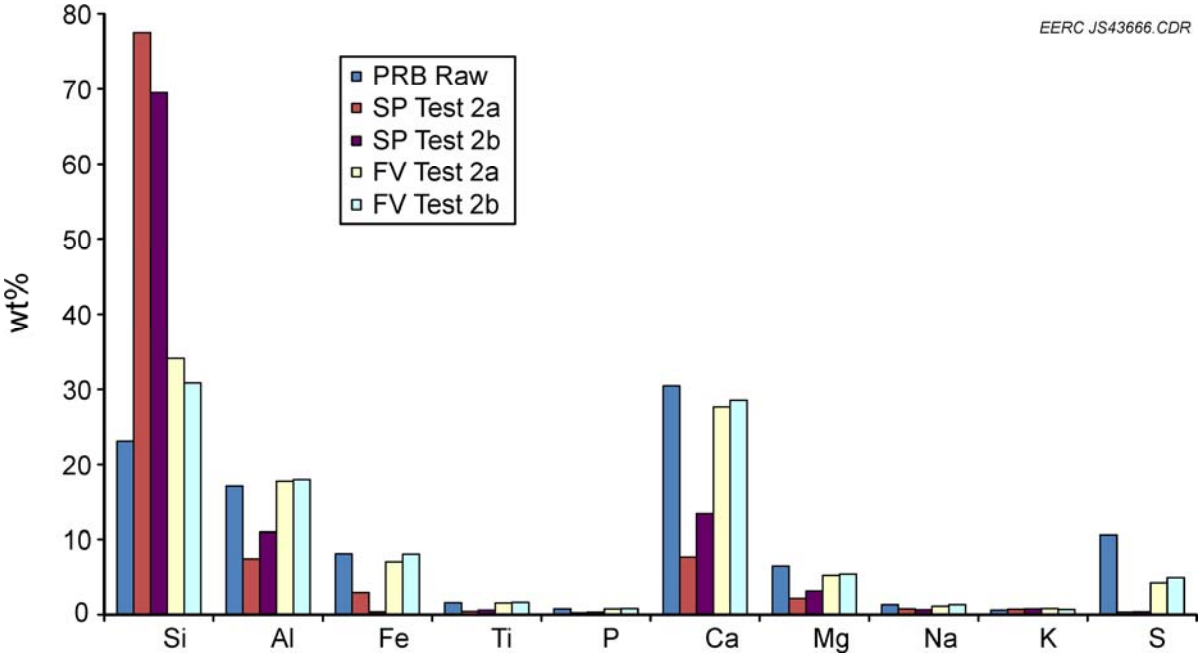

Figure 29. Partitioning of elements from the coal, SP, and filter vessel for Test 2.

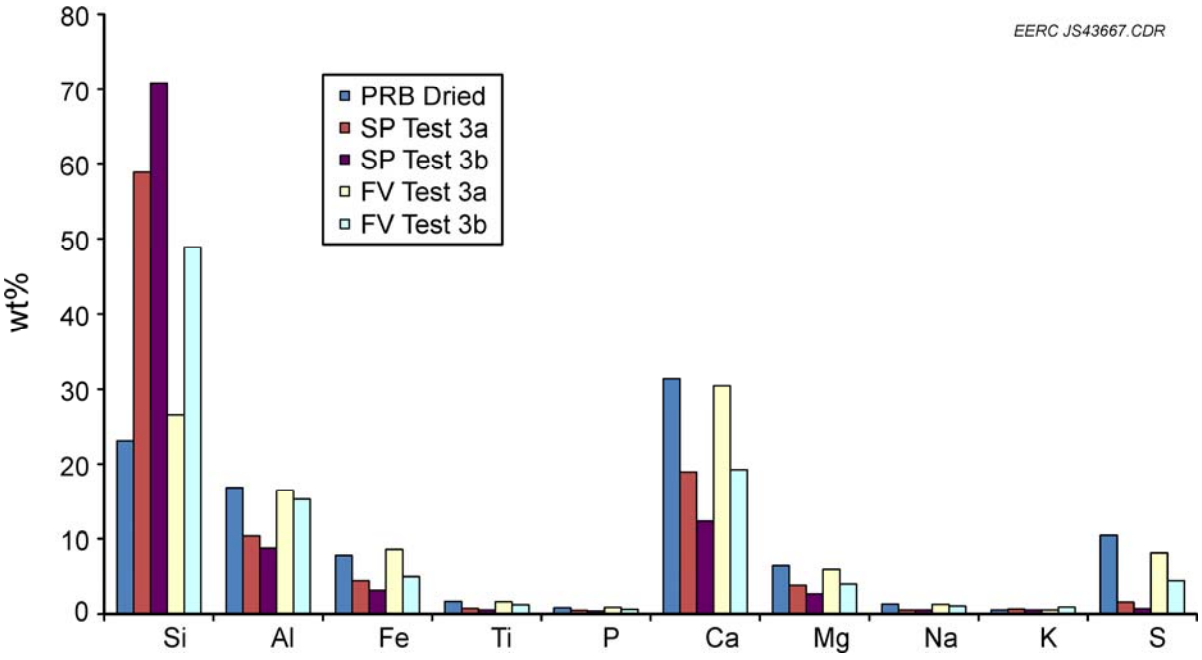

Figure 30. Partitioning of elements from the coal, SP, and filter vessel for Test 3.

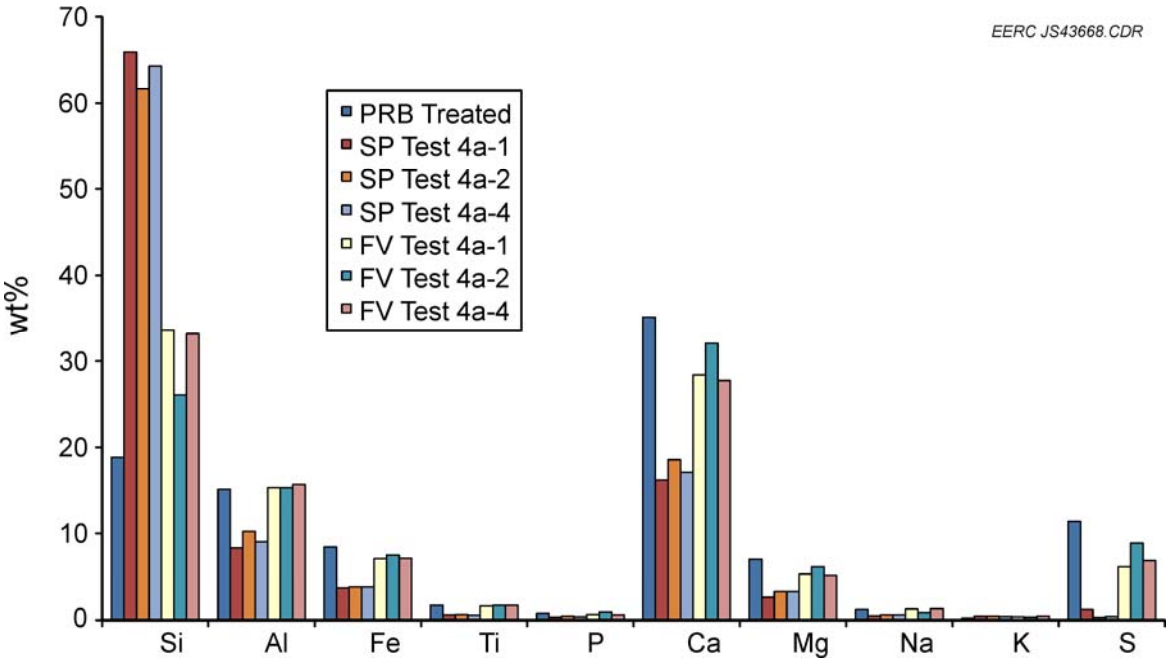

Figure 31. Partitioning of elements from the coal, SP, and filter vessel for Test 4.

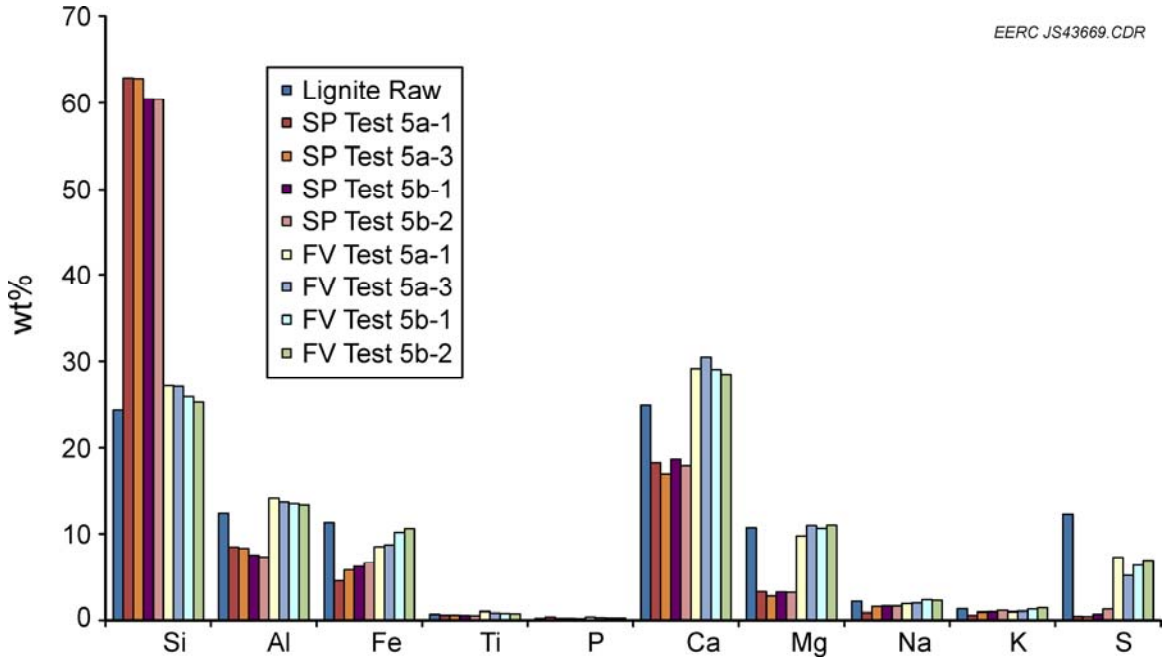

Figure 32. Partitioning of elements from the coal, SP, and filter vessel for Test 5.

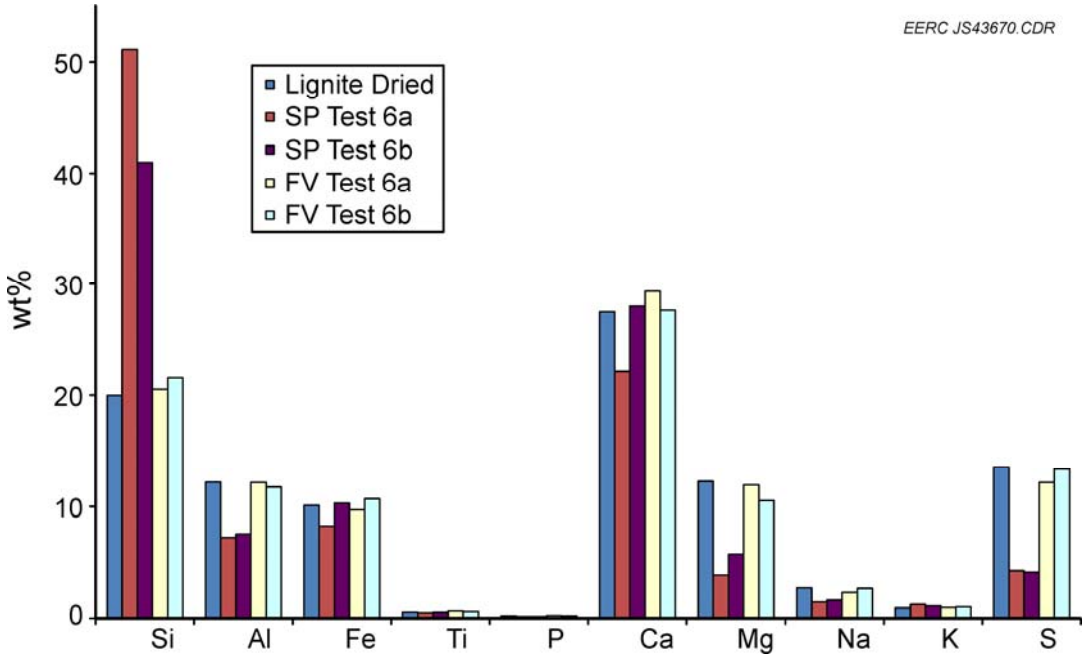

Figure 33. Partitioning of elements from the coal, SP, and filter vessel for Test 6.

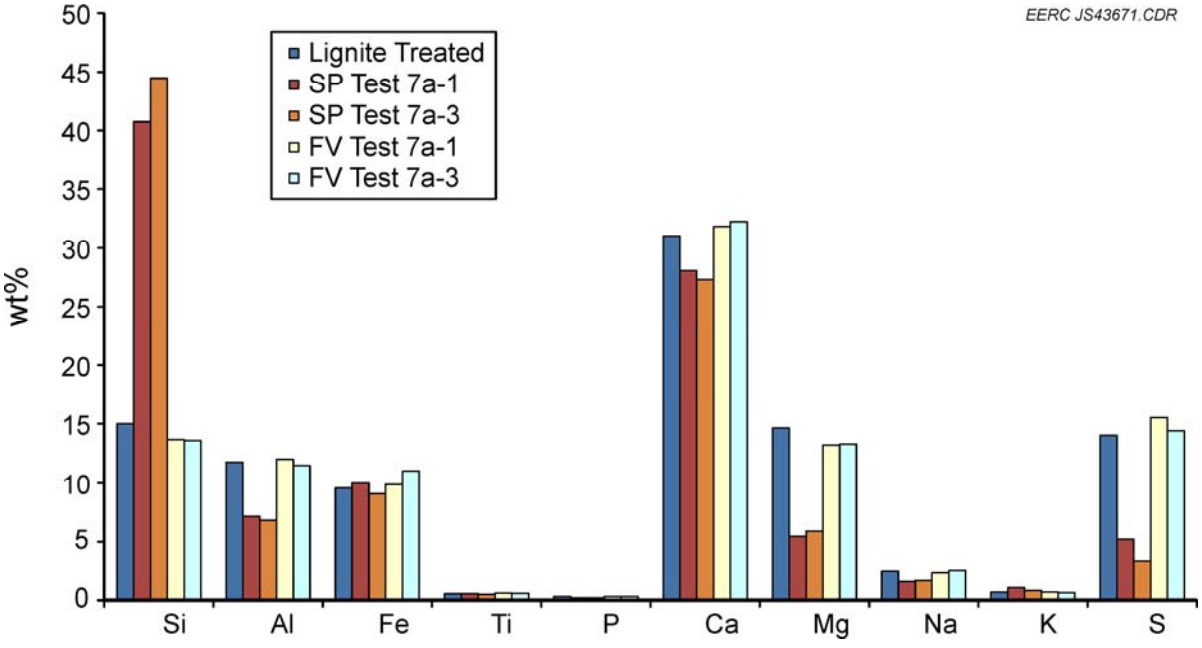

Figure 34. Partitioning of elements from the coal, SP, and filter vessel for Test 7.

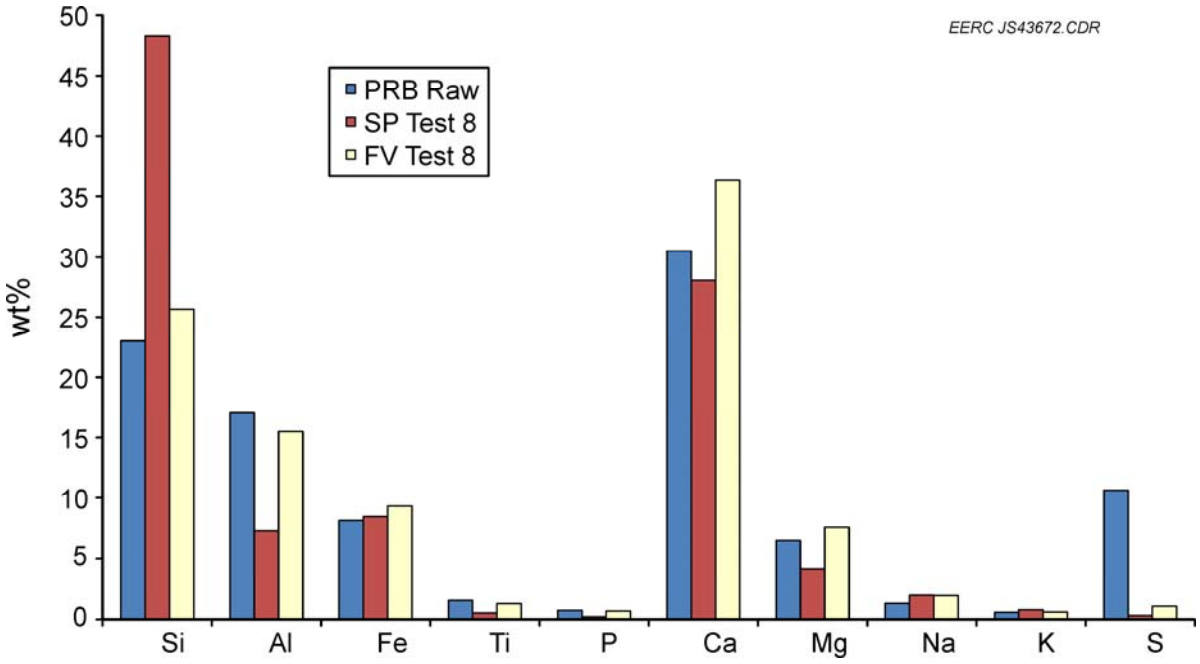

Figure 35. Partitioning of elements from the coal, SP, and filter vessel for Test 8.

gasification systems. The presence of moisture in the syngas inhibits the reaction for sulfur capture with calcium.

The addition of silica sand in the system makes it difficult to determine with certainty any potential impact of the treatment process on the overall ash chemistry. For the lignite test runs, there does appear to be an increase in the calcium content in the filter vessel ash for the dried and treated tests. This is in line with the reduction in silica content noted in the coal ash chemistry. This increase can be beneficial because it promotes additional sulfur capture. It should also be noted that no ash agglomeration issues were observed for any of the fuels over any of the test conditions. Therefore, the small change in ash chemistry with the treated fuels did not result in any detrimental effects and may have improved sulfur capture.

Water samples were also taken during selected test runs just after the HGFV on the TRDU. The water samples were analyzed for total organic compounds (TOCs) and chemical oxygen demand (COD). The concentration of organics is reported on a mg/L-of-liquid-collected basis and on a ppmw-in-syngas basis. The data are presented in Table 21 for the selected SS test periods. The concentration in the liquid-based data does not necessarily represent differences in tar production because the varying levels of moisture that were present in the syngas dilute the samples collected at different rates. Therefore, the data are also presented on a syngas basis.

Samples were collected during the parametric testing for each fuel run; therefore, the impact of fuel type can be evaluated. The tar production does appear to be higher for the raw fuels as compared to the dried and treated fuels. The tests with the raw fuels at higher

Table 21. Analysis of Water Samples Collected

	Liquid Basis		Syngas Basis (average of CEM and GC measurements)			
SS Period	COD, mg/L	TOC, mg/L	COD, ppmw, dry	TOC, ppmw, dry	COD, ppmw, wet	TOC, ppmw, wet
Test 1	1020	350	31	11	30	10
Test 2b	2200	1150	71	37	70	37
Test 3a	1240	960	21	16	21	16
Test 3b	1000	670	14	10	13	9
Test 4a-2	500	160	8	3	7	2
Test 5a-4	600	130	34	7	31	7
Test 5b-2	1440	640	83	37	74	33
Test 6b	440	160	7	3	7	2
Test 7a-3	1200	220	24	4	23	4
Test 8	1580	570	576	208	424	153
Test 8	700	140	246	49	183	37

temperatures clearly indicate reduced tar production, as expected. The lowest tar production occurred during Tests 4a-2 and 6b. Significantly higher levels of organic compounds were produced during Test 8 which included steam and oxygen-blown gasification. The liquid samples collected do not indicate higher concentrations of organics, but this is because the samples are diluted from the steam injection. The calculations on a syngas basis show that the syngas concentration of organic compounds was much higher for Test 8 than for the other tests.

Evaluation of Fuel Performance

A few of the important effects of WRI's fuel-upgrading and gasifier operational modifications process were analyzed in more detail. Figure 36 shows the syngas HHV versus fuel type. The CEM data for the PRB goes against the expected trend because the higher CO contents should lead to a syngas with increased heating value for the treated PRB. This may be a result of higher nitrogen content during the PRB treated test run that occurred because of the air compressor shutdown. The Yokogawa data do show a slight increase in the syngas heating value for the PRB. It is expected that additional testing and optimization of the gasifier settings would clearly show an increase in HHV with the dried and treated fuels. The data from the lignite test help validate this assumption because significantly increased heating values were observed for both the dried and treated fuels. This demonstrates a very significant benefit of WRI's coal-upgrading/gasification process.

Figure 37 illustrates the impact of fuel type and associated WRI gasifier operational modifications on the gasifier CO concentration. Large increases in CO are noted for both the dried and treated fuels. The most significant impact observed was on the CEM lignite data, where the average CO concentration was increased from approximately 8% to 16%.

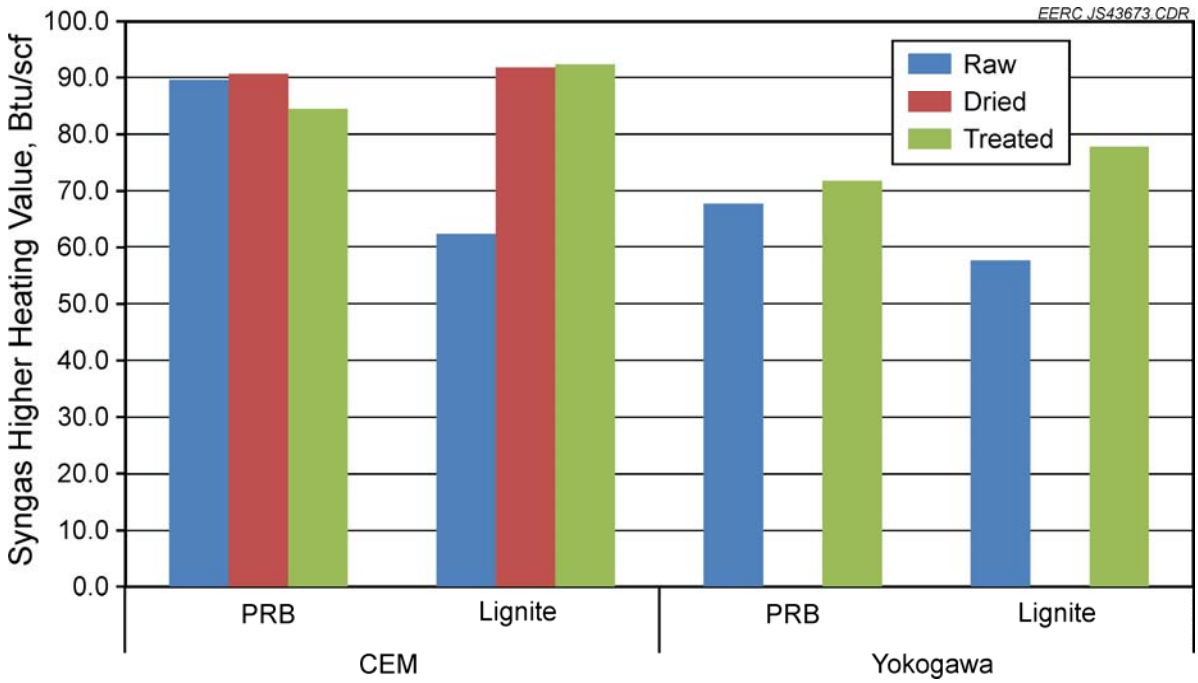

Figure 36. Syngas heating value vs. fuel type.

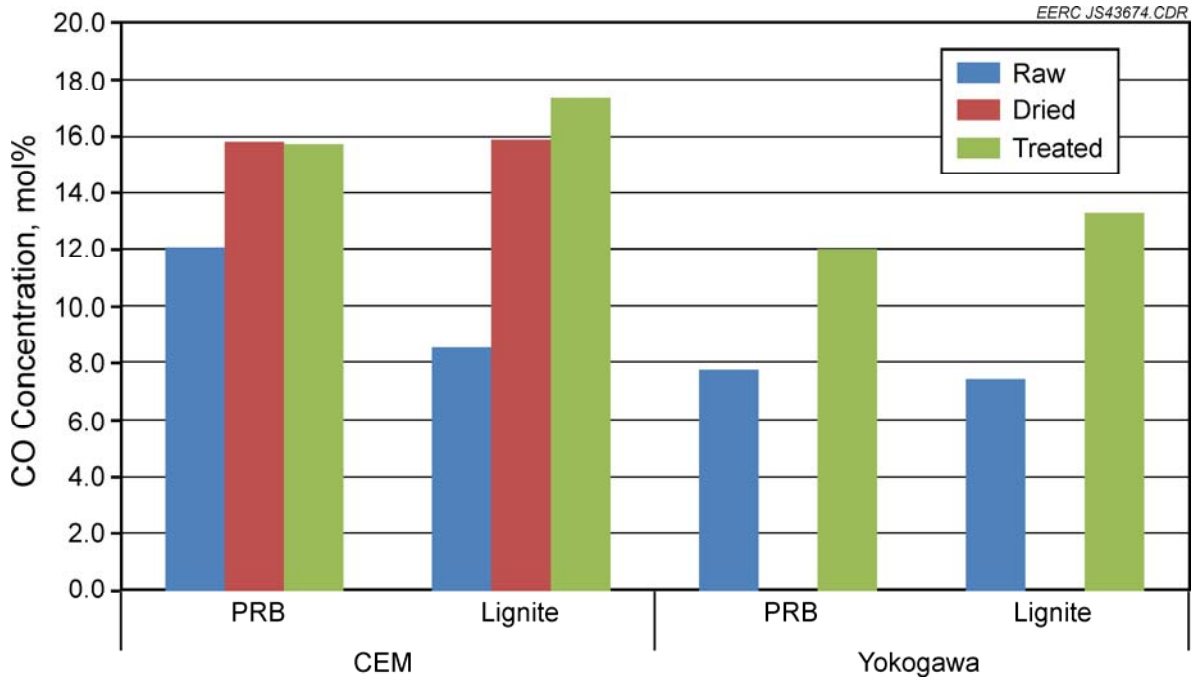

Figure 37. CO concentration vs. fuel type.

The overall impact of temperature on carbon conversion and HHV was also analyzed. From the data shown in Figure 38, no significant impact of temperature is noted on either parameter. Temperature is known to have an impact on carbon conversion; therefore, the data suggest that more testing would be needed to verify and quantify the impact of temperature. Temperature can have a negative impact on syngas HHV because more oxygen is used and more carbon is burned to achieve the higher temperatures. However, it is possible for temperature to have a positive impact on heating value if higher carbon conversion is achieved.

Warm-Gas Cleanup Performance

Heated syngas from the TRDU HGFV was sent through a heat trace tubing bundle from the seventh floor to the first floor of the TRDU tower. The heated tubing bundle was operated at approximately 550°F to prevent syngas components such as moisture and tars from condensing before entering the warm-gas cleanup train. The warm syngas first passed through two shift beds and then through a single fixed bed for desulfurization before being quenched and compressed.

Testing data for the warm-gas cleanup train are presented based on nine individual operating periods. The periods chosen are based on steady inlet gas composition. A summary of the test periods is shown in Table 22. The initial testing started with a hydrogen enrichment test to boost the hydrogen concentration of the syngas stream. The ultrahigh-purity (UHP) hydrogen was used from gas cylinders and mixed with the compressed syngas stream just prior to entering

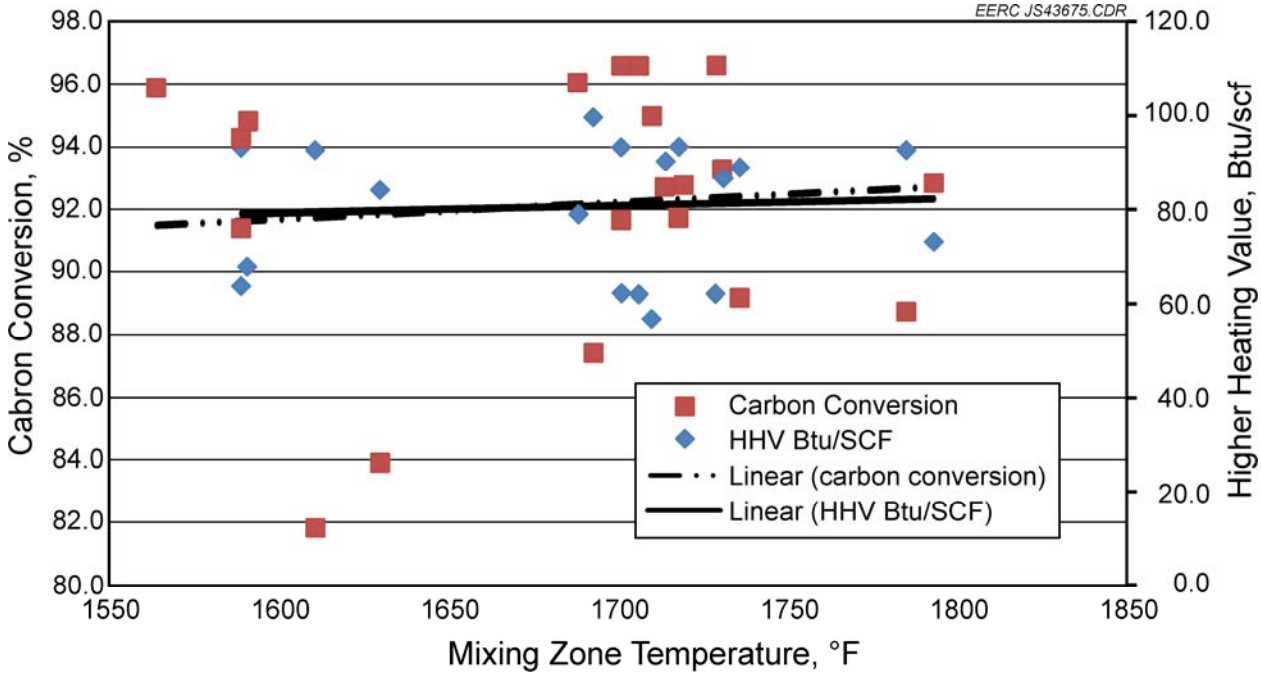

Figure 38. Carbon conversion and HHV vs. temperature.

Table 22. Warm-Gas Cleanup and Membrane Test Periods

Period	Start	End	Description
1	1/17/2012 0:48	1/17/2012 4:37	Gasifier syngas from parametric tests plus H_2 enrichment
2	1/17/2012 10:00	1/17/2012 20:30	Gasifier syngas from parametric tests
3	1/18/2012 1:50	1/18/2012 16:00	Gasifier syngas from parametric tests
4	1/18/2012 16:00	1/18/2012 23:47	Gasifier syngas from parametric tests plus H_2 enrichment
5	1/19/2012 0:00	1/20/2012 7:30	Gasifier syngas from parametric tests
6	1/20/2012 11:00	1/21/2012 13:34	Gasifier syngas from parametric tests
7	1/21/2012 17:30	1/22/2012 0:03	Gasifier syngas from membrane optimization tests
8	1/22/2012 5:00	1/22/2012 16:15	Gasifier syngas from membrane optimization tests
9	1/22/2012 16:30	1/22/2012 18:50	Gasifier syngas plus partial desulfurizer bypass (Membrane 2 only)

the membrane regulators and preheater. The next two runs received syngas from the TRDU parametric test plan. The fourth period was a second hydrogen enrichment test. Periods 5 and 6 were run with syngas from the lignite parametric tests. Periods 7 and 8 occurred when the gasifier was transitioned to oxygen-blown mode for maximizing the hydrogen content of the syngas stream. Period 9 consisted of a partial bypass of the desulfurization beds, which brought higher levels of sulfur to the membrane skid. Only Membrane 2 was used for this test.

Operating data for the fixed-bed reactors are shown in Table 23. Steam injection occurred just prior to Bed 1. Steam injection was increased after Test Period 1 to drive the shift reaction toward more hydrogen production. Steam ran near 170 scfh for Periods 2–6. For Periods 7–9, the steam was turned down because steam was being added to the TRDU. Shift Bed 1 was run at a higher temperature than Shift Bed 2, and was operated near 600°F for most of the testing. Shift

Table 23. Fixed-Bed Reactor Operating Data

	Steam Injection	System Pressure,	Fixed-Bed Temperatures, °F			
Period	Rate, scfh	psi	Shift Bed 1	Shift Bed 2	RVS-1 Bed 3	RVS-1 Bed 4
1	124	114	590	470	Offline	517
2	163	115	595	480	Offline	523
3	165	115	601	451	Offline	504
4	175	115	606	446	Offline	505
5	178	115	610	430	546	504
6	178	115	606	432	550	Offline
7	120	115	594	442	550	Offline
8	50	116	578	409	568	476
9	63	116	588	410	Offline	513

Bed 2 was run at a lower temperature, ranging from 409° to 470°F for the testing. Of the two RVS-1 beds, Bed 4 was used first and ran near 500°F for the testing. Increased temperature increases the reaction rate kinetics of the sorbent and, therefore, improves capture but also decreases the amount of sulfur the sorbent can hold. Bed 3 ran near 550°F when it was online. Temperatures are shown when each bed was online. The beds were switched during SS Periods 5 and 8.

Quench pot temperature data are shown in Table 24. The syngas entered the quench pots at approximately 300°F and was reduced to around 75°F by the end of the sixth pot. The temperature was variable based on the syngas flow rate. Three additional quench pots were used after these, including a final ice knockout pot. The temperature of the syngas was not measured after the last pot but was assumed to be reduced to approximately 50°F before the gas boosters.

Syngas concentration was measured after the shift, desulfurization, quench, and compression steps but just prior to entering the membrane. Table 25 shows the syngas concentration for the SS test periods. The shift catalyst performed well throughout the testing, with CO levels below 1.5% for the duration of the run and averaging 0.7% for the week. Hydrogen concentrations were flow from the gasifier during the parametric test runs, averaging 12.7%. Therefore, the hydrogen level was increased for SS Periods 1 and 4 by injecting hydrogen from a hydrogen gas cylinder. This injection resulted in an average hydrogen concentration of 29.6% for SS Period 1 and 34.7% for SS Period 4. Hydrogen concentration increased during the membrane optimization tests and was 18.5% for SS period 7 and 23.5% for SS Period 8. Nitrogen concentrations were high throughout the week, even for the oxygen-blown tests. The N_2 concentration was still near 50% for the oxygen-blown runs because of the high level of nitrogen purging required for gasifier operation.

Table 24. Quench Pot Data

Period	Pot 1 Inlet, °F	Pot 1 Outlet, °F	Pot 2 Outlet, °F	Pot 3 Outlet, °F	Pot 4 Outlet, °F	Pot 5 Outlet, °F	Pot 6 Outlet, °F
SS1	312.6	244.3	166.3	134.8	104.3	96.6	82.8
SS2	319.7	258.9	177.8	146.3	110.7	102.1	92.9
SS3	321.3	262.0	178.5	147.0	112.1	104.0	73.8
SS4	318.2	264.6	183.2	149.6	111.9	103.2	66.3
SS5	307.0	270.8	198.0	162.2	119.2	107.2	70.8
SS6	308.1	267.6	189.0	152.4	110.0	99.1	87.5
SS7	307.7	284.6	213.6	180.1	134.6	117.2	100.9
SS8	293.6	253.2	192.6	154.6	115.2	98.8	74.6
SS9	284.5	254.6	192.5	157.0	117.9	110.4	54.6

Table 25. Syngas Composition after WGS and Desulfurization

Operating Period	CEM Conc., mol%					GC Conc., mol%					Dräger Tube, mol%
	H_2	CO	CO_2	N_2	CH_4	H_2	CO	CO_2	N_2	CH_4	H_2S
SS1	29.6	0.7	12.5	55.4	0.8	25.9	0.5	11.6	50.1	0.9	1.7
SS2	12.7	1.0	14.7	69.4	0.8	13.0	0.9	14.0	61.8	0.9	1.6
SS3	13.5	1.4	15.4	68.7	0.8	13.0	1.0	14.8	60.9	1.0	0.8
SS4	34.8	0.8	13.2	51.6	0.5	35.6	0.3	12.1	44.2	0.5	0.6
SS5	10.9	0.3	16.2	71.8	0.6	11.4	0.2	14.5	63.1	0.8	1.9
SS6	13.6	0.4	16.4	67.5	0.6	14.6	0.4	16.5	58.5	0.8	0.2
SS7	18.5	0.4	23.8	55.1	1.2	NA	NA	NA	NA	NA	7.0
SS8	20.0	0.4	26.8	49.5	1.9	21.2	0.3	27.8	52.3	2.6	4.9

Dräger tubes were used to monitor the sulfur (H_2S) concentration of the syngas because the sulfur levels were typically below the detection limit for any of the online analyzers. Figure 39 shows the concentration of H_2S through the week. The H_2S levels remained near or below 2 ppm for the majority of the week. The first spike observed in H_2S levels occurred when Bed 4 initially experienced breakthrough on January 19 during SS Period 5. The highest level of H_2S observed for this event was 10 ppm, and for a duration of less than 30 minutes. Bed 3 was brought online

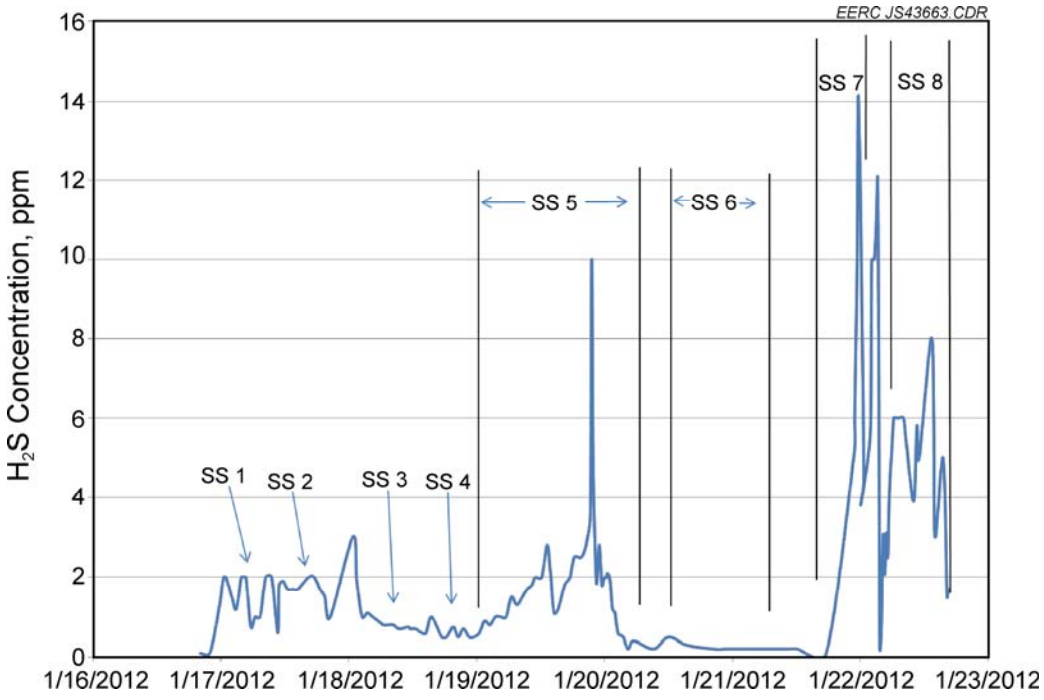

Figure 39. Dräger tube H_2S concentration.

and sulfur immediately dropped to 5 ppm and then went below 1 ppm after about 5 hours. Bed 3 then experienced breakthrough more quickly, likely because of firing the lignite coal, which is higher in sulfur than the PRB. Bed 4 was not fully regenerated, so the membranes were taken offline at 00:03 on 1/22/12. The feed coal was switched back to PRB, and flows were reduced so Bed 3 was again capable of performing the sulfur removal to around 6 ppm. Flows were restarted to the membranes at 04:40. Bed 4 was brought online at 14:29, and sulfur levels started to drop below 2 ppm, but then Membrane 1 was taken off-line and the sulfur spike test started for Membrane 2. The highest H_2S observed during the period was 14 ppm, and the membranes were taken off-line 20 minutes after this peak was observed. The membranes were brought back online, and the sulfur ran between 4 and 8 ppm for approximately 9 hours.

Tables 26 and 27 show the results of sampling for NH_3, HCN, and HCl using Dräger tubes at both hot- and cold-side sampling locations. The components will condense through the quench pots, so sampling, both hot and cold, was performed to understand the impact. The Dräger tubes can be difficult to use at a hot-side sample location because any water condensation will interfere with the results. The data in Table 28 indicate that there was ammonia present in the syngas but the hot sampling technique made it difficult to quantify, with a couple of measurements at 70 ppm. One measurement indicated 5 ppm of HCl also present in the syngas. The cold-side readings, which should be more accurate, indicated a maximum of 10 ppm NH_3 after the quench train, and no HCN or HCl was detected.

Table 26. Hot-Side Sampling for Condensable Trace Components

			Concentration, ppm		
Date	Time	Sample Location	NH_3	HCN	HCl
1/16/12	22:07	Port B	0	0	0
1/18/12	01:35	Port B	0	0	0
1/18/12	05:37	Port B	70	0	0
1/18/12	12:30	Port B	0	0	0
1/19/12	00:13	Port B	70	0	0
1/21/12	13:45	Port B	0	0	5

Table 27. Cold-Side Sampling for Condensable Trace Components

			Concentration, ppm		
Date	Time	Sample Location	NH_3	HCN	HCl
1/17/12	4:31	7th quench pot	10	0	
1/17/12	4:43	Port C			0
1/17/12	8:57	7th quench pot	10		
1/17/12	16:27	Port C	0	0	0
1/18/12	529	7th quench pot	5		
1/20/12	234	Port C	0	0	0
1/20/12	1225	Port C	0	0	0
1/20/12	2233	7th quench pot	0	0	0

Table 28. Mercury Sampling at Sample Port C

Test	Total, μg/m$_3$	Location	Method
SS1	<0.01	1st	ME-ST
SS3	1.51	1st	M30B
SS4	0.89	1st	M30B
SS5	0.95	1st	M30B
SS5	<0.09	1st	ME-ST

The results of mercury and trace metal sampling are shown in Tables 28 and 29. The mercury concentration appears to have dropped by about a factor of 10 through the gas cleanup train and quench pots. Previous testing experience at the EERC suggests that the mercury is removed through the quench train when organics are present in the quench water. Trace metal detection was again an issue for this sample location. The trace metal concentrations did not appear to change significantly through the sample train.

Hydrogen Separation Membrane Performance

Two membranes, designated Membrane 1 and Membrane 2 were tested in parallel. The membrane temperature as well as the gas pressure entering each membrane was separately controlled. Sampling of the inlet syngas was performed by LGA and GC prior to the gas entering the preheater. H_2S, NH_3, HCN, and HCl concentrations were also periodically monitored at the same sampling location as well as before and after the quench pots using Dräger tubes. The permeate and raffinate from the membranes were sampled alternately by another LGA and GC pair operating in parallel. Figure 13 shows the overall system layout.

During the weeklong test, eight periods of stable operation were identified for analysis. At the end of the test, Membrane 2 only was subjected to five levels of increased H_2S concentration for relatively short (0.5 hour) periods. H_2S was increased by partially bypassing the fixed-bed desulfurization unit. Tables 30–32 give the general operating condition for the membranes during these periods. In the table, it should be noted that the syngas entering the membranes was

Table 29. Trace Metal Sampling at Sample Port C

Trace Element, μg/m^3	SS1	SS5
Sb	<0.9	<0.9
As	<3.1	<2.9
Be	<0.2	<0.2
Cd	<1.0	<1.0
Cr	28.5	45.7
Co	<1.0	1.3
Pb	<1.3	1.5
Mn	33.7	<61.5
Ni	5.4	6.5
Se	<0.2	<0.2

Table 30. Membrane 1 Operating Parameters During each SS Period

Operating Period:	SS1	SS2	SS3	SS4	SS5	SS6	SS7	SS8
Start:	17-Jan 0:48	17-Jan 10:00	18-Jan 1:50	18-Jan 16:00	19-Jan 0:00	20-Jan 11:00	21-Jan 17:30	22-Jan 5:00
End:	17-Jan 4:37	17-Jan 20:30	18-Jan 16:00	18-Jan 23:47	20-Jan 7:30	21-Jan 13:34	22-Jan 0:03	22-Jan 16:15
Membrane Inlet, °F	923	919	922	926	923	921	918	925
Membrane Temperature, °F	930	929	930	931	930	930	931	931
Permeate Exit, °F	53	54	55	51	60	60	59	62
Syngas Inlet, °F	916	908	909	919	902	910	922	908
Syngas Inlet Pressure, psi	396	388	401	407	401	401	402	400
Permeate Pressure, in. H_2O	71	53	52	65	33	39	39	26
H_2 Inlet, mol%	29.6	12.7	13.5	34.8	10.9	13.6	18.5	20.0
Wet H_2 Inlet, mol%	29.6	12.7	13.5	34.8	10.9	13.6	18.5	20.0
Raffinate H_2, mol%	22.3	9.6	10.6	29.7	8.9	11.5	15.5	15.6
Inlet H_2, scfh	74.0	26.2	27.5	82.6	16.7	21.4	26.2	17.9
Raffinate H_2, scfh	50.1	19.1	21.1	64.0	13.5	17.5	21.2	15.6
Permeate H_2, scfh	22.6	6.5	5.6	20.2	3.0	4.8	5.5	3.4
Permeate H_2, lb/day	2.8	0.8	0.7	2.5	0.4	0.6	0.7	0.4
H_2 Balance, %	104.9	97.3	98.6	105.2	99.8	105.2	105.6	108.1
Hydrogen Recovery, %	30.8	24.3	20.4	24.3	18.8	22.7	20.9	19.4
Theoretical Max. Recovery, %	89.6	71.3	74.9	92.6	68.4	75.6	81.9	83.5
Partial Press. Differential, psi	116.0	48.5	53.0	140.8	42.9	53.7	73.7	93.1

effectively dry because of the need to remove moisture before compressing it. No direct pressure measurement was available for the syngas entering the membranes; the inlet pressure reported is the pressure of the raffinate. The permeate exit temperature reported is after the H_2 has been cooled after leaving the membranes. During the high-H_2S testing, the outlet gas analyzers monitored only the Membrane 2 permeate stream, so no raffinate H_2 concentration or H_2 balance is available for these time periods.

As shown in Table 30, Membrane 1 was operated near 930°F and 400 psi during the weeklong test run. Because of the relatively low hydrogen levels provided by the gasifier, hydrogen was added to the syngas stream to improve the partial pressure and test the membranes under conditions closer to the recommended DOE guidelines. The inlet hydrogen concentration was increased to 29.6% for SS1 and 34.8% for SS4. This increase significantly increased hydrogen flux through the membrane, and the DOE target of 2 lb/day was met for the membrane under these test periods. The hydrogen production averaged 2.8 lb/day for SS1 and 2.5 lb/day for SS4. The hydrogen balance was reasonable for the test run, typically ±5% for the test runs, with slightly more deviation observed for SS8. Hydrogen recoveries were low because the test and test apparatus were not designed for high hydrogen recovery but, rather, to demonstrate the flux rate of the system. Membrane 1 appeared to experience some performance degradation through the test. This degradation may have been caused by coking that may have been produced by high

CO levels that occurred when the pump for steam injection into the shift bed failed. After the test run was completed, the membrane was returned to the supplier where lower-than-expected performance was confirmed. After oxidation of the membrane, testing at the supplier indicated the membrane returned to its expected flux rate.

Table 31 shows the operating parameters for Membrane 2, with the system operated near 750°F and 200 psi. The DOE target of 2 lb/day of hydrogen production was met during SS4 with a permeate hydrogen flow of 2.3 lb/day. Hydrogen balance for the run was 100 ± 10%. Recoveries were low because the membrane and test conditions were not designed for high hydrogen recovery but, rather, to demonstrate the flux rate of the system. The membrane did develop a slight leak partway through the testing. By the end of the test, the leak rate on pure N_2 was 4.6 scfh at 200 psi.

The membrane operating parameters for the high-sulfur test are shown in Table 32. As expected, the data clearly show a trend of decreasing flux rate with increasing H_2S concentrations. The membrane shows that it can still produce hydrogen at high sulfur levels. The

Table 31. Membrane 2 Operating Parameters During each SS Period

Operating Period:	SS1	SS2	SS3	SS4	SS5	SS6	SS7	SS8
Start:	17-Jan 0:48	17-Jan 10:00	18-Jan 1:50	18-Jan 16:00	19-Jan 0:00	20-Jan 11:00	21-Jan 17:30	22-Jan 5:00
End:	17-Jan 4:37	17-Jan 20:30	18-Jan 16:00	18-Jan 23:47	20-Jan 7:30	21-Jan 13:34	22-Jan 0:03	22-Jan 16:00
Membrane Inlet, °F	749	759	758	754	770	781	806	812
Membrane Temperature, °F	746	748	747	745	744	744	742	735
Permeate Exit, °F	55	55	57	53	62	63	61	65
Syngas Inlet, °F	916	908	909	919	902	910	922	908
Syngas Inlet Pressure, psi	213	190	215	214	211	211	215	204
Permeate Pressure, in. H_2O	74	62	64	72	53	57	58	45
H_2 Inlet, mol%	29.6	12.7	13.5	34.8	10.9	13.6	18.5	20.0
Wet H_2 Inlet, mol%	29.6	12.7	13.5	34.8	10.9	13.6	18.5	20.0
Raffinate H_2, mol%	22.6	11.3	11.6	28.5	9.2	11.0	15.0	20.6
Inlet H_2, scfh	72.7	25.0	27.1	80.6	16.9	21.3	26.8	27.0
Raffinate H_2, scfh	52.3	21.9	22.8	60.1	14.0	16.2	20.3	16.6
Permeate H_2, scfh	12.1	2.0	3.8	18.3	2.5	5.3	6.8	5.9
Permeate H_2, lb/day	1.5	0.3	0.5	2.3	0.3	0.7	0.8	0.7
H_2 Balance, %	90.9	95.5	99.8	98.0	99.1	101.7	105.9	108.4
Hydrogen Recovery, %	16.2	7.9	13.9	22.7	15.6	25.1	25.9	31.4
Theoretical Max. Recovery, %	80.2	37.4	51.6	85.4	37.8	51.8	64.9	66.2
Partial Press. Differential, psi	61.8	23.0	27.8	73.4	21.9	27.6	38.8	47.3

Table 32. Membrane 2 Average Operating Conditions During High-Sulfur Testing

Operating Period:	Baseline	H_2S Level 1	H_2S Level 2	H_2S Level 3	H_2S Level 4	H_2S Level 5
Start:	22-Jan 16:00	22-Jan 16:40	22-Jan 17:12	22-Jan 17:46	22-Jan 18:08	22-Jan 18:41
End:	22-Jan 16:30	22-Jan 17:10	22-Jan 17:36	22-Jan 17:58	22-Jan 18:33	22-Jan 18:53
H_2S Conc. Dräger, ppm	2	32	90	265	427	550
Membrane Inlet, °F	816	778	759	755	755	757
Membrane Temperature, °F	739	746	739	739	740	741
Permeate Exit, °F	66	66	65	65	65	64
Syngas Inlet, °F	807	399	268	193	148	120
Syngas Inlet Pressure, psi	203	225	225	225	225	223
Permeate Pressure, in. H_2O	50	57	55	54	54	55
H_2 Inlet, mol%	20.7	20.7	18.4	19.4	19.5	19.2
Wet H_2 Inlet, mol%	20.7	20.7	18.4	19.4	19.5	19.2
Raffinate H_2, mol%	16.8	n/a[1]	n/a	n/a	n/a	n/a
Inlet H_2, scfh	31.0	48.8	42.4	44.2	44.3	43.4
Raffinate H_2, scfh	17.0	n/a	n/a	n/a	n/a	n/a
Permeate H_2, scfh	7.8	6.7	4.2	3.9	3.4	3.4
Permeate H_2, lb/day	1.0	0.8	0.5	0.5	0.4	0.4
H_2 Balance, %	104.8	n/a	n/a	n/a	n/a	n/a
Hydrogen Recovery, %	33.2	13.6	9.8	8.8	7.6	7.9
Theoretical Max. Recovery, %	70.0	73.0	69.1	70.9	71.2	70.4
Partial Press. Differential, psi	41.2	45.4	40.5	42.5	42.9	41.9

[1] Not available.

hydrogen flow for Level 5 was 3.4 scfh, and the hydrogen leak rate for that condition is estimated to be 1.0 scfh. After sulfur exposure, the membrane was subjected to a leak test followed by a hydrogen bottle gas test. The results are shown in Table 33. The leak rate at 225 psi was 5.2 scfh, but hydrogen production at 74 psi of pure hydrogen was 17 scfh. This indicates the membrane is capable of recovery after being exposed to high sulfur.

Tables 31–37 give the raffinate and permeate gas compositions over the test periods. The gas compositions as determined by both the LGAs and GC are shown. It should be noted that the LGA produces analyses continuously while the GC produces single-point sample analyses at 15-minute intervals.

For the permeate concentration data, the Membrane 1 permeate is considered to be pure hydrogen and the difference is due to analyzer calibration. For Membrane 2, there was a significant leak; therefore, the concentrations of N_2 and CO_2 give some insight into the hydrogen purity.

Table 33. Membrane 2 Leak Check and Hydrogen Exposure after High-Sulfur Test

Date	Comment	Gas	Inlet P, psi	Flow, scfh
1/22/2012	After sulfur exposure	N_2	139	2.9
1/22/2012	After sulfur exposure	N_2	200	4.6
1/22/2012	After sulfur exposure	N_2	225	5.2
1/22/2012	After sulfur exposure	H_2	24	4
1/22/2012	After sulfur exposure	H_2	50	9.7
1/22/2012	After sulfur exposure	H_2	74	17

Table 34. Membrane 1 Raffinate Concentration

Operating	LGA Concentration, mol%					GC Concentration, mol%				
Period	H_2	CO	CO_2	N_2	CH_4	H_2	CO	CO_2	N_2	CH_4
SS1	24.1	0.4	13.4	59.8	0.6	n/a	n/a	n/a	n/a	n/a
SS2	9.6	0.9	15.0	72.1	0.5	12.0	9.2	13.7	68.7	1.6
SS3	10.6	1.2	16.1	71.5	0.7	9.2	1.1	15.4	64.5	2.1
SS4	29.7	0.7	14.4	57.1	0.4	23.8	0.8	14.1	52.2	1.4
SS5	8.9	0.2	16.5	74.9	0.5	8.2	0.4	15.8	70.0	1.8
SS6	11.7	0.3	16.8	70.6	0.5	10.2	0.4	16.7	66.8	1.0
SS7	15.5	0.3	23.7	58.1	1.0	13.5	0.5	22.5	55.0	1.6
SS8	17.1	0.4	28.0	50.5	1.6	14.1	0.7	27.8	48.1	1.5

Table 35. Membrane 2 Raffinate Concentration

Operating	LGA Concentration, mol%					GC Concentration, mol%				
Period	H_2	CO	CO_2	N_2	CH_4	H_2	CO	CO_2	N_2	CH_4
SS1	23.9	0.7	13.1	60.0	0.6	n/a	n/a	n/a	n/a	n/a
SS2	11.2	0.9	14.6	70.4	0.6	12.6	3.0	16.3	66.3	10.8
SS3	11.6	1.5	16.2	70.9	0.5	9.4	1.2	15.6	65.9	1.1
SS4	28.4	0.7	14.4	58.7	0.3	24.5	0.6	14.0	52.1	0.7
SS5	9.2	0.2	16.6	74.3	0.5	8.0	0.3	15.9	69.9	0.9
SS6	10.8	0.2	16.9	71.5	0.4	9.7	0.4	16.2	67.5	0.9
SS7	14.1	0.1	25.2	58.1	0.9	12.4	0.3	24.7	55.4	1.6
SS8	20.0	0.4	25.5	50.8	1.5	13.3	0.5	28.2	49.0	2.9

Figure 40 displays the inlet syngas composition for the entire test period. The components CO and CH_4 are displayed on the secondary axis. Hydrogen concentration ranged from 10% to 15% during the parametric tests without the supplemental hydrogen. The concentration increased to near 20% during the oxygen-blown tests.

Table 36. Membrane 1 Permeate Concentration

Operating	LGA Concentration, mol%					GC Concentration, mol%				
Period	H_2	CO	CO_2	N_2	CH_4	H_2	CO	CO_2	N_2	CH_4
SS1	97.0	0.0	0.1	0.8	0.0	n/a	n/a	n/a	n/a	n/a
SS2	95.9	0.0	0.0	0.2	0.0	n/a	n/a	n/a	n/a	1.5
SS3	97.3	0.0	0.0	0.1	0.0	76.1	1.5	4.3	18.7	1.2
SS4	98.0	0.0	0.0	0.1	0.0	74.4	0.1	n/a	0.0	0.6
SS5	97.2	0.0	0.3	1.5	0.0	73.8	0.2	1.1	1.0	0.9
SS6	98.5	0.0	0.0	0.0	0.0	74.7	0.1	1.5	0.0	0.9
SS7	97.5	0.0	0.0	0.0	0.0	73.2	n/a	1.6	0.1	1.9
SS8	97.3	0.0	0.1	0.2	0.0	70.9	0.3	1.0	1.4	2.8

Table 37. Membrane 2 Permeate Concentration

Operating	LGA Concentration, mol%					GC Concentration, mol%				
Period	H_2	CO	CO_2	N_2	CH_4	H_2	CO	CO_2	N_2	CH_4
SS1	95.2	0.0	0.4	2.5	0.0	n/a	n/a	n/a	n/a	n/a
SS2	69.2	1.1	4.0	24.0	0.2	65.6	2.1	2.2	12.9	0.3
SS3	79.2	0.4	3.3	16.8	0.1	55.6	0.8	3.8	18.4	0.3
SS4	92.4	0.1	1.5	6.1	0.1	47.4	0.3	8.1	28.1	0.4
SS5	63.0	0.3	6.5	31.4	0.2	48.1	0.4	5.8	28.2	0.4
SS6	61.9	0.3	7.3	31.3	0.2	46.2	0.4	7.6	29.5	0.5
SS7	39.2	0.3	16.3	42.9	0.6	74.1	n/a	n/a	0.1	0.1
SS8	66.2	0.3	11.0	21.5	0.7	49.8	0.5	9.8	20.0	1.2

Figures 41 and 42 illustrate the raffinate and permeate flows for both membranes for the duration of the test run. Significant variation in total flow was caused by issues running the gas boosters and providing a steady flow. The lower flow rates toward the end of the testing resulted in better H_2 recovery but lower overall permeate flow.

CONCLUSIONS

WRI's raw and upgraded fuels produced by WRI's proprietary patent-pending process were tested under WRI's patent-pending gasifier operational modifications in the EERC's TRDU, and each fuel was demonstrated to gasify well with minimal operational issues. The biggest system upset for the week was the loss of the main air compressor for a couple of hours, which was caused by cold ambient air temperatures. Fuel feeding for the test run progressed with minimal issues, and no differences were noted in the feedability of the three fuels. The treated fuels were shown to have a significant reduction in moisture and certain volatile metals including mercury. Lower levels of silica were also observed in the treated coals.

The most dramatic transition observed throughout the testing was the change in CO and CO_2 concentrations as the gasifier was switched from raw to WRI upgraded fuels. For both the

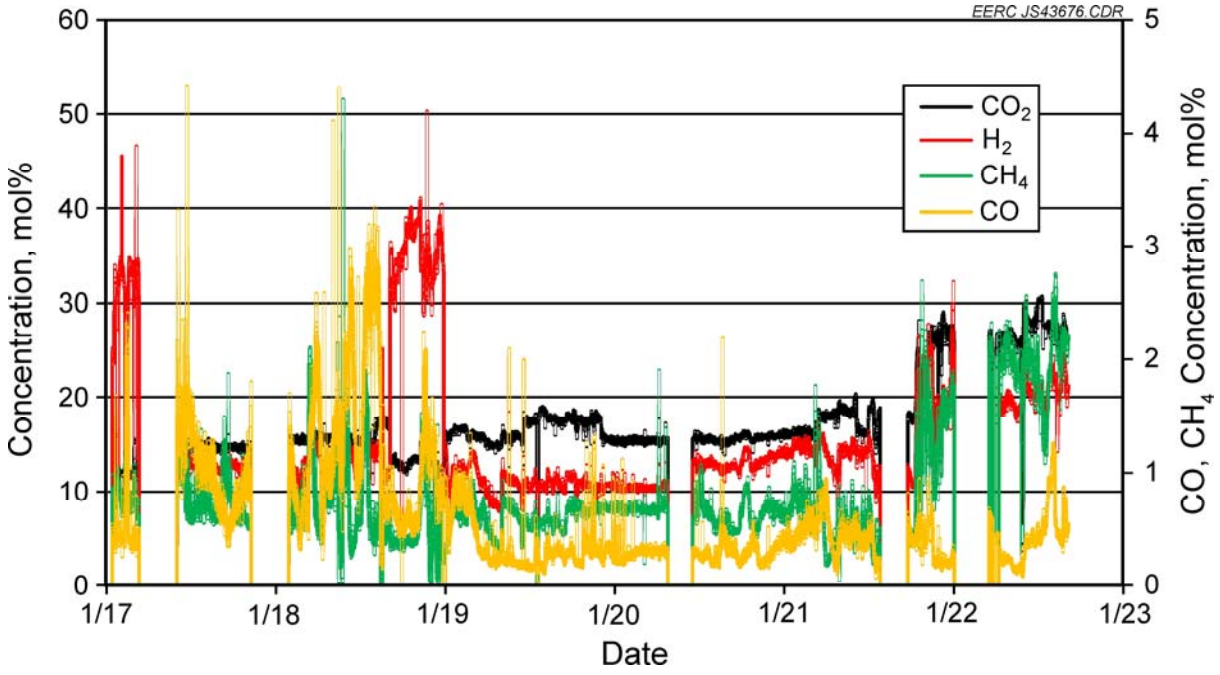

Figure 40. Inlet syngas composition for the test period.

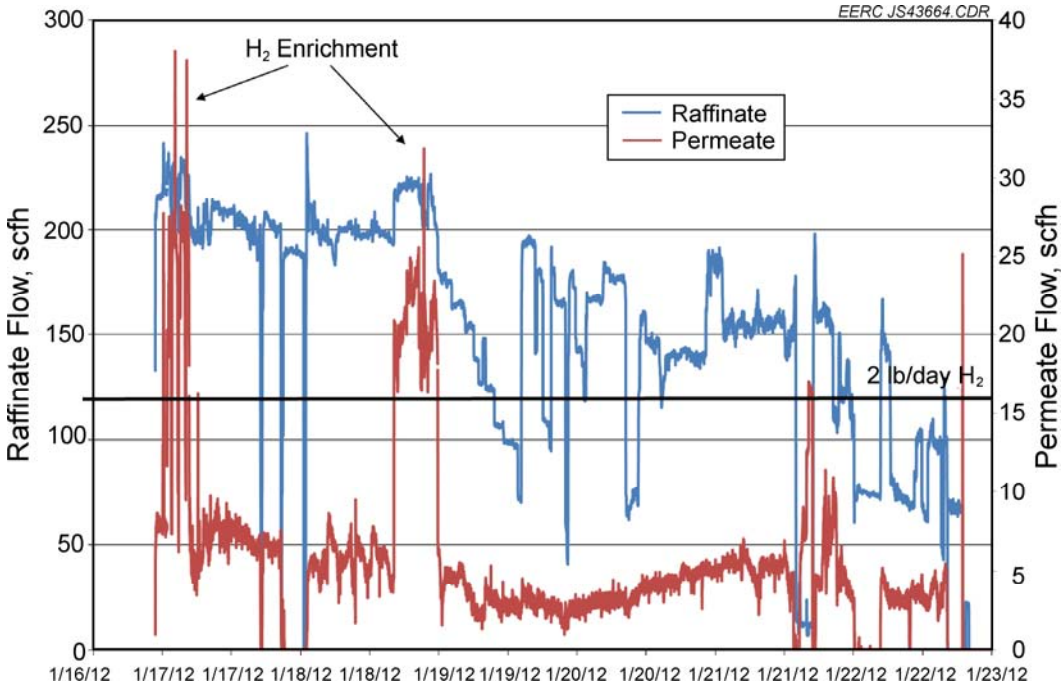

Figure 41. Membrane 1 raffinate and permeate flows.

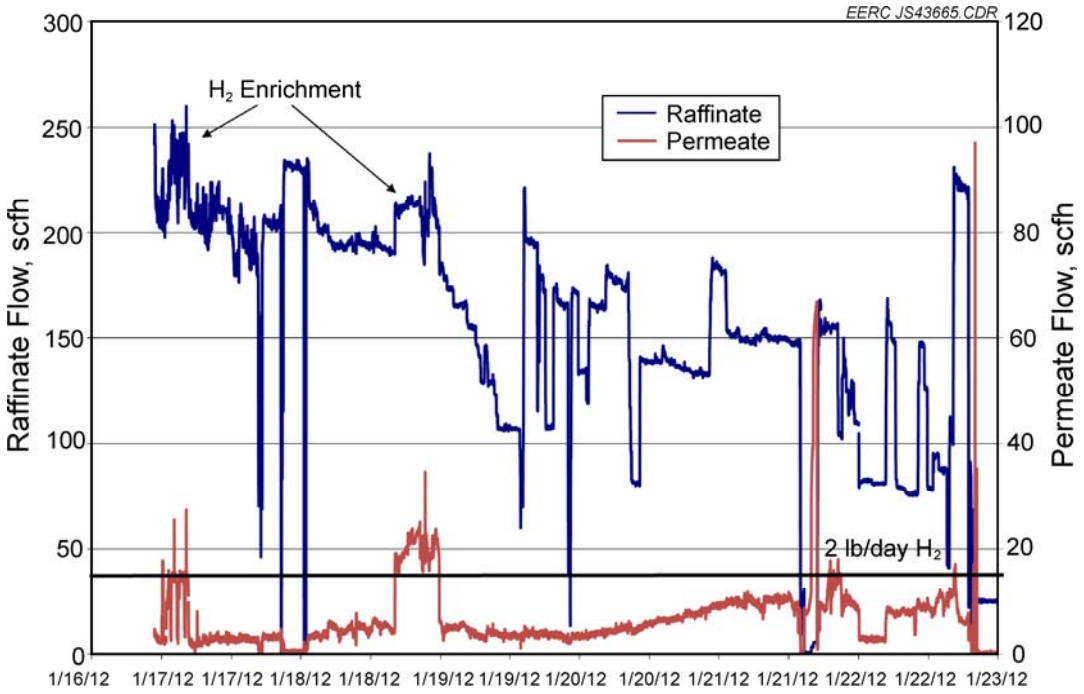

Figure 42. Membrane 2 raffinate and permeate flows.

PRB and the lignite, CO levels significantly increased and CO_2 levels significantly decreased when the dried fuel was brought online. This transition was also observed when switching from the upgraded PRB to the raw lignite, between Tests 4a-4 and 5a-1.

Smaller but significant changes in CO_2 concentration were observed when switching gasifier temperatures. As expected, the higher temperatures resulted in higher CO_2 concentration, increased carbon conversion, and reduced syngas heating value.

The concentration of trace metals in the syngas was also measured using carbon traps with Method 30B and the ME-ST method. The data indicated certain volatile metals including mercury were reduced in the syngas during the treated PRB run.

Particle-size distributions were determined for all of the ash samples collected during the test run and the raw fuels. No major differences were observed in the particle-size distributions for the test runs. The elemental composition of the ash was also analyzed, and the most signficant finding was the high level of sulfur capture occuring in the filter ash under the air-blown test conditions. Otherwise, no significant difference was observed in the ash chemistry between the raw and treated fuel. No ash agglomeration issues were observed for any of the tests.

Water samples produced from the gasifier were analysed for organic content. Lower levels of organics were observed on the dried and treated fuel gasifier runs as compared to the raw fuel runs. Significantly higher conentration organic material was produced during the steam–oxygen gasification tests.

The warm-gas cleanup equipment, sorbents, and catalysts used were shown to be capable of removing sulfur down to less than 2 ppm, and the shift catalyst was able to reduce CO levels to below 1%. Water and tars were condensed out of the syngas prior to compression for the membrane exposure.

Both of the hydrogen separation membranes were shown to be able to produce greater than 2 lb/day of hydrogen. Membrane 1 appeared to experience some performance degradation which may have been caused by coking. The coking could be attributed to a system upset and lack of steam available for the WGS reaction. The membrane was exposed to oxygen at high temperature at the supplier's laboratory to burn out the contaminant, and the membrane performance returned to expected levels. Membrane 2 developed a significant leak during the testing. Both membranes were shown to be capable of producing hydrogen from coal-derived syngas for the entire test period.

In summary, the WRI coal-upgrading/gasification process has demonstrated the amenability of the upgraded coal for improved gasification performance compared with raw and partially dried coals. In addition, proprietary gas injection at selected locations led to enhanced syngas quality. Acceptance of hydrogen separation membranes on the downstream segment to the syngas also validated WRI's patent-pending process.

REFERENCES

1. Schobert, H. *Lignites of North America*; *In* Anderson, L.L., Ed.; *Coal Science and Technology*; Elsevier, 1995; Vol. 23, 696 p.

2. Kong, L.; Karner, F.R.; Benson, S.A.; Steadman, E.N. Petrography and Inorganic Geochemistry of the Rosebud Coal Seam at the Absaloka, Big Sky and Rosebud Mines, Powder River Basin, Montana. *Org. Geochem.* **1993**, *20* (6), 811–822.

3. Alfsen, G.C. An Overview of Hydrogen Production from Coal Gasification. Prepared for the U.S. Department of Energy, Morgantown Energy Technology Center, Dec 1984.

4. Sondreal, E.A.; Swanson, M.L.; Benson, S.A.; Holmes, M.J.; Jensen, M.D. A Review of Gasification Technology for Coproduction of Power, Synfuels, and Hydrogen from Low-Rank Coals. In *Proceedings of the 20th Symposium on Western Fuels*; Marriott Denver Tech Center, Denver, CO, Oct 24–26, 2006; 37 p.

5. Carpenter, B.C. *Optimization of Great Plains Coal Gasification Using ASPEN/SP*. M.S. Thesis, University of North Dakota, Grand Forks, ND, May 1993; 189 p.

6. Hossain, M.M. *ASPEN/SP Computer Model of Great Plains Coal Gasifiers*; M.S. Thesis, University of North Dakota, 1995.

7. Mann, M.D.; Knutson, R.Z.; Erjavec, J.; Jacobsen, J.P. Modeling Reaction Kinetics of Steam Gasification for a Transport Gasifier. *Fuel* **2004**, *83*.

8. Jacobsen, J.P. *Char Reaction Kinetics in a Transport Gasifier*; M.S. Thesis, University of North Dakota, May 2001.

9. Energy Resources Company, Inc. *Low-Rank Coal Study: National Needs for Resource Development*; Report for U.S. Department of Energy Contract No. DE-AC18-79FC1006; Nov 1980.

10. Nexant: Tam, S.; Nizamoff, A.; Kramer, S.; Olson, S.; GTI: Lau, F.; Roberts, M.; Zabransky, R.; NETL: Hoffmann, J.; Shuster, E.; Zhan, N. *Lignite-Fueled IGCC Power Plant;* U.S. Department of Energy Contract No. DE-AC26-99FT40342; May 2005.

11. Swanson, M.L.; Hajicek, D.R.; Collings, M.E.; Henderson, A.K. Gasification of Low-Rank Coals in a Transport Reactor. Presented at the 21st International Pittsburgh Coal Conference, Sept 13–17, 2004, Osaka, Japan, 2004, 19 p.

12. Rutkowski, M.D.; Klett, M.G.; Maxwell, R.C. The Cost of Mercury Control in an IGCC Plant. Presented at the 2002 Gasification Technologies Conference, San Francisco, CA, Oct 27–30, 2002, 11 p.

13. Newby, R.A.; Smeltzer, E.E.; Lippert, T.E.; Slimane, R.B.; Akpolat, O.M.; Pandya, K.; Lau, F.S.; Abbasian, J.; Willians, B.E.; Leppin, D. *Novel Gas Cleaning/Conditioning for Integration Gasification Combined Cycle*; Base Program Final Report for U.S. Department of Energy National Energy Technology Laboratory DE-AC26-99FT40674; Aug 2001.

14. Benson, S.A. *Laboratory Studies of Ash Deposit Formation During the Combustion of Western U.S. Coals*; Ph.D. Thesis, Pennsylvania State University, 1987.

15. U.S. Department of Energy. *Effects of a Transition to a Hydrogen Economy on Employment in the United States;* Report to Congress; July 2008.

16. Ellis, S. Honda Fuel Cell Vehicle Progress. Presented at the Advancing the Hydrogen Economy Action Summit II, Grand Forks, ND, Sept 4, 2008.

17. Holmes, M. Coal-to-Hydrogen. Presented at the Advancing the Hydrogen Economy Action Summit II, Grand Forks, ND, Sept 4, 2008.

18. Gerdes, K. The Potential of Advanced Gasification Pathways to Reduce CO_2 Capture Costs. Presented at the Gasification Technologies Conference, Colorado Springs, CO, Oct 2009.

19. Hoffman, J. Cost and Performance for Low-Rank Coal Power Plants. Presented at the Gasification Technologies Conference, Colorado Springs, CO, Oct 2009.

20. Plunkett, J. Performance and Cost Comparisons of Alternate IGCC-Based Carbon Capture Technologies. Presented at the Gasification Technologies Conference, Colorado Springs, CO, Oct 2009.

21. Klara, J.M. IGCC: Coals Pathway to the Future. Presented at the Gasification Technologies Conference, Oct 4, 2006.

22. Stocker, J.; Whysall, M.; Miller, G. *30 Years of PSA Technology for Hydrogen Purification*; UOP LLC; 1998.

23. Adhikari, S.; Fernando, S. *Hydrogen Membrane Separation Techniques*; ACS Publications Industrial & Engineering Chemistry Research, 2006.

24. Kluiters, S.C.A. Status Review on Membrane Systems for Hydrogen Separation; Dec 2004.

25. Stanislowski, J.; Laumb, J. Gasification of Lignites to Produce Liquid Fuels, Hydrogen, and Power. Presented at the Pittsburgh Coal Conference, Sept 2009.

26. Ockwig, N.; Nenoff, T. *Membranes for Hydrogen Separation*; ACS Publications Chemical Review 2007.

27. U.S. Department of Energy. *Hydrogen from Coal Program RD&D Plan for the Period 2009 Through 2016*; External Draft; Sept 2009.

28. Cicero, D. The U.S. DOE's Hydrogen from Coal Program. Presented at the 235th ACS National Meeting, April 2008.

29. O'Brien, C.; Miller, J.; Gellman, A.; Howard, B.; Morreale, B. Hydrogen Transport Through Palladium-Based Separation Membranes in the Presence of Hydrogen Sulfide. Presented at the Pittsburgh Coal Conference, Pittsburgh, PA, Sept 2009.

30. Howard, B.; Morreale, B. Poisoning and Corrosion of Pd–Alloy Hydrogen Separation Membranes by H_2S. Presented at the Pittsburgh Coal Conference, Pittsburgh, PA, Sept 2009.